AFCRL-TR-60-236

University of California
La Jolla
School of Science and Engineering
Department of Physics

Atmospheric Radiation Tables

Walter M. Elsasser
with
Margaret F. Culbertson

Final Report under Contract AF 19(604)-2413

The research reported in this document has been sponsored by the Geophysics Research Directorate of the AF Cambridge Research Laboratories, Air Force Research Division (ARDC)

AFCRL-TR-60-236

University of California
La Jolla
School of Science and Engineering
Department of Physics

Atmospheric Radiation Tables

Walter M. Elsasser

with

Margaret F. Culbertson

Final Report under Contract AF 19(604)-2413

The research reported in this document has been sponsored by the Geophysics Research Directorate of the AF Cambridge Research Laboratories, Air Force Research Division (ARDC)

PREFACE

In 1942, the author published a monograph entitled "Heat Transfer by Infrared Radiation in the Atmosphere," which was rather favorably received by the meteorological public. The war terminated this particular work, and during it and thereafter the author became engaged in other scientific pursuits not directly related to atmospheric radiation. In the meantime, a vast literature has grown up around the subject, dealing with laboratory experiments as well as theoretical analysis, not to speak of the applications to the atmosphere itself. From the fall of 1950 until 1954, the author, while at the University of Utah, was engaged in a project sponsored by the Air Force Cambridge Research Center whose aim it was in part to extend the methods used earlier for water vapor so that they were applicable to carbon dioxide and ozone. Very extensive new laboratory data on all three optically active atmospheric gases have become known in the last seven or eight years. This finally suggested a new edition of the earlier monograph, and the task was begun in the summer of 1957 at the Scripps Institution of Oceanography, again under the sponsorship of the Air Force Cambridge Research Center.

The present monograph is a second edition of the earlier one in the limited sense that the methods used to determine radiative fluxes in the atmosphere have been retained with only very minor changes. Approximations much more refined but also much more cumbersome to handle than the linear techniques of the 1942 work have been omitted. Instead, radiation tables have been calculated on the basis of the available data, practically all of them fairly new, for the 15-μ CO_2 band, the combined 9.6-μ and 9.0-μ ozone bands, the 6.3-μ water-vapor band, the rotational water-vapor band, and finally for the overall water-vapor spectrum. The only difference, in principle, from the earlier treatment lies in the use of a linear pressure reduction throughout, in place of the former square-root reduction. In the text, the review of the basic theory of band structure and band absorption has been somewhat enlarged. On the other hand, Part III of the earlier monograph which dealt mainly with radiation measurements in the atmosphere itself has been omitted, partly because the new tables are based on laboratory data, but largely because the literature on the subject has swollen to such dimensions that it would be impossible to do justice to it within the confines of this monograph.

Owing to many other obligations, the author has been unable to keep up in detail with the proliferating literature on atmospheric radiation. A purely formal bibliography based on a search of the abstracting literature seemed out of place in a work of this limited character. We have therefore restricted the bibliography to papers that are actually quoted in the text. It is possible, though not too probable, that an occasional paper which has a direct bearing on our work might have been overlooked, and the author apologizes in advance for such omissions.

Another restriction of the present monograph concerns the fact that we give only tables and no nomograms (charts). This is based on the view that a work like the present by its very nature addresses itself not so much to the practical forecaster as to the scientific investigator of the atmosphere. The latter will almost invariably spend some time and effort on the subject of radiative transfer if he becomes engaged in it at all. Given the very numerous graphical or numerical schemes that may be used for this purpose, depending on individual tastes, we felt it to be preferable to leave the construction of nomographs to the investigators concerned. With modern methods of reproduction, this is a relatively simple and cheap task that can be performed quite rapidly.

The very extensive computational work, including the involved two-dimensional smoothing of the radiation tables, was done by Miss Margaret Culbertson, M.A. Without her consistent accurate performance, this monograph could not have been written.

We are greatly indebted to the Thermal Radiation Laboratory of the Air Force Cambridge Research Center for their financial support, and in particular to Drs. John N. Howard, J. I. King, and P. R. Gast for their personal encouragement. This assistance and encouragement has been invaluable in completing the work.

WALTER M. ELSASSER

SCRIPPS INSTITUTION OF OCEANOGRAPHY
LA JOLLA, CALIFORNIA
FEBRUARY 1960

ABSTRACT

This paper contains tabular material on the emission and transmission of the far infrared bands of water vapor, carbon dioxide, and ozone. The values given are entirely based on *laboratory* measurements made w th long optical paths (with the exception only of the water-vapor absorption in the "window" near 10 μ). The final results are presented in the form of radiation tables, the numerical equivalent of the method of the radiation chart given by the author in his 1942 monograph, *Heat Transfer by Infrared Radiation in the Atmosphere* (Harvard University Press). Whereas the earlier monograph was restricted to water vapor, this paper covers all the bands appearing in the spontaneous emission of atmospheric air at common atmospheric temperatures. This comprises five bands, the 6.3 μ band and the rotational band of water vapor, the 14 μ band of carbon dioxide and the 9.6 μ and 11 μ bands of ozone. The ozone bands are found to be of minor importance in atmospheric heat transfer. Of greater importance is the overlap of the 14 μ carbon dioxide band and the rotational water-vapor band, and tables of this overlap are given.

The text is to some extent a new edition of the 1942 monograph. All material concerned with the direct measurement of atmospheric radiation (Part III of the earlier work) has been omitted and, instead, all three gases rather than water vapor alone are being dealt with. The methods (explained again in the text) are those used before, *i.e.*, the numerical integration of the (linear) equations of transfer for a gas in local thermodynamical equilibrium and in the absence of scattering. Only one integration, namely, that over the height of the radiating atmosphere, remains undone, and the use of the tables consists in doing this integration for an atmosphere of a given p-T relation numerically or graphically, on a nomogram constructed from the tables.

The only place at which a refinement of the earlier procedures has been introduced is in taking account of the variation of band contour with temperature (change of population of rotational levels). A crude approximation was used for this so as to keep the numerical work within bounds, but even so it should allow a better representation than was obtained heretofore. It is felt that these tables go nearly as far as one can go with laboratory measurements and with linear methods of approximation for computing transfer. Further progress is likely to involve more elaborate spectroscopic measurements under atmospheric conditions or calculations of a far more elaborate type. While the data given are considered comprehensive for the region of the far infrared spectrum covered by atmospheric emission, a comparison of the results with actual atmospheric measurements has not yet been made.

For the convenience of the user most of the tables have been subjected to a process of two-dimensional smoothing. The resulting accuracy is purely formal, and while convenient for the computer has no physical meaning. It is expected that the resulting errors should be at most of the order of a very few per cent of the black-body flux at the lower temperatures.

CONTENTS

ATMOSPHERIC RADIATION TABLES

WALTER M. ELSASSER[1]

with

MARGARET F. CULBERTSON

University of California, La Jolla

I. INTRODUCTION

This monograph contains numerical tools required to compute approximately the effects of radiative transfer in the atmosphere for the far infrared region of the spectrum. We shall not deal with the transmission and scattering of solar radiation, but only with the long-wave radiation that is emitted, and of course also absorbed, by the earth's surface, by clouds, and by the atmosphere itself. This part of the spectrum extends from a wavelength of about 4 microns to near the microwave range at a fraction of a millimeter wavelength. The main agents of transfer are two water-vapor bands and one band of carbon dioxide. In addition, there are some bands of carbon dioxide of minor importance and a band or rather a cluster of bands of ozone.

It is well established that the net effect of infrared radiation transfer is almost invariably a cooling. Only in a few rather exceptional circumstances does there occur a small amount of heating. Radiative cooling takes place at the ground, especially in clear weather, at cloud tops, and in the free atmosphere. The average radiative cooling of the free atmosphere is not large; it is of the order of one to two degrees per day, but, since this goes on all the time, the cumulative effects are of major importance for the dynamics of the atmosphere. The present monograph provides data from which all these effects of radiative cooling can be calculated simply and with a reasonable degree of accuracy at any given location, provided the temperature and moisture distribution of the atmosphere are known from a sounding.

Far infrared spectroscopy is now about half a century old and highly developed. The principal bands, especially those of simpler compounds such as H_2O and CO_2 are exceedingly well investigated; almost all of their lines have been measured and have been interpreted in quantum-mechanical terms. Moreover, even the lesser bands are now rather thoroughly known and their molecular mechanism understood. Unfortunately, this does not solve the problem of atmospheric transfer. Each band consists of hundreds of lines, and the total transfer is obtained by combining the contributions from all of these lines. Proposals have frequently been made to deal with this problem by means of large-scale computing machines. This can no doubt be done, but it would involve the manipulation of a vast amount of primary data on the part of the investigator, and it would even then be difficult to know whether all the significant data and effects have been taken into account. While electronic computing machines have so far seldom been used for this purpose, Kaplan (1950, 1952) has carried out elaborate manual computations for the 15-μ carbon-dioxide bands. The results are in good agreement with observations; but even after smoothing over the individual lines there remains a good deal of cumbersome detail, which makes it difficult to generalize these results to as broad a variety of conditions as we meet in the atmosphere.

It is hard to see how a rigorous solution of the transfer problem can be found, applicable to a large variety of atmospheric conditions, given the complexity of the spectrum and the intricate way in which the line intensities depend on temperature and the line shapes on pressure. On the other hand, there exist approximations which in the majority of cases are satisfactory. The nature of these approximations is described in detail in section II; their physical background is described in section III. They follow in a straightforward way from the basic formalism of the radiative-transfer equations together with typical structural characteristics of molecular bands. Some important points regarding these approximations should be brought out here.

In the first place, averaging over spectral intervals containing several or many lines is carried out mathematically at an early stage of the formalism, by means of rather straight-forward theoretical models. In terms of these averages, solutions of the transfer equations can be found that are rigorous for a schematical band and should be very nearly correct for real bands. The only features of the bands entering there-

[1] Present affiliation: Chairman, Department of Physics, University of New Mexico, Albuquerque, New Mexico.

after are smoothed-out band contours whose transmission characteristics can be expressed in terms of a very few numerical parameters. These parameters lend themselves to direct observational determination in a manner to be indicated.

Band-spectroscopic observations can be carried out in two ways. The traditional ambition of the spectroscopist has been to work with as narrow a slit as possible in order to resolve all the spectral lines, even the very weak ones. This is, however, not so advantageous when dealing with problems of atmospheric-radiation transfer. Here, we want a slit wide enough so that we do not see the individual lines at all but, instead, measure directly a smoothed-out band contour. For a long time, no such measurements were available, but in the last seven or eight years systematic investigations of far infrared bands with wide-slit techniques have been undertaken, using specially designed absorption cells to simulate or at least approximate the long optical paths encountered in the atmosphere. For the main bands of water vapor and carbon dioxide, this type of work was done at the Laboratory of Astrophysics and Physical Meteorology of Johns Hopkins University and at the Physics Department of Ohio State University. Many of the measurements were made with somewhat differing techniques at both places, providing a welcome mutual check. Furthermore, these measurements were made in the presence of various quantities of air in the absorption cell, allowing one to study directly the very important effects of extraneous pressure upon the absorption characteristics of the far infrared bands. This laboratory work is described in section IV. It is not possible, unfortunately, to cool the extremely bulky absorption cells below room temperature, and so the extrapolation of the band absorption to the low temperatures of the upper atmosphere has to be done by theoretical means. There, again, we have used an approximative averaging method and did not go back to the individual lines.

The tables given here are exclusively based on laboratory measurements of the above-mentioned type that simulate atmospheric conditions. On the one hand, direct reference to finer structural details of the bands is avoided; on the other hand, there is also no reference to data gained in the atmosphere itself. Earlier experience with water-vapor transmission indicates that the actual radiative fluxes will be closely reproduced, probably to within a few per cent in most cases, by these tables; nevertheless, the ultimate check will have to consist of extended measurements under a great variety of atmospheric conditions, to be compared with the predictions obtained from the tables.

The tables form the basis of radiative-cooling calculations. They may also be used to compute the total radiation leaving the earth which is of interest on general geophysical grounds and to determine the flux received by a satellite. All the numerical work may be done once and for all except for one final numerical integration which involves the temperature distribution of the atmosphere as well as the distribution in height of the optically active gases, and therefore it varies with conditions, both in space and in time. Very early, Mügge and Möller (1932) developed a nomogram on which this integration could be done graphically. It was further developed by Elsasser (1942) and has become known as a "radiation chart." We retain this term, although we present the data only in tabular form. Many workers prefer to do the integrations numerically rather than graphically. Also, we find that, if a nomogram is desired, it can be inked by a draftsman and reproduced by some conventional process in very short order and with a minimum of expense. The term "radiation chart" appearing in the following pages designates a *table* with two entries, temperature, T, and optical thickness in the vertical, u, so that, when the empirical relationship between the two, say $u(T)$, is given for any particular atmosphere, the radiative flux may be obtained by integration along the path defined by $u(T)$. This technique is described in section V.

The question has often been asked whether radiative-cooling calculations could be used for purposes of forecasting. We believe that the calculations are, as a rule, prohibitively difficult; moreover, radiative cooling is not usually strong enough to affect the local dynamics of the weather over a relatively short period. Apart from such local effects as nocturnal cooling of the ground, radiative cooling is a "secular" effect in the dynamics of the weather. Its variation with altitude, latitude, season, *etc.* should be of great meteorological importance; these effects can be investigated systematically by means of the data presented here. So far as altitude is concerned, our methods should be reasonably accurate up to a height of, say, 25 to 30 km but should give at least correct orders of magnitude to, say, 40 km. This is discussed in section 3.2. A number of investigators have carried out computations of radiative cooling based on earlier and, we believe, already fairly accurate data. The material contained in this monograph should permit a further check of such work and an extension to a greater variety of atmospheric conditions.

II. PRINCIPLES OF RADIATIVE TRANSFER

1. Kirchhoff's law, Planck's law, and the equation of transfer

The problem encountered in determining the infrared fluxes in the earth's atmosphere is much simpler than the general radiative transfer problem occurring in geophysics or astrophysics. There are two essential simplifying facts which hold to a very high degree of approximation. The first is the absence of scattering. A parcel of air containing optically active gases will partly absorb and partly transmit incident radiation, but it will not appreciably scatter the transmitted radiation. In the second place, every particle of air is effectively in local thermodynamical equilibrium. That is, the excitation of molecular levels and the radiation ensuing therefrom are the same as they would be if the parcel were in an enclosure in thermodynamical equilibrium at a given temperature, T. The condition of the parcel, including its emitted radiation, can therefore be described by density, temperature, pressure, and the relative concentrations of the optically active substances in the parcel; the radiation issuing from the parcel is, in particular, independent of the characteristics of the radiation incident upon the parcel. In the next chapter, we shall briefly return to these conditions and their physical background; for the time being, we shall admit them as valid.

A surface which absorbs all radiation of any given wavelength falling upon it is called completely opaque. A surface which is completely opaque at all wavelengths is called *black*. An enclosure surrounded by black walls, the whole kept at a constant temperature, T, is filled throughout by black-body radiation of temperature T. This is true no matter what else is inside the enclosure. If local thermodynamical equilibrium prevails in the enclosure, *Kirchhoff's law* can readily be proved. Consider a piece of matter inside the enclosure, and consider a given direction of travel for the radiation. Incident upon the piece, there is in the given direction black-body radiation of intensity, say, $I_b(\lambda)$ for any given wave length, λ. The fraction A of this radiation may be absorbed. Let E be the radiation emitted by the piece. Then, in equilibrium,

$$I_b = (1 - A)I_b + E,$$

expressing the fact that the total radiation leaving the piece is again black. Therefore,

$$E/A = I_b, \tag{1}$$

which is Kirchhoff's law. This is valid at any specified wavelength.

In this paper, we shall use as a unit the *wave number*, which is the reciprocal of the wavelength; we designate it by ν throughout, and

$$\nu = 1/\lambda = \nu'/c, \tag{2}$$

where ν' is the conventional frequency and c the velocity of light.

We shall now indicate *Planck's law* of black-body radiation together with the numerical constants that have been used in the present tables. We encounter two situations of interest. On the one hand, we consider unidirectional beams of radiation of intensity $I_b(\nu)$ per unit area as emitted by a black body; on the other, we are interested in the black-body *flux* B_ν that emerges from a unit area of a black surface into all directions of the hemisphere. The two are connected by the simple relationship

$$B_\nu = \pi I_b(\nu) \tag{3}$$

which will be proven later on. It is customary to express Planck's law in terms of fluxes. Then

$$B_\nu = \frac{p\nu^3}{e^{q\nu/T} - 1} \tag{4}$$

where, in terms of fundamental constants,

$$p = 2\pi hc^2, \quad q = hc/k$$

(h, Planck's constant, k Boltzmann's constant) and numerically (figures from *American Institute of Physics Handbook*, McGraw-Hill, N. Y., 1957; see, also, Cohen *et al.*, 1955)

$$\begin{aligned} p &= 3.7413 \cdot 10^{-5} \text{ erg/cm}^2 \text{ sec} \\ q &= 1.4389 \text{ cm deg.} \end{aligned} \tag{5}$$

The absolute temperature is related to the centigrade scale by

$$T = t + 273.16.$$

We shall frequently use the derivative with respect to the temperature of the black-body function. By letting

$$x = q\nu/T,$$

this can be written

$$\frac{dB_\nu}{dT} = \frac{pT^2}{q^3} \cdot \frac{x^4 e^x}{(e^x - 1)^2}, \tag{6}$$

where

$$p/q^3 = 1.25585 \cdot 10^{-5},$$

using the values from (5). In our tables, we have

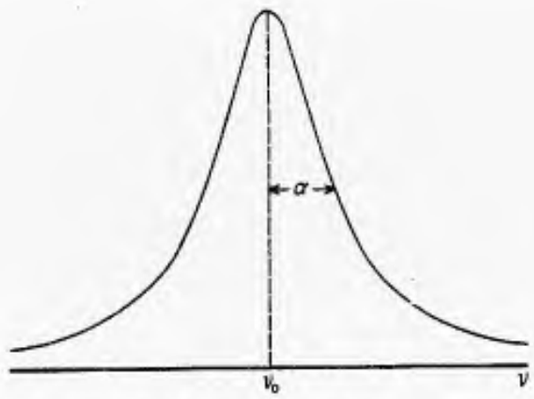

FIG. 1. Shape of spectral line.

adopted as a unit one gcal per sq cm per day. In these units, the factor becomes

$$p/q^3 = 2.5915 \cdot 10^{-8} \text{ (gcal/cm}^2\cdot\text{day)}. \tag{7}$$

For the sake of completeness, we mention the figure for the total black-body radiation (Stefan-Boltzmann formula)

$$B = \int_0^\infty B_\nu d\nu,$$

$$B = 1.1696 \cdot 10^{-7} T^4 \text{ (gcal/cm}^2\cdot\text{day)} \tag{8}$$

$$\frac{dB}{dT} = 4.6784 \cdot 10^{-7} T^3 \tag{9}$$

In order to derive the equation of radiative transfer, we now return to the case of a straight-line beam, leaving the integration over the hemisphere for later. We shall use u to designate optical thickness (mass of optically active gas per sq cm). Let k be the absorption coefficient, defined by the relation

$$dI_a = -kIdu; \tag{10}$$

that is, in a layer of optical thickness du, the fraction kdu of the incident intensity is absorbed. By Kirchhoff's law (1) the amount emitted by the layer is

$$dI_e = kI_b du, \tag{11}$$

and hence

$$dI = -k(I - I_b)du, \tag{12}$$

which is the equation of radiative transfer for the one-dimensional case in the absence of scattering.

2. A single spectral line

Next we shall be concerned with straight absorption, expressed by the integral of (10)—

$$I = I_0 e^{-ku}. \tag{13}$$

Here, k is a function of ν, and in band spectra it is in general a very complicated one. The far infrared bands which are responsible for radiative transfer in the atmosphere appear, on sufficient spectral resolution, to consist of very numerous spectral lines, and we shall proceed by first considering the absorption of a single spectral line. We shall then study band patterns made up of many individual lines.

The shape of spectral lines can depend on a variety of factors, but in most of the atmosphere the far infrared lines have the so-called Lorentz shape. We shall designate the integrated intensity of a line by S. Then the distribution of absorption over the line is expressed by the formula (fig. 1)

$$k(\nu) = \frac{S}{\pi} \frac{\alpha}{(\nu - \nu_0)^2 + \alpha^2}. \tag{14}$$

This is normalized, so that

$$\int_{-\infty}^{+\infty} k d\nu = S. \tag{15}$$

The parameter α is called the half-width of the line; it is a function of pressure and, to a lesser degree, of the temperature. For a constant temperature, α is directly proportional to the total pressure, which in the atmosphere is essentially the air pressure, since the partial pressures of the optically active gases are quite small.

We now define the transmissivity of a spectral interval $\Delta\nu$ as

$$\tau = \frac{1}{I_0 \Delta\nu} \int I d\nu = \frac{1}{\Delta\nu} \int_{\Delta\nu} e^{-k(\nu)u} d\nu, \tag{16}$$

by (13). By substituting here the expression (14), we get

$$\tau = \frac{1}{\Delta\nu} \int d\nu \exp\left[- \frac{S\alpha u/\pi}{(\nu - \nu_0)^2 + \alpha^2} \right]. \tag{17}$$

If we take the interval wide enough, we may use $-\infty$ and $+\infty$ as limits of integration. We introduce the abbreviation

$$x = Su/2\pi\alpha. \tag{18}$$

By substituting the variable,

$$\tan\frac{s}{2} = \frac{\nu - \nu_0}{\alpha},$$

(17) becomes

$$\tau = \frac{\alpha}{\Delta\nu} \int_{-\pi}^{+\pi} e^{-x\cos s - x} \frac{d}{ds}\left(\tan\frac{s}{2}\right) ds.$$

By an integration by parts and some further manipulations, this finally assumes the form

$$A = 1 - \tau = (2\pi\alpha/\Delta\nu) x e^{-x}[J_0(ix) - iJ_1(ix)]. \tag{19}$$

Here, A will be called the *absorptivity*. J_0 and J_1 are Bessel functions of order zero and one, respectively. This formula is due to Ladenburg and Reiche (1911).

There are two important limiting cases. When x is small, the power series for the Bessel functions yields

$$A\Delta\nu = 2\pi\alpha x = Su. \tag{20}$$

This is the region of linear absorption, the absorption being proportional both to line strength and to the optical path. The condition of validity of this approximation is clearly $x \ll 1$ which, by (18) and (14), means

$$k(\nu_0)u \ll 1;$$

i.e., for this approximation to hold, the absorptivity must be small at the line center; it is then *a fortiori* small in the wings of the lines (fig. 2).

In the opposite extreme, x is large. The asymptotic development of the Bessel functions then gives

$$A\Delta\nu = 2\sqrt{S\alpha u}. \tag{21}$$

The absorption is now proportional to the *square root* of the line intensity and of the optical thickness. One can readily verify that, as fig. 2 shows, the central part of the line has been completely absorbed away, and further absorption can occur only in the wings of the line.

Formula (21) may be obtained more directly by neglecting the term α^2 in the denominator of (14). If this simplified form for k is substituted into (16), one may obtain (21) by an elementary integration.

For a band containing many lines, (20) leads to

$$A\Delta\nu = \sum_i S_i u,$$

the summation extended over all the lines in the interval. This is a good approximation when each term of the sum is sufficiently small, since mutual overlapping of neighboring lines is unimportant for weak absorption. On the other hand, for the strong absorption case expressed by (21), overlapping of neighboring lines in a band becomes of paramount importance, and the total absorption will always be less than the sum of the contributions (21) of the individual lines. Clearly, A cannot exceed unity, whereas the preceding expressions for A are unbounded and therefore inapplicable to sufficiently thick layers. The next developments are concerned with taking into account the mutual overlapping of lines in a band.

3. Periodic band pattern

A simple and in some cases fairly realistic model of a band suggests itself readily: we allow a single line of

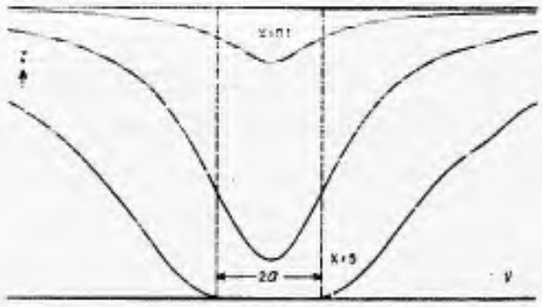

FIG. 2. Absorption of single line for various absorber thicknesses.

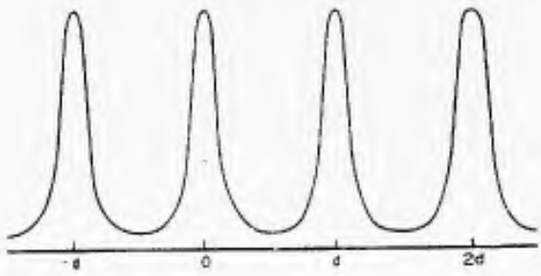

FIG. 3. Periodic band pattern.

the form (14) to repeat itself periodically (fig. 3). Thus, we let

$$k(\nu) = \sum_{n=-\infty}^{n=+\infty} \frac{S\alpha/\pi}{(\nu - nd)^2 + \alpha^2}, \tag{22}$$

where d is clearly the distance between adjacent lines. It is possible to express (22) in terms of an analytical function owing to the fact that, if such a function has only single poles, it is uniquely defined by these poles (by Mittag-Leffler's theorem; see Whittaker and Watson, 1940, Ch. 7). We find that (22) is equivalent to

$$k(\nu) = \frac{S}{d}\frac{\sinh\beta}{\cosh\beta - \cos s}, \tag{23}$$

where

$$\beta = 2\pi\alpha/d, \quad s = 2\pi\nu/d. \tag{24}$$

The transmissivity (16) may now be written

$$\tau = \frac{1}{2\pi}\int_{-\pi}^{+\pi} e^{-k(\beta)u}ds.$$

To evaluate this, form

$$\frac{d\tau}{du} = -\frac{1}{2\pi}\int ke^{-ku}ds.$$

We introduce the variable

$$\cos\varphi = \frac{\cosh\beta\cosh s - 1}{\cosh\beta - \cosh s}$$

and find

$$\frac{d\tau}{du} = -\frac{S}{2\pi d}\int_0^{2\pi} d\varphi \exp\left[-\frac{Su}{d\cdot\sinh\beta}(\cosh\beta+\cos\varphi)\right]$$
$$= -(S/d)e^{-y\coth\beta}J_0(iy/\sinh\beta),$$

with

$$y = Su/d. \tag{25}$$

By integrating the last expression with suitable boundaries,

$$\tau = \int_y^\infty e^{-y\coth\beta}J_0(iy/\sinh\beta)dy. \tag{26}$$

We shall consider limiting cases of this formula. The parameter β measures the ratio of line width to the distance of neighboring lines, by (24). For large β (that is, strongly overlapping lines), we have $\coth\beta = 1$ and $J_0 = 1$; hence,

$$\tau = e^{-y},$$

and the band exhibits the behavior of a continuous absorption spectrum. This case, however, is not realistic for the atmosphere. We should note that the degree of overlapping does not only depend on β but also on the thickness u of the layer. The case of large β corresponds to a "smearing out" of the absorption coefficient even if u is so small that the absorption of the individual line is represented by the "linear" formula (20). On the other hand, overlapping may occur in thick layers (large u) where the individual lines absorb only in the wings. This is the normal case for atmospheric bands, generalizing the square-root law (21).

We therefore approximate for small β

$$1/\sinh\beta = 1/\beta - \beta/6$$

and

$$\coth\beta = 1/\beta + \beta/3.$$

By substituting into (26) and using the asymptotic expansion for J_0, one obtains

$$A = 1 - \tau = \operatorname{erf}\left[(y\beta/2)^{\frac{1}{2}}\right] = \operatorname{erf}\left[\sqrt{\pi u S}\alpha/d\right], \tag{27}$$

with the usual definition

$$\operatorname{erf}(x) = \frac{2}{\sqrt{\pi}}\int_0^x e^{-x^2}dx. \tag{28}$$

For small values of x, we have

$$\operatorname{erf}(x) = 2x/\sqrt{\pi},$$

and (27) reduces to the square-root absorption law (21). In practice, it is found that a square-root law holds only for a rather limited range of optical thickness; then the curve for A bends around to reach unity asymptotically. It may be noted that in the derivation of (27) the region of a linear absorption law, which must always exist for sufficiently small u, has been obliterated.

The bands of CO_2 consist of fairly regularly spaced lines, and for them the absorption law (27) is not too poor an approximation. On the other hand, the bands of water vapor and ozone have a highly irregular fine structure and cannot be well described by our approximation. This model of the periodic band was introduced by Elsasser (1938, 1942) and is sometimes referred to as the Elsasser band.

4. Statistical band model

We now treat another model for band absorption, based on statistical considerations, due to Goody (1952, 1954). Let $\Delta\nu$ be a spectral interval in which there are n lines of mean distance d;

$$\Delta\nu = nd. \tag{29}$$

Let $P(S_i)$ be the probability that the ith line have an intensity S_i and let P be normalized;

$$\int_0^\infty P(S)dS = 1.$$

We assume that any line has equal probability of being anywhere in the interval $\Delta\nu$. The *mean* absorption clearly does not depend on ν provided we are far enough away from the edges of the interval. We shall therefore determine it for $\nu = 0$, the center of the interval. We have from (14), if we let the center of the ith line be at $\nu_0 = \nu_i$,

$$k_i(S_i, \nu_i) = k(\nu = \nu_i, \nu_0 = 0).$$

The mean transmissivity is found by averaging over all positions and all intensities of the lines; thus,

$$\tau = \frac{1}{(\Delta\nu)^n}\int_{\Delta\nu} d\nu_1 \cdots \int_{\Delta\nu} d\nu_n \int_0^\infty P(S_1)e^{-k_1 u}dS_1 \cdots \int_0^\infty P(S_n)e^{-k_n u}dS_n.$$

But all the integrals are alike; hence,

$$\tau = \left[\frac{1}{\Delta\nu}\int d\nu \int P(S)e^{-ku}dS\right]^n = \left[1 - \frac{1}{\Delta\nu}\int d\nu \int P(S)(1-e^{-ku})dS\right]^n.$$

By using (29), it is at once seen that the last expression approaches an exponential when n becomes large; we write

$$\tau = \exp\left[-\frac{1}{d}\int P(S)[A_1\Delta\nu]dS\right], \tag{30}$$

with the abbreviation

$$[A_1\Delta\nu] = \int_{\Delta\nu} (1 - e^{-ku})d\nu \tag{31}$$

where A_1 is nothing but the absorptivity of a single line taken over the interval $\Delta\nu$. The expression (30) is clearly valid for any line shape, $k(S, \nu)$, whatever.

We shall next consider two special cases. First, let all the lines have equal strength. The integral in (30) can simply be omitted and we have, by using again (29),

$$\tau = e^{-nA_1}. \tag{32}$$

This reduces to the algebraic sum of the individual line absorptions, $1 - \tau = nA_1$, when the exponent is small, the lines absorbing weakly. Otherwise, the absorptivity is always less than nA_1. This is due to the fact that overlapping of lines diminishes the absorption and that in an irregular array there remain occasional wider absorption gaps which are filled up but slowly as the thickness of absorber increases.

If we use the square-root absorption law (21), formula (32) becomes

$$\tau = \exp\,(-2\sqrt{uS\alpha}/d). \tag{33}$$

Next, let the lines be of different strength and consider a simple Poisson distribution for the probability of their strength—namely,

$$P(S) = \frac{1}{S_0} e^{-S/S_0}. \tag{34}$$

By letting $k = KS$, we find from (30)

$$\tau = \exp\left[-\frac{1}{d}\int \frac{KuS_0}{1 + KuS_0}\,d\nu\right].$$

We now introduce the Lorentz shape (14)—

$$K = \frac{\alpha}{\pi(\nu^2 + \alpha^2)}.$$

This vanishes fast enough for large $|\nu|$ that we can extend the integration in (34) from $-\infty$ to $+\infty$, giving

$$\tau = \exp\left[-\frac{uS_0\alpha}{d\sqrt{\alpha^2 + uS_0\alpha/\pi}}\right]. \tag{35}$$

This is Goody's formula. It should be noted that it can be expressed as a function of *two* parameters only, apart from u, namely S_0/d and α/d, in complete analogy to the periodic band case (26). Usually, in atmospheric bands $\alpha \ll d$, the lines are narrow compared to their mutual distance. If α is small, we may in a first approximation neglect α^2 under the square root, and (35) becomes

$$\tau = \exp\,(-\sqrt{\pi uS_0\alpha}/d), \tag{36}$$

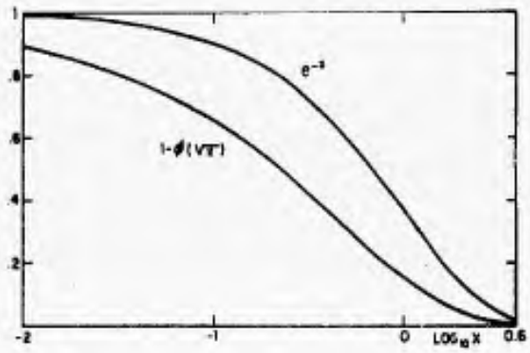

FIG. 4. Comparing transmission for periodic band, equation (27) with random band, equation (36) both for limit of widely spaced lines. (ϕ is the error integral (28).)

which differs from the corresponding formula (33) for lines of constant intensity only by a slight numerical factor in the exponent.

In fig. 4, the two functions (27) and (36) are compared, with a logarithmic scale for the argument, which is the same for both cases provided we identify S in the former with S_0 in the latter. Actual band spectra are neither as regular as is implied in the one formula nor as irregular as is assumed in the other; hence, one might expect most real transmissivity functions to lie between these two cases.

The basic formulas (30) and (31) of the statistical transmission theory are very general, and it is possible to deal with sets of lines having a shape different from the Lorentz shape. The Doppler shape becomes important in the upper layers of the stratosphere. This will be dealt with in section III. Calculations of this more general type have been carried out by Kaplan (1953) who has also used this method to treat the statistical superposition of several period bands of the type described in section II; see, also, Plass (1958).

5. Pressure. Semi-empirical method

We shall here merely state the facts regarding the pressure effect on absorption; some of the physical background will be discussed in section III. The finite width of a Lorentz line is produced by the collisions of the radiating molecule with other molecules; from kinetic theory, the number of collisions is proportional to $p/\sqrt{T}$; we write, therefore,

$$\alpha = \alpha_0 \frac{p}{p_0}\sqrt{\frac{T_0}{T}}, \tag{37}$$

where the width α_0 refers to standard conditions, p_0, T_0. Since the relative concentration of the optically active gases in the atmosphere is usually quite small, p essentially designates pressure of the ambient air. The pressure effect expressed by (37) is very important in atmospheric transfer calculations; the temperature

effect in (37) is much smaller and may be ignored when no great accuracy is required.

Let us now look at a relatively simple transmissivity formula such as (35). Although we have succeeded in smoothing over the rapid variation of absorption caused by the numerous lines, there remains a dependence on some parameters, and the application of such a formula to a great variety of atmospheric conditions will be too cumbersome to be practical. On the other hand, much simplification occurs when the lines are very narrow. Then (36) applies for the statistical band and (27) for the periodic band. Both depend only on one combination of parameters. In the atmosphere, the spectral lines become the narrower the higher we go, as seen from (37); since the lines are already fairly narrow at one atmosphere of pressure, they will be even more so higher up in the atmosphere. This suggests that, in a fair approximation, transmissivity functions may be expressed as generalizations of (36), say

$$\tau = \tau(u \cdot L),$$

where L is designated as *generalized absorption coefficient* and is a slowly varying function of ν over the band. In order to take account of the pressure dependence as given by (37), we note that only the product $u\alpha$ appears in (36) and (27). We therefore introduce a "reduced" optical thickness,

$$u^* = u \frac{p}{p_0} \sqrt{\frac{T_0}{T}}, \tag{38}$$

and write

$$\tau = \tau(u^* \cdot L). \tag{39}$$

It is possible to check the accuracy of (39) by means of laboratory measurements. Numerous wide-slit observations on the relevant far infrared bands are now available. These are made with variable optical path lengths, u, and with variable air pressures. By fixing on a given interval of the spectrum, one can then empirically obtain the function (39) and can check how far the pressure reduction (38) represents the actual data. By doing the same thing for a number of spectral intervals, one can furthermore see how much the different τ's for various intervals differ from each other. It is then possible to justify the use of a single τ for the spectrum of one substance, as it appears that the different τ's for different intervals are rather close to each other. Once this τ is adopted, one can determine the variation of L with frequency over the band. This is simply done by sub-dividing the band into a number of intervals (much smaller than the total band width but still wide enough so that the individual lines are completely smoothed out). One then determines L for each interval so that the resulting functions (39) fall upon each other as closely as possible; one next draws a smooth curve through these L-values as function of ν. This is the desired curve of the generalized absorption coefficient.

By means of the laboratory observations, one can check directly the accuracy of this procedure. Details for particular gases will be given in section IV. We should note here already that the appropriate scale is logarithmic throughout. Thus, we shall give (39) the form

$$\tau = \tau (\log u^* + \log L), \tag{40}$$

and we shall use decadic logarithms in all cases. The absorption is found to be widely distributed over several cycles of the logarithmic scale, and it would be impossible to do justice to the observations with a linear scale. As a result of this, no great accuracy is required in the determination of the optical length, u. This is advantageous in applications to the actual atmosphere, since it means that no great accuracy is required in determining the distribution of the optically active gases as function of height.

6. Stratified medium

So far we have assumed straight beams of radiation passing through an absorbing medium. This corresponds to laboratory experiments with absorption tubes but does not of course represent the geometry of the atmosphere. We assume the atmosphere to be horizontally stratified and of infinite extent in the horizontal direction. Let the axis of the polar coordinates ϑ, φ be in the vertical. It is convenient to integrate the radiative currents (beams) over a hemisphere. This leaves us with two integrated currents, one whose vertical component is downward and one whose vertical component is upward. These currents integrated over the hemisphere will be designated as *fluxes*; thus, there are an upward flux and a downward flux, both obtained by integrating straight-line beams.

Given a level in the atmosphere, it will be crossed by a family of beams with upward components of intensity $I(\vartheta)$, assuming independence of φ. Simple geometry then shows that the net upward flux is

$$f = 2\pi \int_0^{\pi/2} I(\vartheta) \cos \vartheta \sin \vartheta d\vartheta, \tag{41}$$

and similarly for the downward flux. For black-body radiation, I is independent of ϑ, and we find

$$f_b \equiv B_\nu = \pi I_b, \tag{42}$$

which is identical with (3).

Next consider a layer of optical thickness u upon which isotropic flux I_0, $(\partial I_0/\partial \vartheta = 0)$, is incident on one side. If there was only a vertical beam, the intensity emerging on the other side would be $I = I_0 \tau(u)$.

By integrating now over the hemisphere, we see with the help of fig. 5 that

$$f = 2\pi I_0 \int_0^{\pi/2} \tau(u \sec \vartheta) \cos \vartheta \sin \vartheta d\vartheta.$$

We write this, by using (42), as

$$f = f_0 \tau_F(u), \tag{43}$$

where τ_F will be designated as the *flux transmissivity* and is defined by

$$\tau_F(u) = 2 \int_0^{\pi/2} \tau(u \sec \vartheta) \cos \vartheta \sin \vartheta d\vartheta. \tag{44}$$

We can rewrite this as

$$\tau_F(u) = 2u^2 \int_u^\infty \tau(x) dx/x^3, \tag{45}$$

which lends itself rather readily to numerical computations. Since the transfer equations used here are linear, the integration over the angles may be carried out at any stage of the integration, and hence flux transmission in the atmosphere can be taken into account by a simple formal device—namely, by treating the atmosphere as if there were only two beams of radiation, one going vertically upwards, the other vertically downwards. It suffices to replace in the beam formalism I by f and, at the same time, τ by τ_F. With these substitutions, the transfer formulas for the two vertical beams carry over unchanged into those for the two vertical fluxes, as may readily be proved explicitly.

The shape of τ_F is in all practical cases extremely similar to that of the beam transmissivity, τ, except that there is a slight shift on the log u scale. For most practical purposes, it suffices to set

$$\tau_F(u) = \tau(1.60u)$$

or, equivalently,

$$\tau_F(\log u) = \tau(\log u + 0.20). \tag{46}$$

In the work described below, we have usually carried out the integration (45) for the empirically obtained beam transmissivities of the atmospheric gases, but the advantage gained thereby over (46) is small.

7. Uniform isothermal layer

The following results are due to Pederson (1942) and, independently, to Strong and Plass (1950). Although they are not used in the present work, we quote them here for the sake of completeness. They refer to the case where the integration over the height in the atmosphere can be carried out analytically. This can be done in a model, representing the stratosphere,

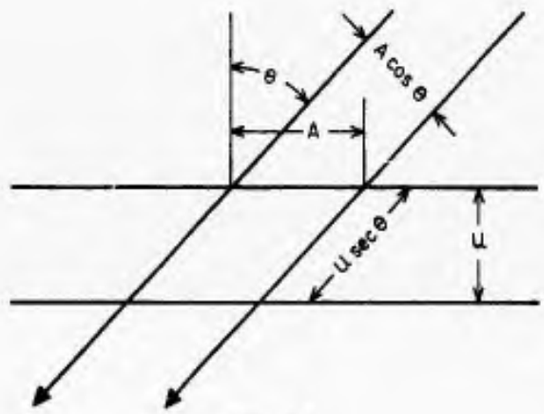

FIGURE 5.

where an isothermal layer of uniform chemical composition extends from a lower boundary (indicated by the subscript 0) upward to infinity. For an isothermal layer, (37) reduces to

$$\alpha = \alpha_0 p/p_0. \tag{47}$$

Within the layer, the density decreases upward according to the barometric law. Since there is uniform mixing, we have, for the optical thickness in the vertical, u,

$$du = c\rho dz$$

where c is the mixing ratio of the optically active gas and ρ the density of the air. Hence, by the barometric law,

$$gdu = cdp = cp_0 d\alpha/\alpha_0, \tag{48}$$

where g is the acceleration of gravity. We compute the absorptivity of a single line, by using (14). We slightly generalize by admitting oblique beams making an angle ϑ with the vertical. The absorptivity of the layer is found after some calculations to be

$$A(\alpha_0, \alpha) = \frac{2\alpha}{\Delta\nu} \int_0^\infty \left\{ 1 - \left[\frac{x^2 + (\alpha_0/\alpha)^2}{x^2 + 1} \right]^\gamma \right\} dx \tag{49}$$

where

$$\gamma = Scp_0 \sec\vartheta / 2\pi g \alpha_0. \tag{50}$$

If the term (α_0/α) in the numerator is neglected (corresponding to wing absorption), the integral can be simply evaluated by means of gamma functions. Plass and Fivel (1955) have, moreover, shown that (49) can be expressed in terms of Legendre functions—namely,

$$A(\alpha_0, \alpha) = \frac{2\pi\gamma\alpha_0^\gamma}{\Delta\nu \cdot \alpha^{\gamma-1}} \times \left[P_\gamma \left(\cosh \ln \frac{\alpha}{\alpha_0} \right) - \frac{\alpha_0}{\alpha} P_{\gamma-1} \left(\cosh \ln \frac{\alpha}{\alpha_0} \right) \right].$$

As Goody (1954) has pointed out, such expressions

are of limited applicability because they do not take into account overlapping; and, indeed, A goes to infinity for infinite γ. The same authors have, however, introduced the periodic Elsasser band into this model of the stratosphere and succeeded in analytically evaluating the resulting integrals.

III. PHYSICS OF THE ATMOSPHERIC BANDS

1. Spectroscopic characteristics

This section is intended to justify in more detail the techniques and approximations used from the viewpoint of molecular physics. These arguments mainly corroborate the validity of the formalism already presented, and most of it may therefore be passed over rapidly by those interested only in the meteorological aspects of the problem. However, section III.4 deals with the modification of the band-absorption contour by the temperature which will be used extensively later on.

The optically active gases of the atmosphere, CO_2, H_2O, and O_3 are all triatomic molecules. The band-spectroscopic properties of such molecules are described in the well-known work by Herzberg (1945) to which we may refer the reader for all particulars. We shall here give just such details as are desirable for the consistency of our own account.

Carbon dioxide. Spectroscopic evidence indicates unambiguously that the three atoms of CO_2 form a symmetrical straight-line array, the carbon atom in the middle being flanked by oxygen atoms on either side. Such a configuration cannot have a static electric dipole moment. An electric dipole moment will, however, be induced by vibrational motion of an asymmetrical type. Fig. 6 shows the three normal modes of vibration of such a configuration. From what has been said, it follows that the symmetrical motion ν_1 should not give rise to an electric dipole moment and should not, therefore, be optically active. It has been identified in the Raman spectrum near 7.5 μ. In the vibration ν_2, the electric moment is perpendicular to the axis of the molecule. The 15-μ band represents this particular vibration, the band being a "fundamental," that is a transition from the ground state to the first excited vibrational state. Another fundamental corresponds to the transition of the first vibrational state, ν_3. This is the 4.3-μ band which appears at the short-wave edge of the black-body curve for atmospheric temperatures.

A vibrational level diagram of the CO_2 molecule may be found in Herzberg's book. The only transitions of interest to us here besides the one already mentioned are some rather faint bands which appear near 10 μ and which, in spite of their weakness, might have a not entirely negligible effect upon heat transfer in the atmosphere. Band-spectroscopically, they are vibrational harmonics. We shall revert to the details in section IV.

Owing to its straight-line arrangement, the CO_2 molecule has spectroscopics closely akin to those of a diatomic molecule. The 15-μ band in particular has all three branches of a typical band of such a molecule, the P, Q, and R branch, corresponding to a jump of the rotational quantum number by $+1$, 0, and -1. In a very crude approximation, the lines of the P and R branches are equidistant; thus, if it was not for the superposition of these two branches, the periodic Elsasser model would be an excellent approximation to the actual transmissivity. As it is, the observed transmissivities are somewhat changed toward the random Goody model. The Q branch is quite closely clustered near the center of the 15-μ band and for that reason does not contribute importantly to radiative transfer. It will not be taken into account separately in the semi-empirical developments of section IV.

Water vapor. The water molecule forms an isosceles triangle which is obtuse and has an apical angle of 104.5 deg. Fig. 7 shows the three normal modes of vibration for such a structure. The 6.3 band has been identified as the fundamental ν_2 of fig. 7. The two fundamentals, ν_1, and ν_3, are found close together, in a band near 2.7 μ, well on the short-wave side of the

FIG. 6. Normal modes of a linear molecule.

FIG. 7. Normal modes of molecule forming an isosceles triangle.

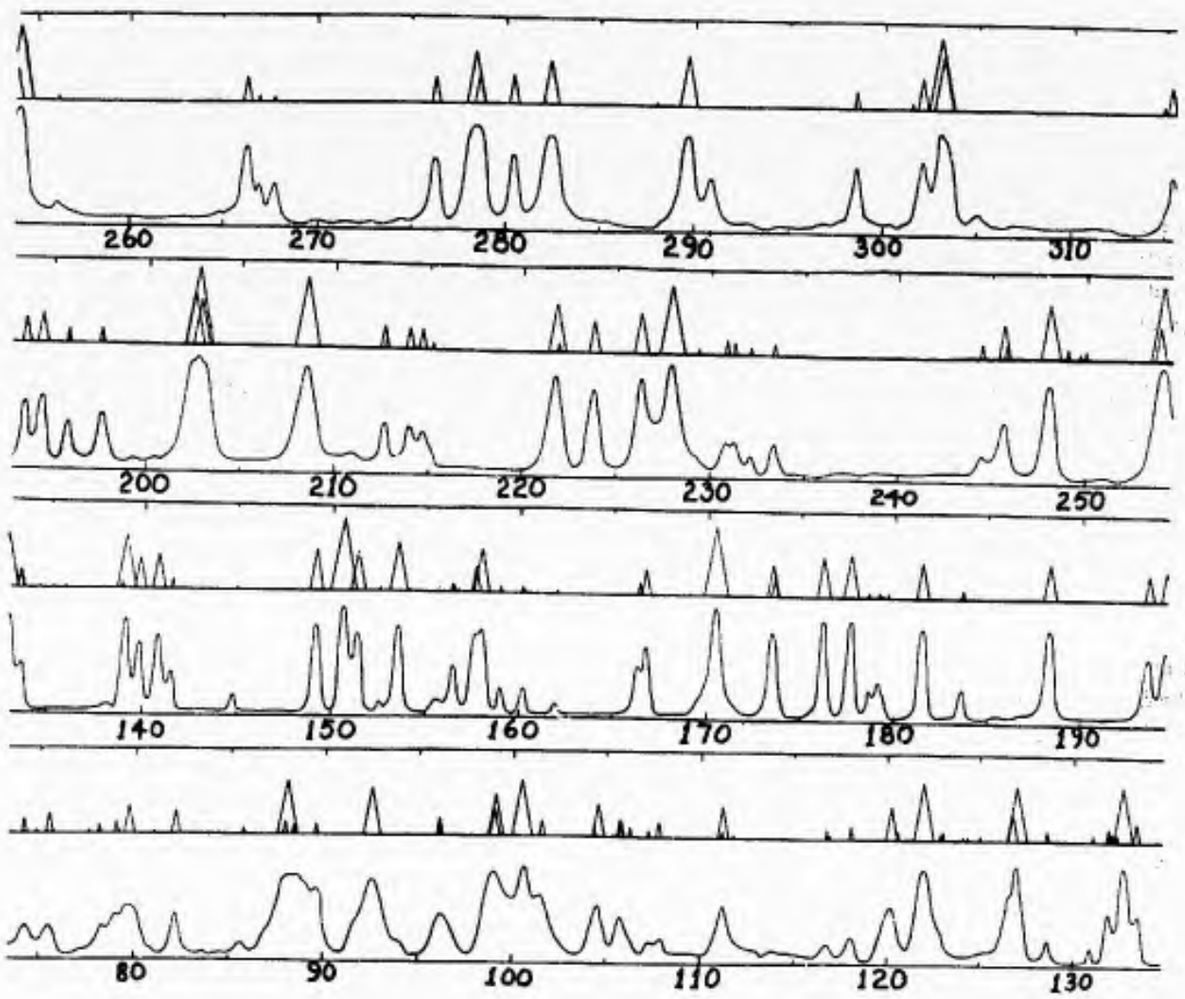

FIG. 8. A section of the rotational water-vapor band after Randall, Dennison, Ginzburg, and Weber (1937) taken with large spectral resolution. Numbers are cm^{-1}; triangles above spectrum give lines computed from quantum mechanics by position and intensity (= area of triangle).

region which interests us here. This band and the bands representing higher harmonics are of meteorological interest in that they give rise to absorption of sunlight by the atmosphere.

The band on the long-wave side of 20 μ represents the purely rotational spectrum of water vapor. The water molecule forms, with respect to rotation, an asymmetrical top, and the line structure of the spectrum does not have the simplicity of a symmetrical rotator which we found in the CO_2 molecule. There is no clearcut regularity at first sight; a typical stretch of the rotational band as it appears with very high spectroscopic resolution is shown in fig. 8 (Randall *et al.*, 1937). Above each section of the spectrum, there is a line studded with triangles which represent positions and intensities (= areas of triangles) calculated from quantum mechanics. Such a spectrum may be approximated by the Goody transmission formula, and the laboratory observations indicate that, with suitably chosen parameters, formula (35) can be made to give an excellent fit to observed transmissivities taken with a sufficiently wide slit. The fine structure of the 6.3-μ band is essentially similar to that of the pure rotational band.

There is no clear evidence that water vapor has absorption bands in the region between the two bands mentioned—that is, between about 8 μ and 13 μ. We shall return to this point in section IV.

Ozone. The analysis of the far infrared spectrum of ozone remained unsatisfactory for many years, except that it seemed certain that the molecule forms an isosceles triangle. In 1948, Wilson and Badger reinvestigated the spectrum and discovered a faint band centered at 9.0 μ, hitherto overlooked. If this is interpreted as the fundamental ν_1 of fig. 7, then the well-known absorption peak at 9.6 μ can without difficulty be interpreted as ν_3, and the 14-μ band, which is somewhat weaker than the latter, can be interpreted as ν_2. These assignments are corroborated by the more recent investigations of Hughes (1952–53) who finds an apical angle of 117 deg and by the analysis of Kaplan, Migeotte, and Neven (1956). The infrared bands of

ozone are of interest for the radiative cooling of the stratosphere where their thermal effects may be quite important. In our semi-empirical approach of the next section, we shall deal in detail with absorption in the 9- to 11-μ region. We shall merely give absorption data for the 14-μ band without entering into the problem of overlapping with the CO_2 band at the same location. Likely, no appreciable error is committed in most cases if the 14-μ band of ozone is omitted altogether in radiative-transfer calculations.

2. The shape of spectral lines

The Lorentz shape (14) of the far infrared lines is fundamental for the whole theory of atmospheric transmission. We shall therefore give an approximate treatment, showing how this distribution of intensity in a spectral line arises (see, also, Born, 1933, p. 435). An isolated molecule would emit an almost purely harmonic wave, say $Ae^{2\pi i\nu t}$, and the only deviation from purely harmonic behavior would be produced by the damping that results from the emitted wave itself; in the far infrared, the spectroscopic effect of this damping is exceedingly small. During the time a radiating molecule is in collision with another molecule, the radiating wave train is altered; owing to the intermolecular forces, the frequency of the emitting molecule is temporarily shifted by an appreciable amount. Now the fraction of time a molecule spends in collision with other molecules is very small (about 10^{-3} at STP). Lorentz therefore assumes that the principal effect of the collision is to destroy the phase coherence of the emitted wave train; one may assume the collision to be instantaneous, but such that after the collision the molecule starts emitting with another phase, the new phases being randomly distributed. This is equivalent to saying that the spectrum of an assembly of molecules consists of a set of wave trains of variable lengths with arbitrary initial phases. From general statistical principles, the time between collisions is distributed according to an exponential (Poisson) law, the probability that a collision occurs between t and $t+dt$ being e^{-t/t_0} where t_0 is the mean time between collisions. We must also average over all the initial phases of the wave trains, and we can express this by using not the spectrum itself but the power spectrum (the absolute value squared of the Fourier transform). Hence, the desired spectrum is

$$\int_0^\infty \frac{dt}{t_0} e^{-t/t_0} \left| A \int_0^t e^{2\pi i\nu t} dt \right|^2 = \frac{|A|^2}{2\pi\nu t_0} \int_0^\infty e^{-t/t_0} \cos(2\pi\nu t) dt = \frac{|A|^2}{2\pi\nu t_0} \cdot \frac{1}{(2\pi\nu)^2 + (1/t_0)^2}. \quad (51)$$

If we set $1/t_0 = 2\pi\alpha$, this becomes equivalent to (14) apart from constant factors and apart from the dependence on $1/\nu$ in front of the right-hand side of (51). However, since ν varies but very little over the line width, this factor may be set equal to a constant in an excellent approximation. Now, since $2\pi\alpha$ is the number of collisions per molecule per unit time, the dependence of α on pressure and temperature is, from the kinetic theory of gases, just given by (37).

An elaborate quantum-mechanical theory of Lorentz line broadening has been given by Van Vleck and Weisskopf (1945). Their calculations apply more closely to lines in the visible, rather than in the far, infrared. An extension of the theory to the latter region was given by Anderson (1949) who showed that, in addition to broadening of the line, pressure produces a slight shift of the line center. Plass and Warner (1952) have investigated the effect which this has on atmospheric transfer and find it as a rule negligible. If the time which the radiating molecule spends in collision is not completely negligible, there appear deviations from the Lorentz shape at large distances from the line center. References may be found in the paper by Plass and Warner where it is also shown that these latter effects may be neglected in atmospheric transfer. Anderson found that the line width varies to some extent as a function of the rotational quantum number in each sub-band and also from sub-band to sub-band. In our preceding theoretical developments, it has been assumed that all lines have the same width. It seems safe to say that such added analytical complexity as would be introduced by accounting for a width varying from line to line would not be repaid by significantly novel physical results. We confine ourselves to interpreting the formal line width, α, of our transmission theory as the average width of the lines.

A second cause of line broadening next to collisions is the Doppler effect owing to the motions of the radiating molecules. Let us assume for the moment a highly rarefied gas where there is no collision broadening. All molecules in a given quantum state radiate at wave number ν_0, but, as the theory of relativity shows, this appears shifted as seen by a stationary observer to the wave number

$$\nu = \nu_0(1 \pm v/c), \quad (52)$$

where v is the velocity of the molecule relative to the observer. Now the fraction of molecules between v and $v + dv$ is, from kinetic theory,

$$n(v)dv = \sqrt{\frac{m}{2kT}} e^{-mv^2/2kT}, \quad (53)$$

where the symbols have their usual meaning. To obtain the Doppler distribution, we merely replace in (53)

the variable v by ν, by using (52); if, moreover, we normalize to an integrated line intensity S, we readily find for the distribution of the absorption coefficient

$$k(\nu) = \frac{S}{\delta\sqrt{\pi}} \exp\left[-\left(\frac{\nu - \nu_0}{\delta}\right)^2\right], \tag{54}$$

where

$$\delta = \frac{\nu_0}{c}\frac{2kT}{m} \tag{55}$$

is a measure of the Doppler width of the line, the half-width at half maximum being $\delta(ln2)^{\frac{1}{2}}$.

In the upper atmosphere, we find a combination of collision broadening and Doppler broadening, whereas, in the lower atmosphere, Doppler broadening is usually much less than collision broadening and may safely be neglected in the computations. When both broadening effects are present simultaneously, the resulting line shape is a combination (mathematically speaking a convolution) of the two (see Mitchell and Zemansky, 1934). Let K be a shape function normalized to unity, so that

$$k_L = SK_L, \quad k_D = SK_D$$

where k_L and k_D are defined by (14) and (54) respectively; then the resulting line shape of a line of total intensity S will be

$$k(\nu - \nu_0) = S\int d\nu' K_L(\nu - \nu')K_D(\nu' - \nu_0).$$

This function has been exhaustively studied by Plass and Fivel (1953). Their findings may be summarized by saying that, on the whole, the effect of Doppler broadening upon a Lorentz-broadened line is small. We may distinguish here between "strong" and "weak" lines. This terminology refers to the Strong-Plass formalism discussed in section II.7 which is more realistic for the atmosphere than a uniform absorbing layer. A line is strong when $\gamma \gg 1$ and weak when $\gamma \ll 1$, where the parameter γ is defined in (50). The intuitive physical meaning is as follows: in the Strong-Plass atmosphere, the line gets narrower as one goes upwards, owing to the decrease in half-width proportional to the decrease in p. This produces an intensification of the absorption in the line center which makes up for the decrease of optical thickness in the upper layers. For a weak line, the absorption remains always in the region of the linear law (20). For a strong line, on the other hand, the center is always completely opaque, and absorption occurs in the wings so that the square-root absorption law (21) holds. For a weak line, it may be shown that the total absorption is independent of the mechanism of broadening, a plausible enough result. In atmospheric transfer, the strong lines (and, in particular, the very strong lines) are much more important. Now, as we go up in the stratosphere, the Lorentz width decreases, whereas the Doppler width, which depends only on $\sqrt{T}$, is fairly constant. For any line, there exists a level at which the Lorentz width and Doppler width become equal. Now, if the line is strong, transfer takes place in its wing, whereas no transfer occurs in its central parts. The intensity of a Lorentz line decreases only slowly, as $(\nu - \nu_0)^{-2}$, with distance from the line center, whereas the Doppler line decreases exponentially. Thus, the effect of Doppler broadening in the wings should be small for strong lines. Since most of the lines contributing appreciably to atmospheric transfer are strong, this means that the approximation in which Doppler broadening is neglected should still be very good, well above the height at which the two widths are equal. This is quantitatively confirmed by the calculations of Plass and Fivel.

So far, we have only dealt with pure theory. The measurement of the detailed intensity distribution of a line in the far infrared is exceedingly difficult, at the limits of the possible, because the only spectral sources available are thermal ones, and their intensity is not far enough above noise to permit unlimited resolution. Numerous experimental investigations of line broadening have been carried out, however, in the visible and in the near infrared, and the Lorentz distribution (14) has been well verified under the physical conditions where it applies. It has also been verified in the microwave region where good resolution is readily available. In the far infrared region, it has been verified so far as feasible; the line width in the far infrared atmospheric bands is of order 0.05 to 0.15 cm^{-1} at $p = 1$ atm. The Doppler width, on the other hand, is much smaller; it is several times 10^{-3} cm^{-1} at atmospheric temperatures. Goody (1954, p. 156) has gathered numerical data on line width (see also Kaplan and Eggers, 1956). Fortunately, the precise values of the width of individual lines are not significant for our semi-empirical approach. The height in the atmosphere up to which Doppler broadening may be neglected as compared to Lorentz broadening is of importance. Goody gives the following heights at which $\alpha = \delta$, the Lorentz width equals the Doppler width, for various atmospheric bands: 23 km for the 6.3-μ water-vapor band, 35 km for the rotational water-vapor band, and 34 km for the CO_2 band at 15 μ. Furthermore, the work of Plass and Fivel (1953) indicates that in the case of the stronger lines the Doppler width may be neglected even somewhat beyond the point where it becomes equal to the Lorentz width. In the case of very strong lines ($\gamma > 100$) which carry an appreciable part of atmospheric transfer, Plass and Fivel calculate that Doppler broadening should be negligible up to a height of 50 km. In view of the above figures, it seems safe to say that taking into account

Lorentz broadening only and ignoring Doppler broadening should yield a reasonable approximation up to heights approaching 40 km. As a matter of fact, the determination of radiative transfer in the upper stratosphere does not depend so much on the spectroscopic complexities just mentioned; the main problem is that the quantities of optically active gas present at these altitudes are so minute that it becomes nearly impossible to reproduce these conditions in the laboratory. In other words, the integrated curves of total band absorption which will be given later are likely to be rather inaccurate at their lower end. This is likely to be a much larger source of error than any other.

3. Local equilibrium and blackness

We shall next discuss the question as to how far Kirchhoff's law (1) is quantitatively valid for far infrared atmospheric radiation. The transfer equations used here are based entirely upon this law. In most radiative-transfer problems involving visible light, as encountered in astrophysics as well as in certain technical applications, there is an appreciable amount of scattering of the radiation. This leads to a transfer formalism much more complicated than the one used here (Chandrasekhar, 1950). In the far infrared, on the other hand, scattering is unimportant except perhaps for solid particles. We shall not enter here into a discussion of the detailed mechanisms of scattering for which quantum mechanical theories are available (Heitler, 1954). The scattering which occurs in the atmosphere cannot be attributed to individual molecules but is due to the statistical density fluctuations of the air molecules (Rayleigh Scattering; see Born's *Optik*, p. 371 ff.). In any event, molecular scattering, whether individual or collective, is inversely proportional to the fourth power of the wavelength. This, as is well known, is the reason that the sky is blue, scattering being important at the short-wave end of the visible spectrum and becoming rather weak at its long-wave end. As we go to the infrared, it becomes still weaker, and, in the far infrared, molecular scattering is totally negligible, as simple calculations by the Rayleigh formula show.

Next in importance to the absence of scattering is the existence of local thermodynamical equilibrium. By this is meant the fact that the thermodynamical state of the atmospheric gas as a whole (air plus optically active substances) may be characterized by a single temperature, T, so that the mean population of any state of energy E is given by the Boltzmann formula, $n(E) = P^{-1}\exp(-E/kT)$, where P is the partition function. In order that this be so, it is necessary that when the population of any particular quantum state or group of quantum states becomes enriched or depleted, this change is rapidly distributed over all the quantum states of the whole gas so that no accumulation in any one state occurs. In the concrete circumstances of infrared radiation transfer, this means that the molecular levels which become excited by the absorption of the infrared flux must redistribute their excitational energy by collisions before they re-radiate it. This means that the relaxation time of rotation-vibrational energy must be short compared to the lifetime of the excited molecular states. A close analysis of the available data shows this to be the case. The quantitative information has been discussed extensively by Goody (1954, p. 146), and we shall therefore not repeat the detailed arguments here. Goody estimates that local thermodynamical equilibrium prevails in the atmosphere up to a level of 50 km. It may therefore safely be assumed that within the range of validity of the present tables any deviations from local thermodynamical equilibrium will be far smaller than many other errors involved.

In dealing with the solution of radiative-transfer problems, one must, as a rule, fulfill boundary conditions. The most important boundary is of course the ground, but the top and bottom of a cloud layer are also significant. Experience shows that in the far infrared the optical properties of most solids or liquids become extremely simple; most solids are essentially black, excepting only the metals and certain crystals. By a black body, we mean again one which absorbs completely all radiation falling upon it, independent of frequency. Conventional ground is black to within the limits of error of most measurements. Dorsey (1940) gives values of reflectivity of liquid water as function of wave length at normal incidence: approximately 2 per cent at 5 μ, 1 per cent at 10 μ, 5 per cent at 15 μ, and 10 per cent at 60 μ. So far, the calculations of atmospheric transfer have always assumed that the lower boundary of the atmosphere is black. Also, the errors committed in assuming the same for the sea surface appear small enough so that considering the sea as a black body is usually a good approximation. To justify this further, note that opaque regions of the atmosphere are those for which the free path of radiation between emission and absorption is small. Radiative transfer is then also small, and some reflectivity of the water surface is unimportant. On the other hand, in the regions of the spectrum where the moist atmosphere is relatively transparent, the radiation travels a long way, and radiative cooling becomes important. The measurements quoted by Dorsey show that the reflectivity of liquid water is large in the regions where the water-vapor phase has absorption bands but small in the region centered about 10 μ where vapor is transparent. This argument would seem to indicate that the effective reflectivity of the sea surface in radiative-transfer problems is much

smaller than would be indicated by a mere arithmetical average of the above figures for reflectivity.

Observation shows that a cloud layer (other than cirrus) which is more than a few meters thick is completely black in the far infrared. Clouds, therefore, are considered in the computations as black boundaries of the radiative fluxes. Since the top of a cloud as a rule cools rapidly by radiation into space, the lapse rate in a cloud is usually adiabatic, and heat transport takes place by convection.

4. Temperature dependence of band contour

In section II.5, we introduced the generalized absorption coefficient $L(\nu)$ such that the transmissivity as function of wave length and optical path is given by $t(u^*L)$ where u^* is the pressure-reduced optical path. If it be assumed that L is independent of temperature, then the temperature appears in the transfer equations only *via* the black-body flux B, which of course is strongly temperature dependent. There is, however, a secondary dependence on temperature, through $L(\nu)$ itself. We shall explain how this temperature effect arises and how it is taken into account in our computations.

The change of absorption with temperature is due to the change of the population of the energy levels of the molecules with temperature. The population of the ith level, of energy E_i, is given by the Boltzmann formula.

$$n(E_i) = P^{-1}e^{-E_i/kT} \tag{56}$$

where P is the partition function, the sum of the Boltzmann factors of all states. Now the excited rotational states of a molecule at atmospheric temperatures are very numerous, as evident from the large number of lines in a band. Short of carrying out extremely elaborate quantum mechanical calculations which would take into account all these levels, only a rather schematical model of molecular behavior can provide us with the necessary correction terms in a simple enough form.

The model adopted here is as follows. Assume for a moment that we replace the band spectrum by the Fourier spectrum of a symmetrical rotator in *classical* physics. This latter spectrum is obtained by distributing an ensemble of classical symmetrical rotators over the frequency range involved according to a Boltzmann formula. The kinetic energy of such a rotator is

$$E = (2\pi\nu)^2 I/2,$$

where I is the amount on inertia. Thus, the Boltzmann distribution of such an ensemble is given by

$$n(E) = P^{-1}\exp(-c\nu^2/T) \tag{57}$$

where c is some constant. This shows that if we plot $\log n$ against ν we get an inverted parabola. In this simple model, the generalized absorption coefficient would be

$$L(\nu) = \text{const. } \nu^3 n(\nu). \tag{58}$$

The variation with ν^3 arises from radiation theory for fixed n; it is, however, much less rapid than the exponential variation of $n(\nu)$; hence, in the model $\log L(\nu)$ appears in a first approximation simply as an inverted parabola. Now the two sides of a rotation-vibration band are generated by adding and subtracting, respectively, the frequency of rotation to the frequency ν_0 of the vibrational jump. Hence, we might ask ourselves whether $\log L(\nu)$ of a molecular band may be schematized by means of a full inverted parabola. It turns out that this is somewhat too crude an approximation, mostly owing to the asymmetry of real bands (produced by centrifugal stretching of the molecule). We have therefore adopted a scheme in which the two sides of a band are approximated by different parabolas (there is of course only one "side" to the rotational band of H_2O). We thus let

$$\log L = -a(\nu - \nu_0)^2 + b \tag{59}$$

where we have neglected the dependence of L on ν^3 expressed in (58) as compared to the exponential dependence of $n(\nu)$ on ν. Here, ν_0 is the band center. The parameters a and b were obtained for each side of a band from the measured data (section IV) by a graphical trial-and-error method. This sufficed since the fit of the parabolas to the actual contour of $\log L$ in any event is only moderately good. On the other hand, it should be remembered that the parabolas themselves are not used but only certain differences derived from them: the band contours observed at room temperature are corrected by means of the temperature dependence of these substitute parabolas.

To find the temperature dependence, we notice first that by the definition of P we have from (56) for a simple rotator

$$P = \int_0^\infty \exp(-E/kT)dE = kT.$$

In view of this, we use (57) and (58) to define the variation of the generalized absorption coefficient on each side of a band, neglecting again the dependence on ν^3 in (58). Thus,

$$L(\nu - \nu_0) = \frac{\text{const.}}{T}\exp\left[-\frac{c}{T}(\nu - \nu_0)^2\right] \tag{60}$$

where c is a constant. Now let L_0 refer to laboratory temperature T_0(293K, say). Then (60) readily gives

the desired temperature-correction formula—namely,

$$\log L = \log L_0 - a\frac{T_0 - T}{T}(\nu - \nu_0)^2 + \log\frac{T_0}{T}, \quad (61)$$

where $a = c/T_0$. Moreover, if in (59) we let $L = L_0$, the present a becomes identical with that of (59). Thus, on obtaining a and b as used in (59) by a trial-and-error process, the correction (61) is fully determined. The method outlined was applied numerically to all the bands for which computations were made.

IV. LABORATORY TRANSMISSIVITIES

1. Formulary

The quantities to be determined from laboratory measurements are the transmissivity, τ, and the generalized absorption coefficient, L. By (39) τ is a function of the product, u^*L, where u^* is the reduced optical path given by (38). In the laboratory, the temperature is effectively constant because it is not feasible to lower the temperature in the rather bulky absorption apparatus. Hence, it suffices to write

$$u^* = up/p_0, \quad (62)$$

where p is the total pressure (almost entirely air pressure as a rule) and p_0 is the standard pressure of 76 cm Hg. *In the remainder of this monograph, we shall for simplicity omit the asterisk and write u for the reduced path throughout.*

We shall consistently use a logarithmic scale for u as well as for L and therefore write

$$\tau = \tau(\log u + \log L). \quad (63)$$

All logarithms in this work are to base 10. In the graphs of this section, where τ is plotted as a function of its logarithmic argument, we simply use $\log u$ as the abscissa, it being understood of course that this designates $\log u + \log L$.

The unit of u has been chosen differently for CO_2 and O_3 on the one hand and for water vapor on the other. For carbon dioxide and ozone, u is measured by the length in cm of a column of the pure gas at standard temperature and pressure. For water vapor, u is measured in cm of precipitable water—that is, grams per sq cm of the column. The latter unit is of course chosen so as to conform with common meteorological practice.

To determine τ for any given region in the spectrum, one chooses an interval wide enough to comprise a large number of individual spectral lines (*e.g.*, by taking the slit of the spectrograph wide enough) and plots the observed mean transmission of the interval against $\log u$ for a variety of values of u, where u now is the path length reduced for pressure according to (62). If this is done for a number of intervals in the spectrum, it is found for the gases considered here that the curve has closely similar shapes for different intervals of one and the same gas. One then adopts a standard transmissivity curve for any one gas. This curve undergoes a shift along the $\log u$ scale when one passes from one interval in the spectrum to an adjacent interval. If this shift is plotted as a function of ν, one obtains a series of points which thereafter are replaced by a smooth curve approximating them. This is the curve of $\log L$ where L is the *generalized absorption coefficient.*

The functions $\tau(u)$ and $\log L(\nu)$ provide the material wherewith to construct a radiation chart as described in the next section. Different substances have different transmissivity curves; most empirical transmissivities can be fitted by a Goody curve of type (35) on suitable choice of the two available parameters; this is particularly true of H_2O and O_3. Again, CO_2 has a somewhat simpler band structure, and its transmissivity curve does not differ too widely from the simple error integral (27). In the case of water vapor, we have used the same transmissivity curve for both bands, the 6.3-μ band as well as the rotational band, but the region between the two bands, the "window," requires a more involved treatment.

With the exception of the values for the water-vapor window which are in part the result of computations, all our curves are based on laboratory measurements only, as made with equipment allowing long optical paths and the addition of air to study pressure effects. For carbon dioxide and water vapor, the measurements have been made at two laboratories, and, in fact, independent sets of data are available in the case of each band so as to provide a mutual check. These are the Laboratory of Astrophysics and Physical Meteorology at Johns Hopkins University under the direction of Professor John Strong and the Physics Department of Ohio State University with its old tradition of infrared spectroscopy. The measurements for ozone come from different laboratories; there are also two independent sets.

2. Carbon dioxide

The experimental work on the 15-μ carbon-dioxide band used here has been available only in the form of technical reports. A report by Cloud (1952) was used

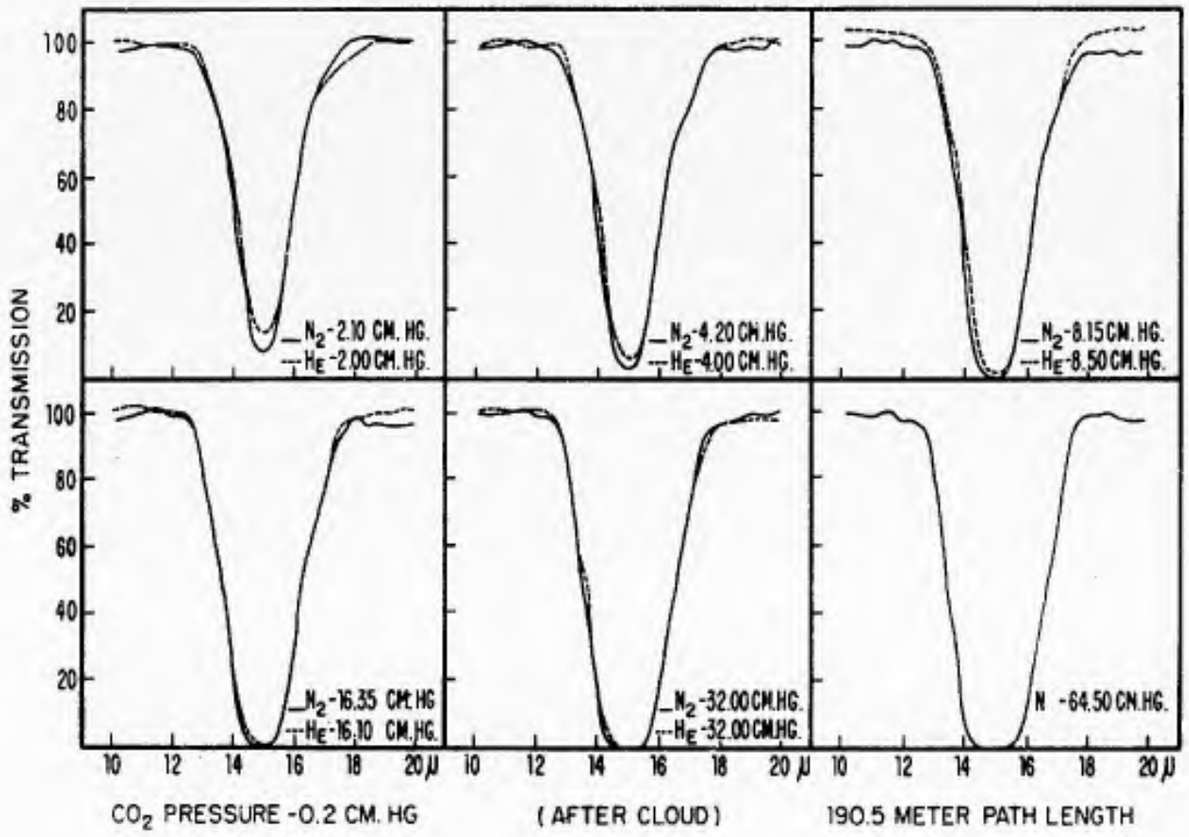

FIG. 9. The 15-μ carbon-dioxide band taken with a wide slit. Type of data used for our computations.

by Elsasser and King (1953) to derive a transmissivity curve and a curve of the generalized absorption coefficient which are presented below. The first computation of the CO_2 radiation chart was based on these values. It was ultimately modified by using further, independent, experimental data contained in a report by Howard, Burch, and Williams (1955) and by Yamamoto and Sasamori (1958).

The work of Cloud was done with the 100-ft transmission tube at Johns Hopkins University. Mirrors at the ends of the tube provide a six-fold traversal, the total path length being 190.5 m. Nitrogen was admitted as a line-broadening agent, which may be shown to have for all practical purposes the same broadening effect as atmospheric air. In some cases, helium was used instead; it gives very nearly the same effect as nitrogen. Both the partial pressure of CO_2 and that of N_2 were varied between extremely wide limits, covering almost all the conditions to be met with in the atmosphere. The 15-μ band was scanned with a very wide slit which obliterated all finer detail of the spectroscopic structure. A series of traces obtained by Cloud is shown in fig. 9. The CO_2 pressure in this particular series was 0.2 cm of Hg. The partial pressures of nitrogen and helium were as indicated for each diagram.

The evaluation was carried out by using a table given by Cloud in which he indicates the mean transmission under various conditions for spectral intervals 1-micron wide. Series of values were grouped together that have, for a given spectral interval, various amounts of CO_2 in the path and also various amounts of nitrogen, and the reduced paths were determined from (62). This quantity, here briefly called u as explained above, was plotted as abscissa—or, rather, log u was so plotted. The points then define a transmissivity curve, $\tau(u)$. If this is done for several intervals, a number of such curves which run parallel to each other is obtained. If the transmissivity curve is indeed the same for different intervals, one can bring all these curves to coincidence by a shift along the log u scale, each shift defining a mean generalized absorption coefficient for the interval considered relative to some reference interval. The final result, representing a standard transmissivity curve for carbon dioxide is shown in fig. 10. The measured points fall so nearly upon the adopted curve, within the inevitable errors of observation and processing, that the points shown were not distinguished according to interval, CO_2 path, and N_2 pressure. The process also furnishes a curve of the generalized absorption coefficient to which we shall return.

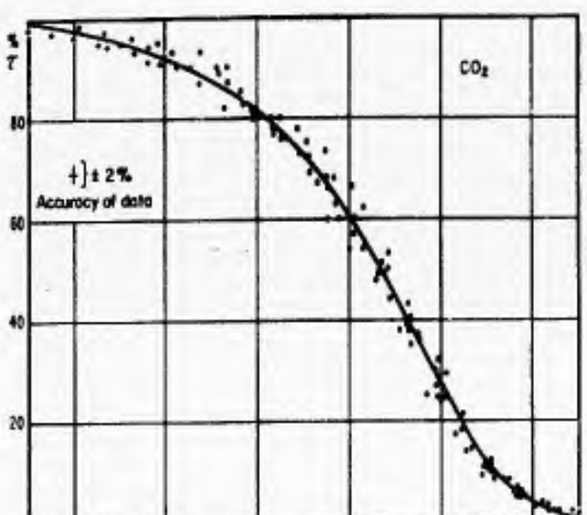

FIG. 10. Transmissivity curve for carbon dioxide.

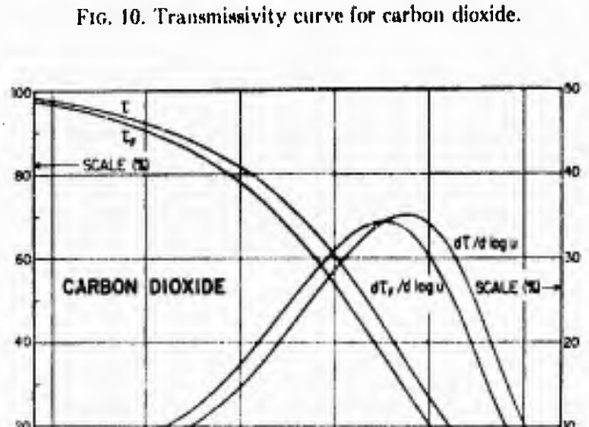

FIG. 11. Beam and slab transmissivities and their derivatives for carbon dioxide.

Some further smoothing of the transmissivity curve was done numerically when the carbon dioxide radiation chart was constructed. This served to regularize first and second differences. It is important to do this smoothing, since later on flux-divergence charts are to be obtained by numerical differentiation with respect to u; these become unnecessarily irregular unless the curves to be differentiated are smooth to begin with. Obviously, the increase in accuracy is purely formal and not physical. The flux transmissivity τ_F was computed numerically by using (45). For use in a flux-divergence chart, the logarithmic derivative, $d\tau/d \log u$, was computed numerically, and the same was done for the flux transmissivity, τ_F. The two transmissivity curves and their logarithmic derivatives are shown in fig. 11. It will be seen that τ and τ_F run very closely parallel, as implied by the approximation (46), and the same is true for the corresponding derivatives.

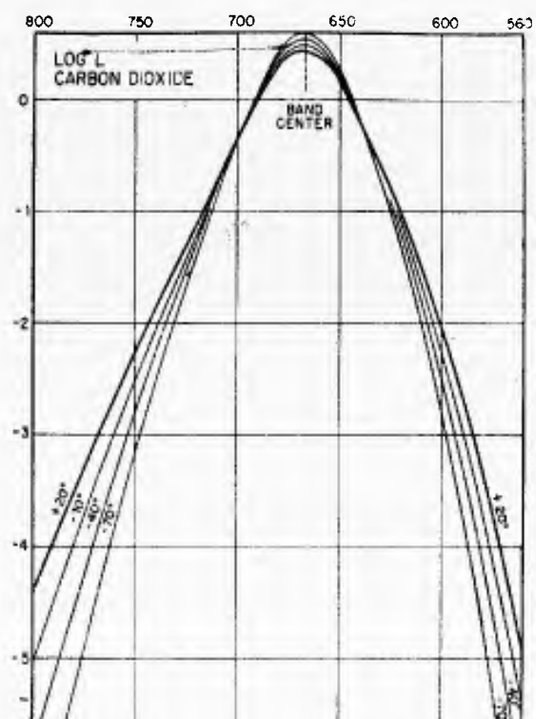

FIG. 12. Generalized absorption coefficient for 15-μ carbon-dioxide band.

We found later that the flux-divergence chart can be constructed more efficiently and reliably by differentiating only the completed radiation chart with respect to u. Hence, the function $d\tau_F/d \log u$ was not actually used later on in the calculations.

The generalized absorption coefficient derived from the shift of the τ-curves for various spectral intervals is shown in fig. 12. The main curve, drawn somewhat heavier, is the one obtained from the laboratory measurements; it is assumed to correspond to a temperature of 20C. The lower part of the curve, however, on both edges of the band, is a rather arbitrary extrapolation. This curve of L was now approximated on each side of the band center (667 cm^{-1}, from spectroscopic data) by a half-parabola, using a trial-and-error procedure. The coefficients of equation (59) are $b = 0.10$; for the short-wave side $a = 3.4 \cdot 10^{-4}$, and for the long-wave side $a = 4.6 \cdot 10^{-4}$. From this, the corresponding band contours for other temperatures were computed by using formula (61). It may be noted that the point $b = 0.10$, representing the apex of the two half-parabolas, is considerably lower than the apex of the actual L-curve for 20 deg which is at 0.44 in fig. 12. This discrepancy is due to the fact that the representative parabolas were chosen so as to match the L-curve over a reasonable fraction of the band contour rather than just at the apex.

Fig. 13 shows the actual absorption, $1 - \tau(uL)$,

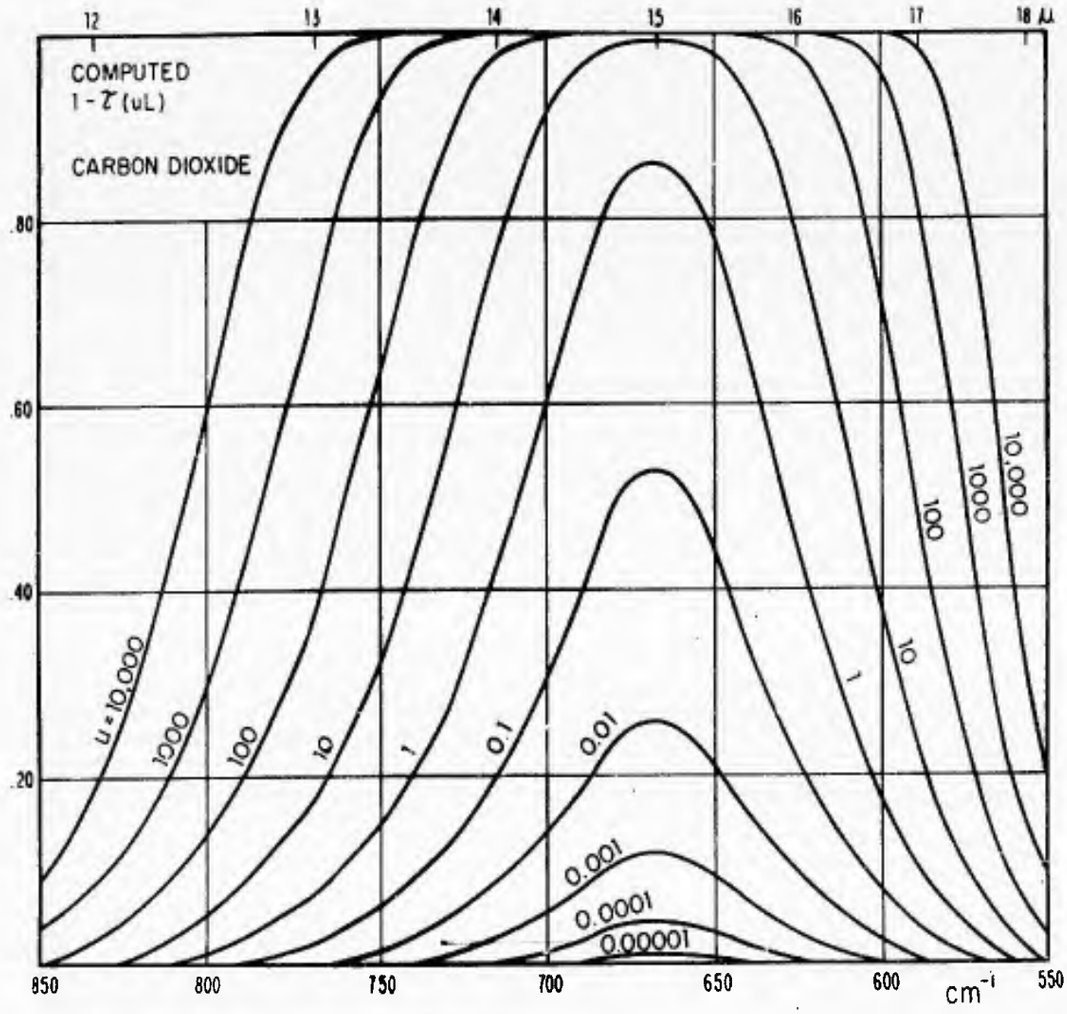

FIG. 13. Actual absorption of 15-μ carbon-dioxide band. Corresponds to curve marked "trial" in fig. 14.

computed from the values of τ given in fig. 10 and those of log L for 20C given in fig. 12. Successive curves differ by a factor of ten in u. To the degree in which our method of approximation is accurate, these curves should duplicate the actual observations of the type shown in fig. 9. We next made a further check of figs. 10 and 12 against the observations, by using the data obtained independently by Howard, Burch, and Williams at Ohio State University (1955). The latter authors used an absorption cell 22 m long in which by means of mirrors multiple traversals could be achieved. For measurements in the 15-μ carbon-dioxide band, 4, 8, and 16 traversals were used. Nitrogen was used as a broadening agent. Howard, Birch, and Williams give their results in the form of band areas. This is the area under a given absorptivity curve (maximum absorptivity = 1) with wave number in cm^{-1} as abscissa. In order to make the measurements of Cloud comparable with these results, we planimetered his curves and converted from the wavelength scale to a wave-number scale. The results of both sets of observations are shown in fig. 14. If now the areas under the curves of fig. 13 are planimetered and the resulting points joined, one obtains the curve marked "trial curve." It is somewhat too high for long paths (right upper corner of fig. 14) but appears too low compared to the Ohio State measurements at short paths. When our work was almost finished, a paper by Yamamoto and Sasamori appeared (1958) in which, for short paths, measurements by Kaplan and Eggers (1956) are also taken into account. The final curve of band areas, then, is likely to lie somewhere near the Ohio State values and near Yamamoto's curve. The curve ultimately adopted, as shown in fig. 14, was deliberately taken somewhat low for the following reason. Short paths correspond usually to data taken high up in the atmosphere; that is, we want to get our maximum accuracy when computing cooling of the stratosphere. Now the experimental data of Howard, Burch, and Williams indicate that the pressure dependence of the absorption is not quite linear in p but somewhat slower, approximately as $p^{0.88}$. Thus, a linear pressure correction as applied in practice tends to underestimate the band area, and we have tried to compensate for

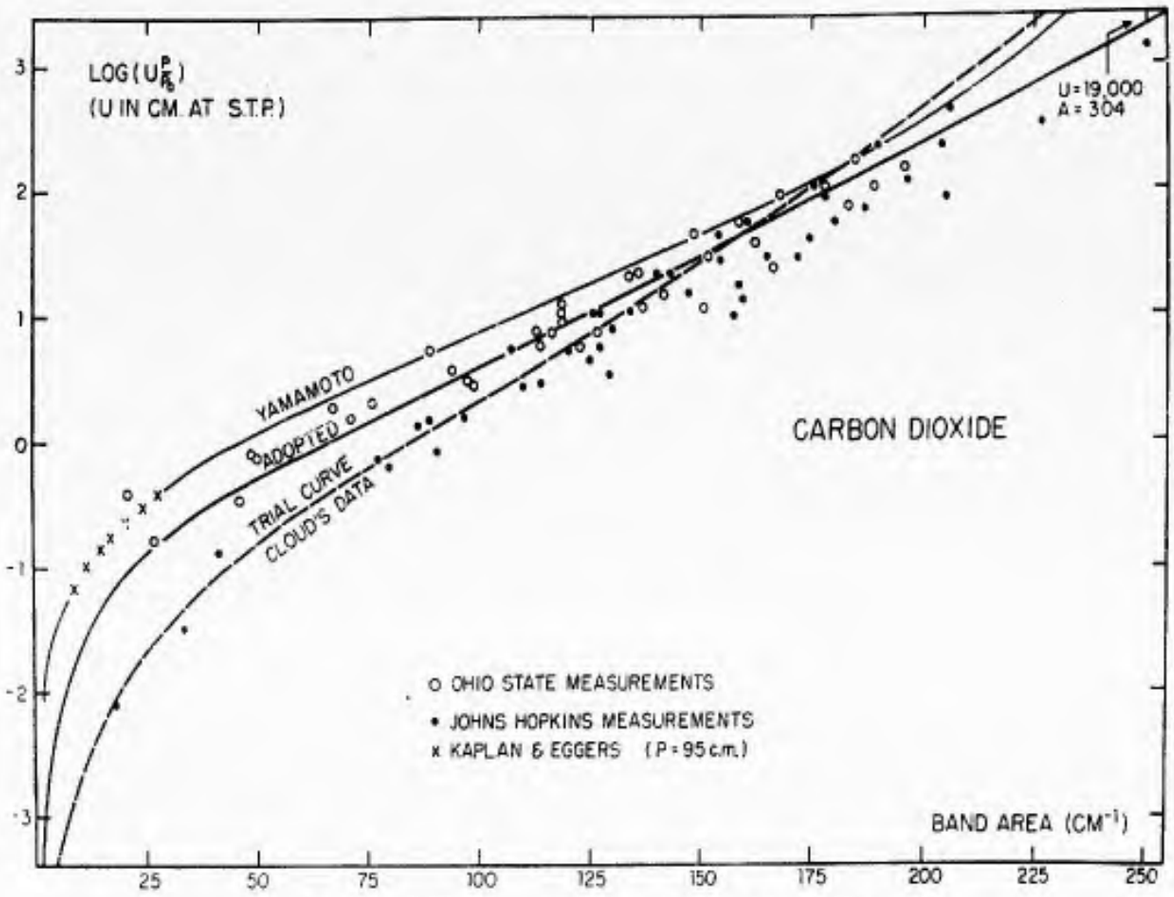

FIG. 14. Computed and measured band areas for carbon dioxide, 15-μ band.

this by shifting the adopted curve to the right in the lower-left corner of fig. 14.

The computation of the CO_2 radiation chart as described in the next section was based on the generalized absorption coefficient of fig. 12 and hence corresponds to the dashed curve of fig. 14. The chart needs now to be corrected so as to correspond to the solid curve. A simple approximation is suggested by the fact that a band covers only a comparatively narrow region of the spectrum; hence, the black-body intensity should not change very appreciably by function of frequency over the band. If the black-body intensity was independent of ν over the band, the ordinates of a radiation chart for given u would be directly proportional to the band area. Hence, we corrected the finished radiation chart in the following way: for any value of u (and all temperatures involved), we multiplied the chart ordinates by A/A_1 where A is the band area (abscissa of fig. 14) corresponding to the adopted solid curve and A_1 is the band area corresponding to the dashed trial curve. Since, however, fig. 14 refers to beam transmission and the chart to slab transmission, the correction for a given $\log u$ in the chart is read off fig. 14 at the argument value $\log u + 0.20$, according to equation (46).

It should be noted in particular that the absorption contours of fig. 13 have not been corrected; they do correspond to the dashed curve of fig. 14. If necessary, they may also be corrected by relabeling the curves of fig. 13 with different values of u. This can readily be done by using again the two curves of fig. 14.

There exist quite a number of other bands of CO_2 in the infrared, but their importance for atmospheric radiation transfer is small if not entirely negligible. A very strong band is centered at 2350 cm^{-1} or a wavelength of 4.26 μ. It represents the fundamental of the normal vibration ν_2 (see section III) whereas the 15-μ band is the fundamental of the normal mode ν_3. This band is situated in a region of the spectrum where for normal atmospheric temperatures the black-body intensity is very small. Only in very hot air such as may be found at mid-day in tropical climates does the black-body curve extend appreciably into the region covered by this band. In such cases, radiative transfer caused by this band may become of some importance. Such conditions are, however, sufficiently rare so that in all probability these effects should be very small in climatological averages. We have therefore omitted a separate treatment of this band.

In addition to the two strong bands representing

fundamentals of the CO_2 molecule, there is a large number of much weaker bands corresponding to higher harmonics of the normal modes. All these may be found tabulated in Herzberg's book. The only ones that should be of importance for atmospheric radiation problems are those that begin (or terminate, as the case may be) in the vibrational ground state (0, 0, 0) of the molecule, since in all bands where the lower vibrational state differs from the ground state there will be no appreciable population of the lower state at temperatures prevailing in the atmosphere. This criterion eliminates all the weak bands on the long-wave side of 4 μ. It appears, therefore, that these minor bands do not play a significant role in the radiative transfer of the atmosphere.

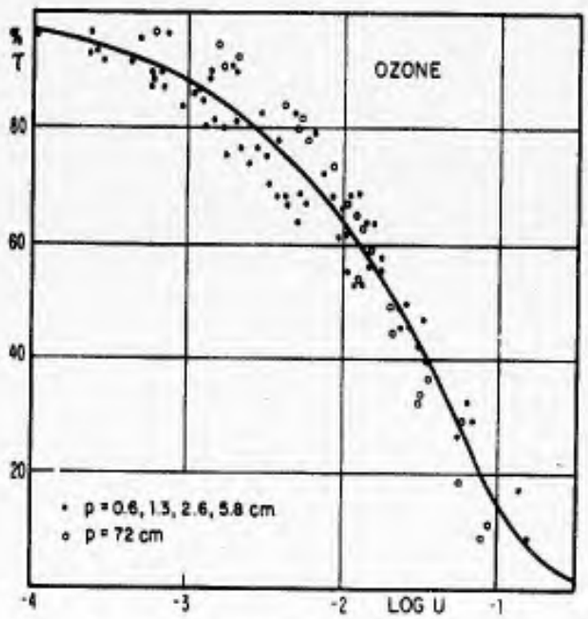

FIG. 15. Transmissivity curve for ozone.

3. Ozone

The procedure followed to construct a radiation chart for ozone is perfectly analogous in all details to the one used for carbon dioxide; hence, we can be short in our description. The laboratory transmissivities used to begin with were those of M. Summerfield (1941). The absorption cell was 90 cm long; the length of the ozone column reduced to STP ranged from 0.2 mm to 5 mm, the latter being considerably in excess of the amount usually found in a vertical path in the atmosphere. Oxygen was used as a broadening agent. The amount of ozone in the path was determined by means of the continuous absorption in the Hartley band in the ultraviolet part of the spectrum which is known to be pressure independent. Summerfield's data were used by Elsasser and King (1953) as in the case of CO_2 to obtain the transmissivity curve for reduced path which is shown in fig. 15. This differs clearly from the corresponding curve for carbon dioxide, fig. 10, not only in shape but also in that there is a much larger scatter of the observed points, indicating that the linear pressure correction, up/p_0, which

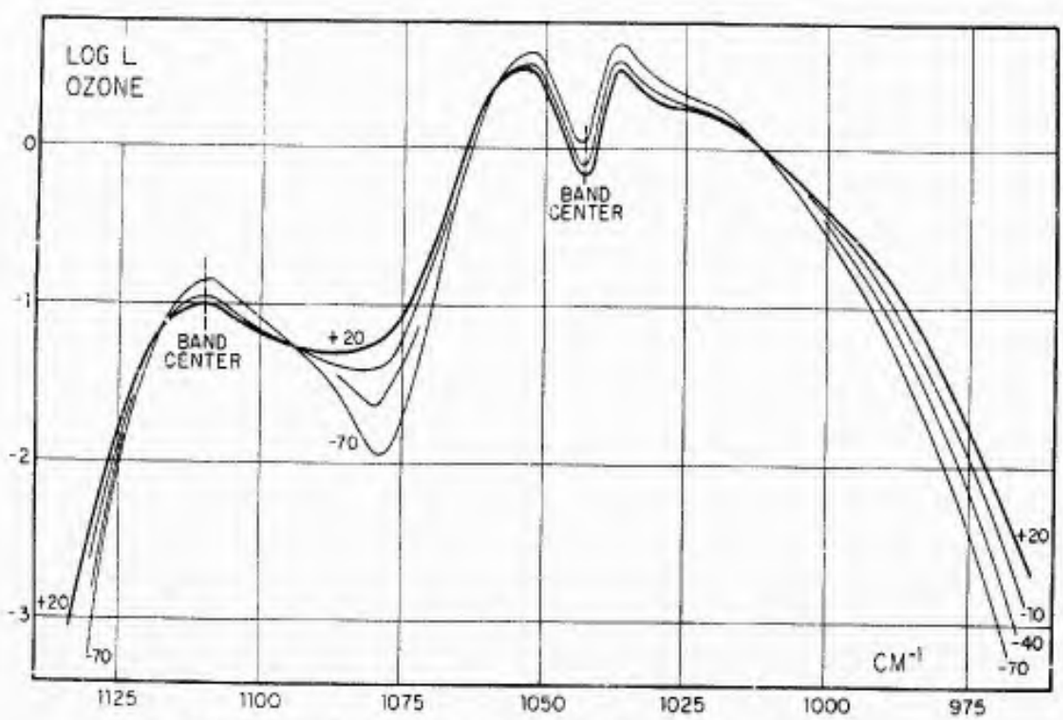

FIG. 16. Generalized absorption coefficient for 9.6-μ and 9-μ bands of ozone.

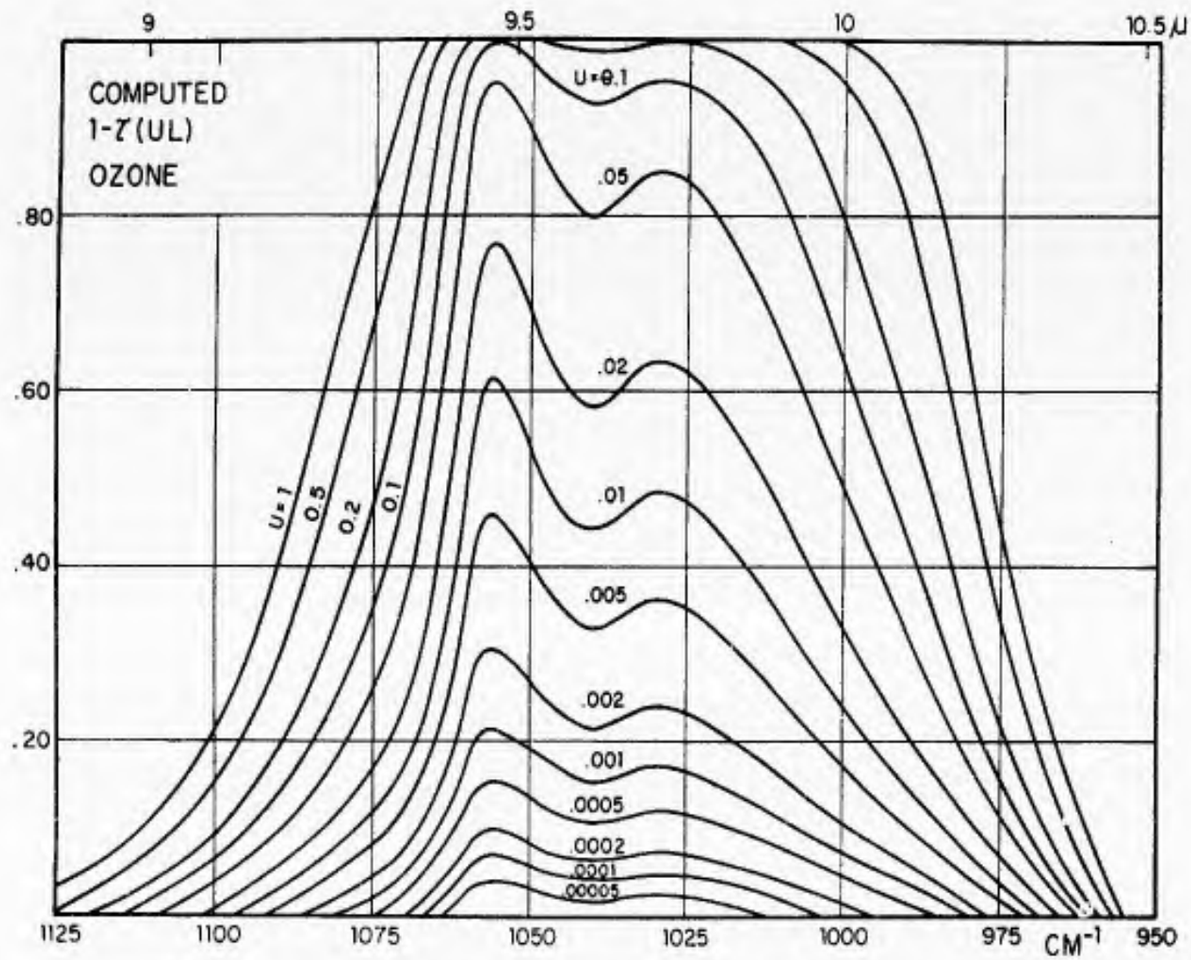

FIG. 17. Actual absorption for 9.6-μ ozone band. Corresponds to curve marked "computed" in fig. 18.

was a very good approximation for carbon dioxide is a rather poor one for ozone. The curve of fig. 15 was subjected again to some numerical smoothing so as to regularize first and second differences. Then a flux-transmissivity curve, τ_F, was computed by numerical integration by using (45).

The generalized absorption coefficient derived from Summerfield's data is shown in fig. 16. The main band is the 9.6-μ band which, as indicated in section III, may be interpreted as the fundamental of the normal mode ν_3. The exact band center is at 1043 cm^{-1}. On the short-wave side, there is a weaker companion centered at 1110 cm^{-1} (9.0 μ) which is the fundamental ν_1. In order to obtain the band contour at lower temperatures by the method described, the following values for the parameters of equation (59) were used. For the main, 9.6-μ band: $b = 0.40$, on the short-wave side $a = 14 \cdot 10^{-4}$, and on the long-wave side $a = 4 \cdot 10^{-4}$; for the satellite band at 9 μ: $b = 1$, on the short-wave side $a = 40 \cdot 10^{-4}$, and on the long-wave side $a = 14 \cdot 10^{-4}$. Some of the curves for lower temperature are shown on fig. 16.

After the construction of the ozone radiation chart had been completed, we became aware of a new and very extensive set of measurements by Walshaw (1957) which had just been published. Walshaw's absorption tube is 35 cm long with a double traversal by the beam. The amount of ozone was determined from the absorption of an ultraviolet band known to be pressure independent. Air was used as the broadening agent of the infrared band. Self-broadening of ozone was found to be 1.61 times the broadening produced by the same amount of air, and this figure was used to reduce all data to the condition of infinite dilution of ozone in air. Walshaw presents his results in terms of band areas under the 9.6-μ absorption band. In determining these areas, however, he eliminates the 9-μ band altogether by extrapolating the 9.6-μ band graphically across the area where the two bands overlap. In order to make our results comparable to those of Walshaw, we did the same to the actual absorption contours, $1 - \tau(uL)$, for 20C, computed by means of the data of fig. 15 and fig. 16. The result, after elimination of the 9-μ band by graphical means, is shown in fig. 17.

Fig. 18 shows a plot of Walshaw's data, using our standard pressure reduction, plotted against the band

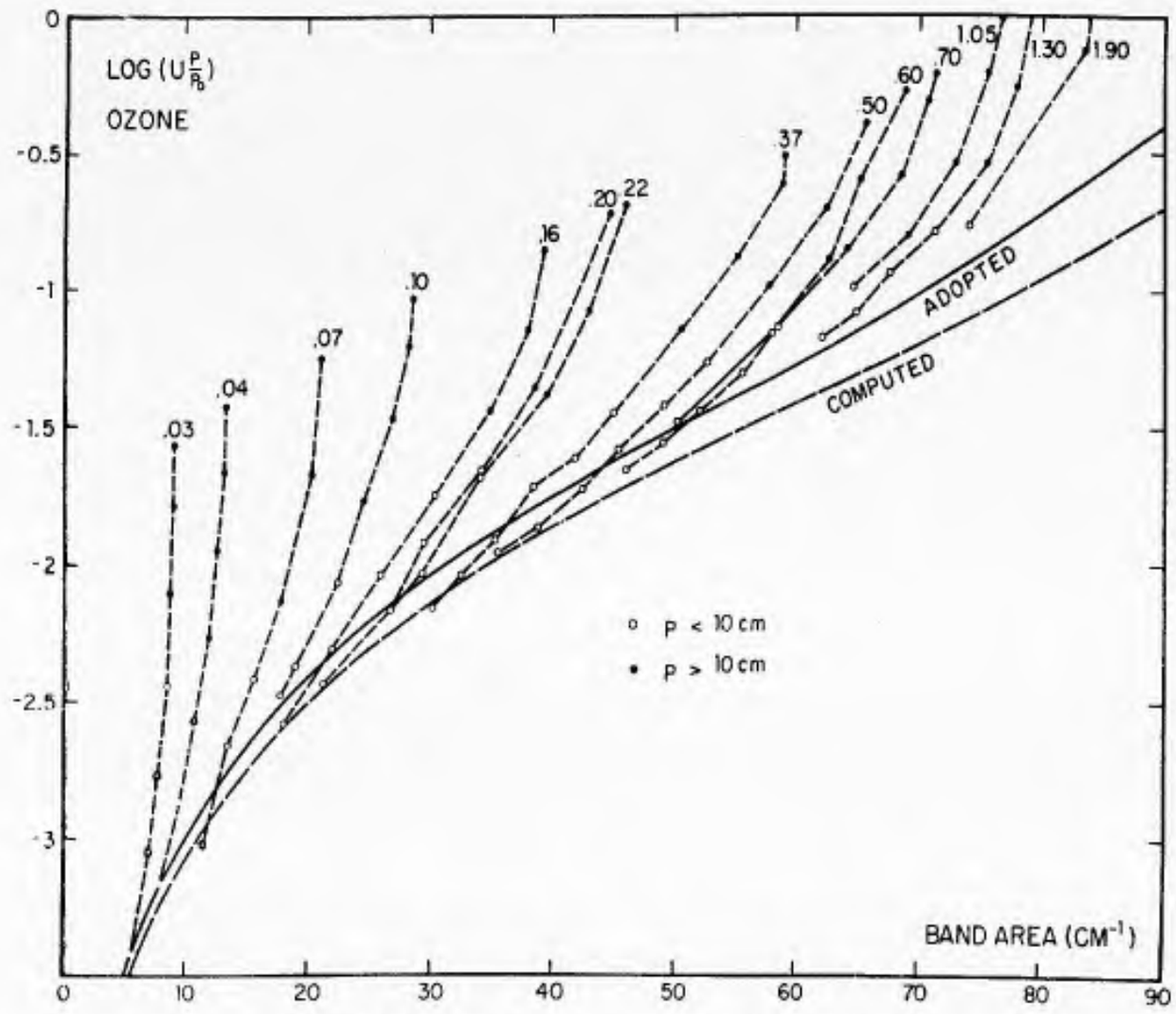

Fig. 18. Computed and observed band areas for 9.6-μ ozone band.

area of the 9.6-μ band. The values derived from the band areas of fig. 17 are given by the dashed curve marked "computed." Walshaw's measurements were made in series of runs, each run containing an approximately constant amount of ozone. Points of the same run are connected by dashed lines, the figure at the top of each line giving an approximate mean value of the ozone column in cm at STP. The pressure of the broadening air increases upward in each run. The points for which the effective air pressure (actual air pressure plus equivalent air pressure corresponding to self-broadening) is less than 10 cm Hg are marked by open circles; the points for which the effective air pressure is more than 10 cm Hg are marked by full circles. It is at once clear that the linear pressure reduction scheme used in our work is a poor approximation: the points are very far from clustering about a single curve as they should if this pressure correction was valid. We did not, however, feel inclined to introduce a more complicated pressure correction, since this would make the use of a radiation chart quite cumbersome. Instead, we decided to make a chart that is applicable mainly to the stratosphere where most of the ozone is concentrated. The "computed" curve of fig. 18 was corrected by reducing all band areas by 10 per cent; this gives the solid curve. Correspondingly, all values of the computed radiation chart were corrected by multiplying them by a factor of 0.90 throughout. Again, as in the case of CO_2, it should be noted that the absorption contours of fig. 17 have not been so corrected. The correction brings the calculated curve close to Walshaw's measured points in the region of low enough pressures and suitable ozone concentrations to be representative of the stratosphere. We also suggest that one might obtain a tolerable approximation to the actual pressure dependence on using a linear pressure reduction, p/p_0, up to some fixed pressure p_1, while at higher air pressures using a fixed pressure correction, p_1/p_0. This would clearly be equivalent to assuming that Walshaw's curves coincide with our solid curve for broadening pressures lower than p_1, whereas for broadening pressures above p_1

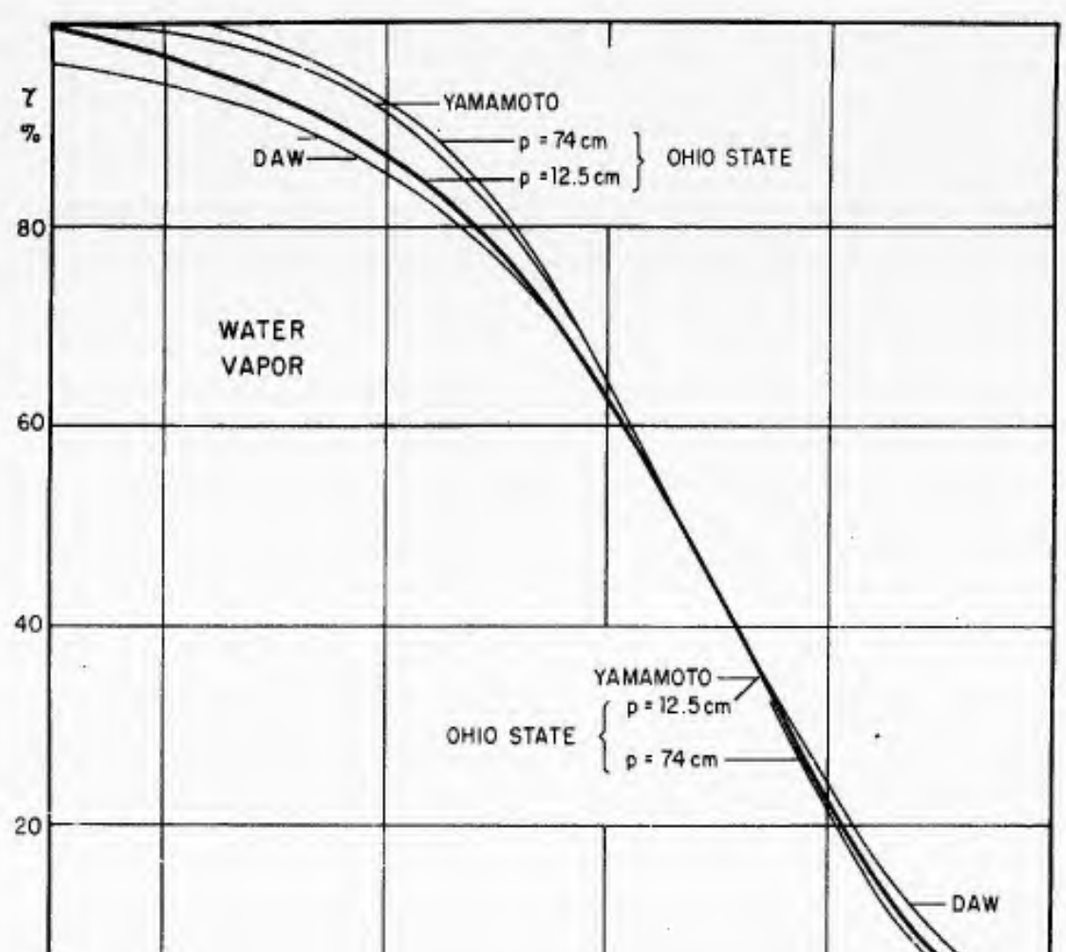

FIG. 19. Transmissivity curves for water vapor. Heavy curve adopted.

the absorption would be pressure-independent, corresponding to a vertical course of Walshaw's curves. The latter, as fig. 18 shows, is not too far from the truth.

There is one other absorption band of ozone in the far infrared, centered at 710 cm^{-1}, or very nearly 14 μ. This band is considerably less intense than the 9.6-μ band. The analysis of its contribution to radiative transfer is complicated by the fact that it is superposed upon the very strong 15-μ carbon-dioxide band. In all likelihood, however, the band is only of minor importance for radiative transfer. For possible future use, we give in table 9 a rough estimate of the generalized absorption coefficient taken from older measurements of Hettner, Pohlmann, and Schumacher (reproduced in Herzberg's book).

4. Water vapor

The far infrared spectrum of water vapor is more extensive than that of carbon dioxide or ozone. It consists of two bands, the 6.3-μ vibration-rotation band which is the fundamental of the normal mode ν_2 and the purely rotational band at the long-wave end of the spectrum. The region between the two, in the neighborhood of 10 μ, is generally known as the "window" and will be so designated throughout.

It so happens that the region of the window is the least well known part of the water-vapor spectrum, whereas the two bands surrounding the window are now reasonably well known in respect to their intensity. We have therefore chosen to compute radiation charts for the two bands separately and only at the end a radiation chart for the entire water-vapor spectrum. This should facilitate the construction of improved radiation charts for the overall spectrum when further data on the window have become known.

The first water-vapor radiation chart, which was in fact the first radiation nomograph of all, was constructed by Mügge and Möller (1932). The next such chart was developed by Elsasser (1942) based on more

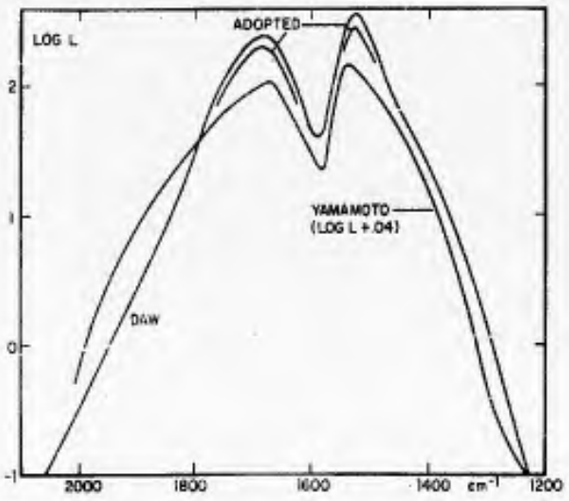

FIG. 20. Comparison of contours for 6.3-μ water-vapor band.

detailed spectroscopic data. Subsequently, such charts were designed by a number of authors—notably, Möller (1943), Bruinenberg (1946), Robinson (1950), Hales (1951), Yamamoto (1952), and Yamamoto and Onishi (1953). The present water-vapor radiation chart differs from Yamamoto's only in minor details, though it is based almost entirely on experimental data obtained later than Yamamoto's work.

The experiments carried out by Howard, Burch, and Williams (1955) furnish transmissivity curves for water vapor not only for the 6.3-μ band, but the same curve applies also for five other bands located in the near infrared. There is no reason to question that it should also be valid for the rotational band where the primary data are inadequate for the construction of a separate transmissivity curve. Thus, we have used the same transmissivity curve for both the 6.3-μ band and the rotational band. Howard, Burch, and Williams find that the shape of the transmissivity curve depends somewhat on pressure. Their two curves, representing a total pressure of 74 cm and 12.5 cm, respectively, are plotted in fig. 19, together with curves derived by

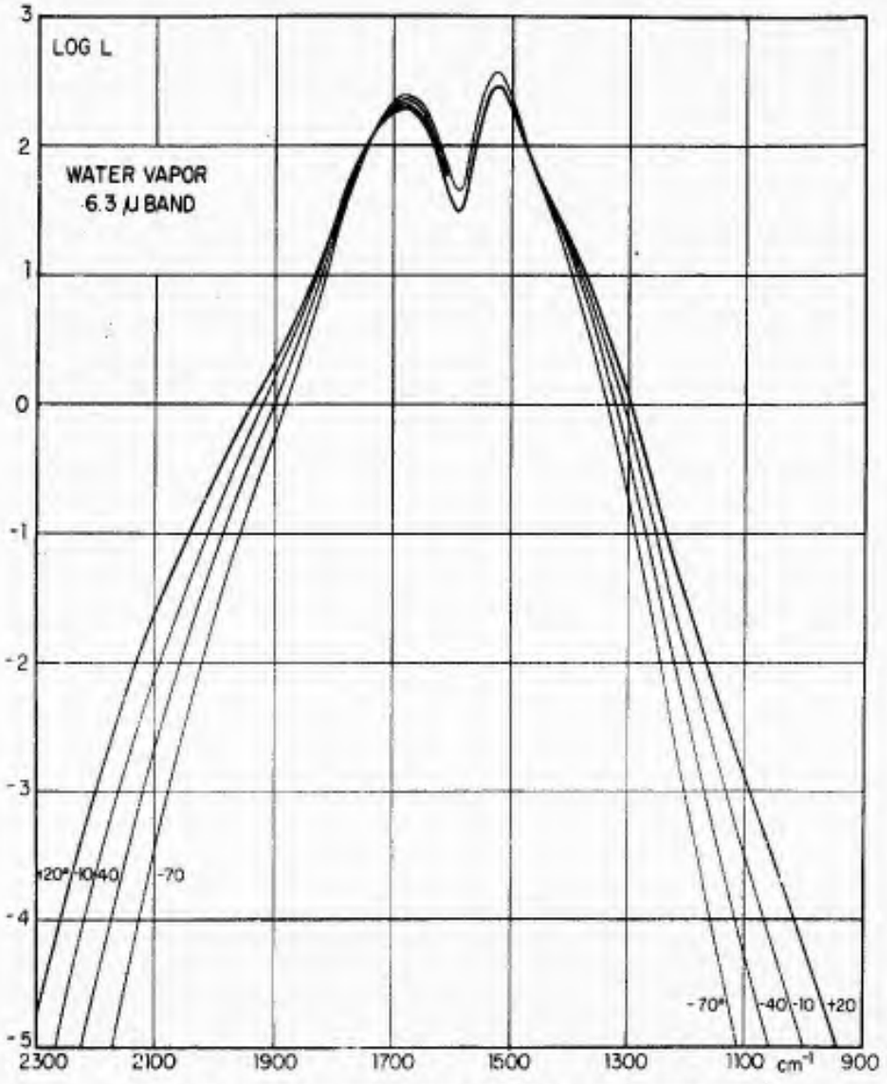

FIG. 21. Generalized absorption coefficient for 6.3-μ water-vapor band.

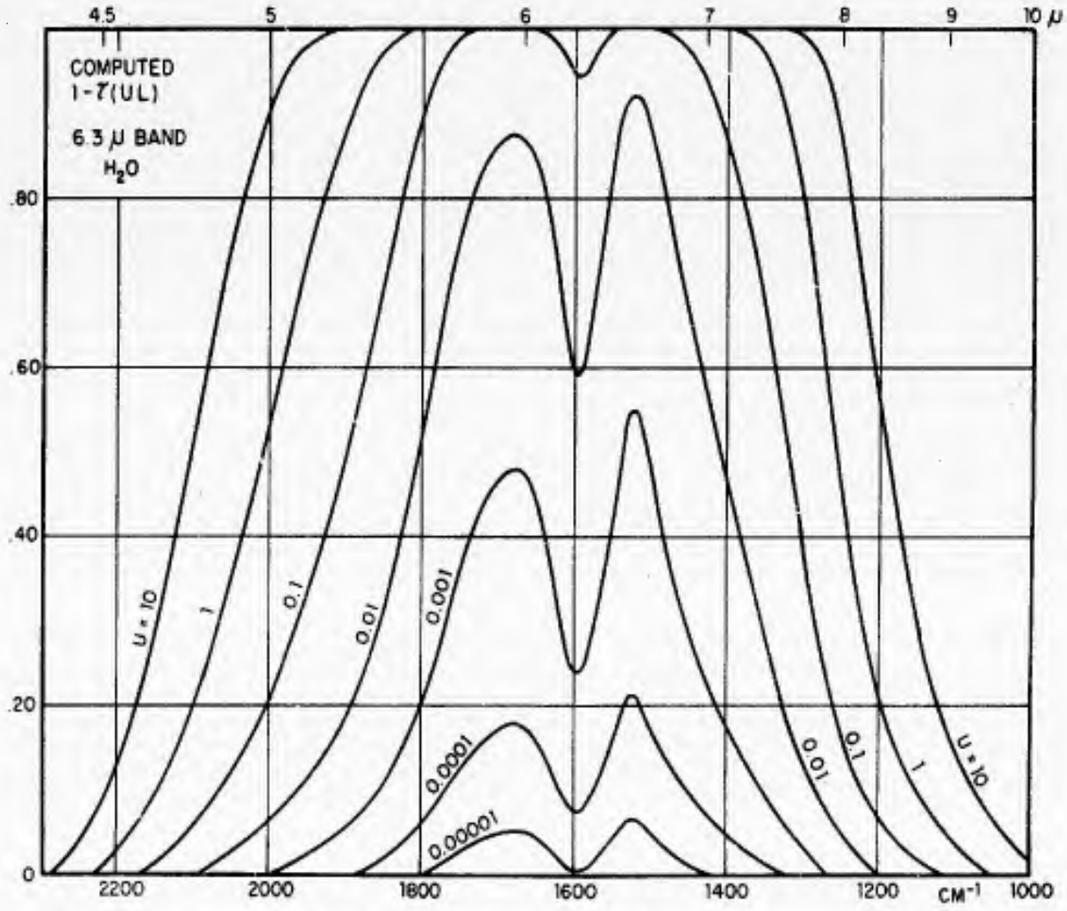

FIG. 22. Actual absorption of 6.3-μ water-vapor band. Corresponds to curve marked "computed" in fig. 23.

Yamamoto (1952) and Daw (1956). All curves have been shifted along the abscissa so that they coincide at the point of 50 per cent absorption. For our computations, we adopted the curve of Howard, Burch, and Williams corresponding to the lower air pressure since we felt that it is more important for the water-vapor radiation chart to be accurate at somewhat higher levels in the atmosphere than right near the ground. The differences between the various curves are, in any event, small.

We first discuss the 6.3-μ band. Yamamoto (1952) has constructed a curve of the generalized absorption coefficient using older experimental data. Daw (1956) measured the band in great detail by means of the equipment at Johns Hopkins University, the experimental procedures being somewhat similar to those of Cloud for CO_2 as outlined above. He constructed a curve of the generalized absorption coefficient compatible with his transmissivity curve of fig. 19. The curves of Yamamoto and Daw are compared in fig. 20. It appears from this that Daw's curve is somewhat high, though it is likely that its shape is correct. A final curve obtained by shifting Daw's curve downward, the top of which is sketched in fig. 20, was adopted after a trial-and-error procedure so as to give a satisfactory fit with the band areas shown in fig. 23, below.

The curve of the generalized absorption coefficient was next corrected for temperature according to the method given above in (61). The center of the band is at 1595 cm^{-1}, and each side of the band was corrected separately, as for CO_2. The coefficients of (59) are as follows: $b = 2.22$, for the band's short-wave side $a = 1.75 \cdot 10^{-5}$, and for the long-wave side $a = 2.4 \cdot 10^{-5}$. The resultant curves are shown in fig. 21. We can now obtain the band areas for a series of reduced optical path and for 20C; these are plotted in fig. 22. Next, we compared these results with the experimental data obtained by Howard, Burch, and Williams who give areas under the band for a variety of optical paths and broadening pressures. All the points are shown in fig. 23 together with the curve that goes through the band areas represented in fig. 22. It should be noted that the observed points which fall conspicuously below the curve represent measurements made on water vapor without the admixture of air or with exceedingly small amounts of air added. Clearly, such points are not characteristic of conditions in the actual atmosphere

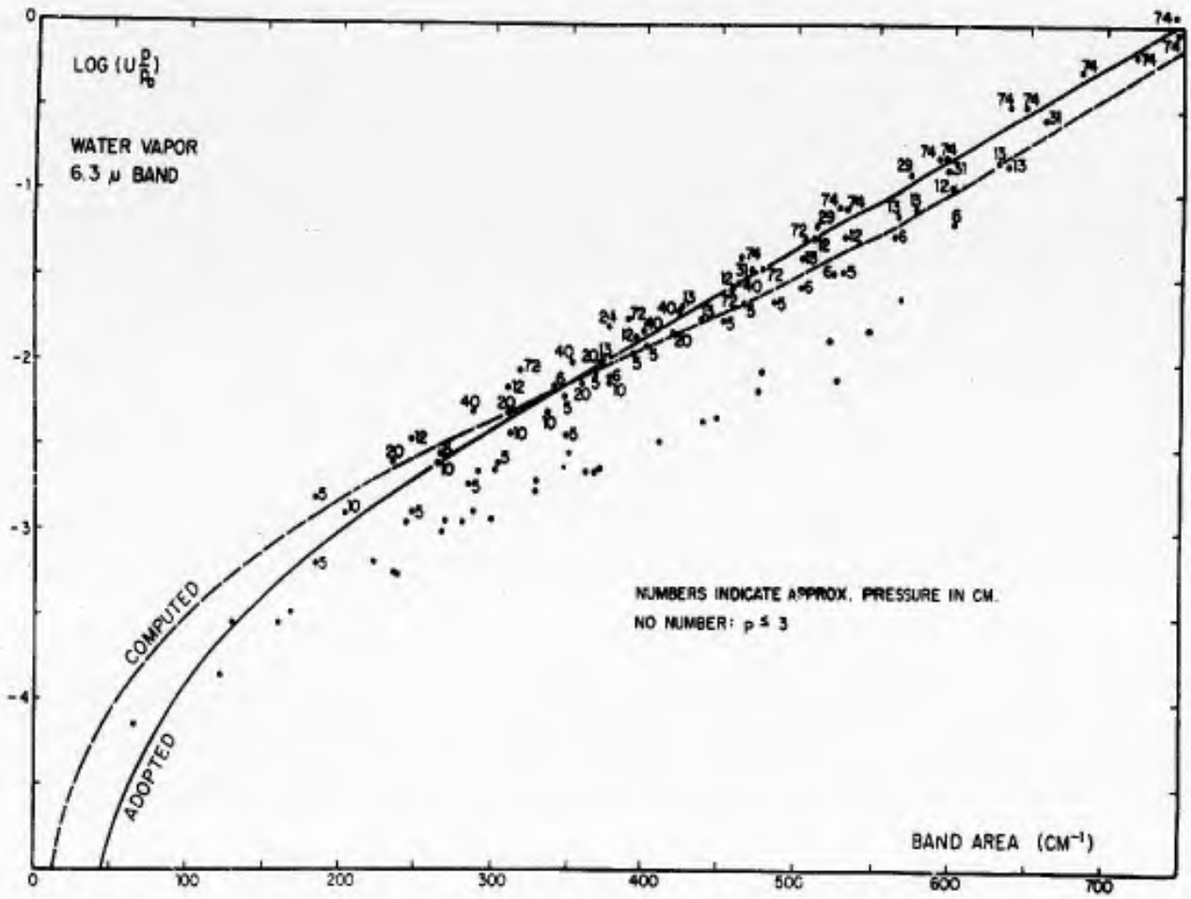

FIG. 23. Computed and measured band areas for 6.3-μ water-vapor band.

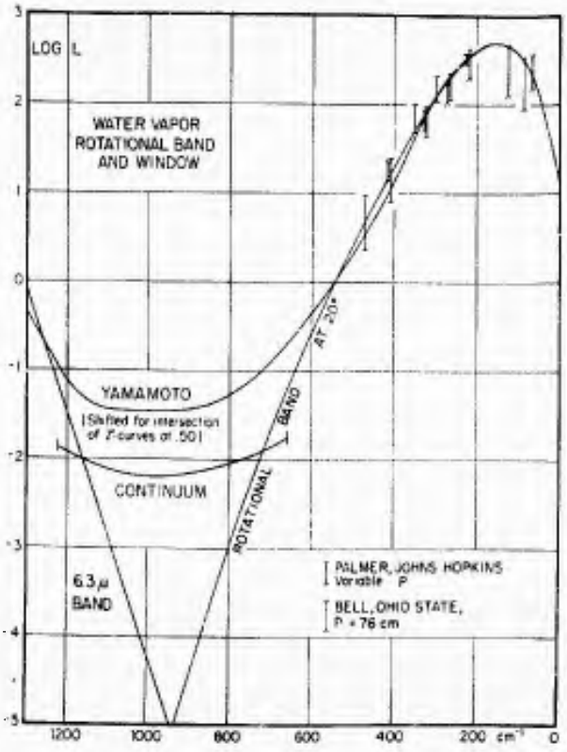

FIG. 24. Generalized absorption coefficient of rotational water-vapor band, and "window."

and may safely be disregarded. A corrected band-area curve, fitting the observed points, was then adopted, as shown in fig. 23. The subsequent procedure was the same as described in the case of CO_2. First, a radiation chart was constructed by means of the preliminary curve representing Daw's results as evaluated in fig. 22. These values were then corrected by multiplying for any given value of u by the ratio A/A_1, where A is the band area corresponding to the adopted curve and A_1 the band area corresponding to the preliminary curve at the point $\log u + 0.20$. Again, it should be remembered that fig. 22 corresponds to the preliminary curve of fig. 23 and that, if the band areas of fig. 22 are to be used for practical applications, they should be corrected correspondingly.

Next, we come to the rotational band. The technique of measurement becomes exceedingly difficult in the very far infrared. Earlier investigators, Yamamoto in particular, had therefore relied on direct summing of the line intensities computed from quantum mechanics. It is possible, for this band, to compute the absolute line intensities, provided only the electrostatic dipole moment of the water molecule has been measured. Yamamoto's band contour obtained in this fashion is shown in fig. 24. (Disregard for the moment

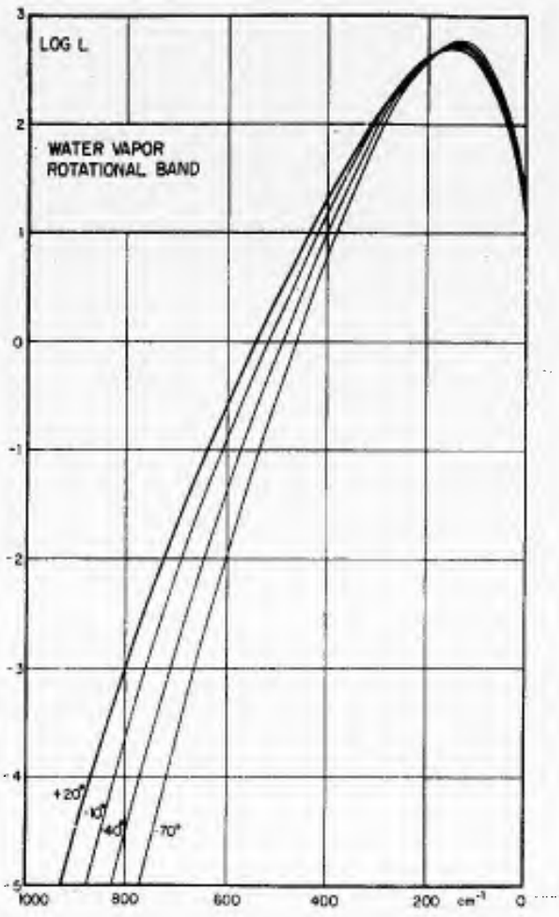

FIG. 25. Generalized absorption coefficient for rotational water-vapor band.

the region of the window.) It has been shifted along the u-axis so as to compensate for the shift of Yamamoto's transmissivity curve in fig. 21. There are no published recent measurements on this band performed with a wide enough slit so as to average out the individual lines. We were most fortunate to obtain by personal communication the results of two independent sets of measurements of this type. Dr. C. Harvey Palmer, Jr.,[1] in 1958, made a series of wide-slit observations with the long absorption tube at Johns Hopkins University at a variety of air pressures. The vertical lines in fig. 24 are located at the centers of the respective spectral intervals and indicate the limits of the series of points measured. A few points which represent pure water vapor not broadened by atmospheric air fall outside these intervals and have been omitted. Professor E. E. Bell of Ohio State University, in 1956, made a series of absorption measurements in moist air at atmospheric pressure only. These have been reported in an interim technical report to the Air Force of which Professor Bell kindly provided a copy. It is seen that, in the spectral region of $\nu > 200$ cm^{-1}, the agreement among the observations of Palmer and Bell and between these and Yamamoto's calculated curve is good. For waves longer than 200 cm^{-1}, the agreement of Bell's measurements with Yamamoto's curve is moderate. We did not feel compelled to deviate from Yamamoto's computed curve, however, given the extreme delicacy of measurements in this spectral region. Moreover, in this region the blackbody intensity is so weak that its contribution to atmospheric transfer is quite small. The band contour on the short-wave side, beyond about 500 cm^{-1}, is an arbitrary extrapolation. For lower temperatures, a band contour was again determined by means of (61). The parameters entering into equation (59) are $b = 2.96$ and $a = 0.98 \cdot 10^{-5}$. The resulting curves are shown in fig. 25. Finally, fig. 26 shows the computed band contours for a variety of reduced pressures at 20C.

We next come to the region of the window between the two water-vapor bands. Absorption there is weak; it is also known that there are a number of very weak lines in the interval. There is evidence, on the other hand, that much of the absorption comes from the "wings" of the very strong lines concentrated at the peak of the rotational band as well as of the 6.3 μ vibration-rotation band. Returning to (14), we see that at large distances from the line center the term α^2 in the denominator may be neglected as compared to $(\nu - \nu_0)^2$. The net effect of the wings of all the distant lines is then a continuous absorption with

$$k(\nu) = \sum_i \frac{S_i \alpha_i}{\pi(\nu - \nu_i)^2} \tag{64}$$

where the summation extends over all the distant lines. This quantity for the window has been computed by L. Kaplan (unpublished) and the results have been evaluated and compared with some atmospheric observations by Roach and Goody (1958). There are various reservations to be made. The observations are inadequate to establish beyond doubt the accuracy of the computations. Moreover, there are theoretical reasons for doubting the extrapolation of the Lorentz formula (14) to very large distances from the line center. Still, at the present time, the values given in the paper of Roach and Goody seem to be about the best we have, and so they were utilized in our computations. The scheme employed is shown on the left-hand side of fig. 24. In the first place, the extrapolated generalized absorption coefficients of the two main bands were assumed to give rise to absorption. Upon this was superposed the absorption of a continuum assumed to extend from 660 cm^{-1} to 1220 cm^{-1}. The absorption coefficient, k, for the latter is also shown in fig. 24. Now this continuous absorption is expressed

[1] Personal communication of data obtained at the Laboratory of Astrophysics and Physical Meteorology of Johns Hopkins University.

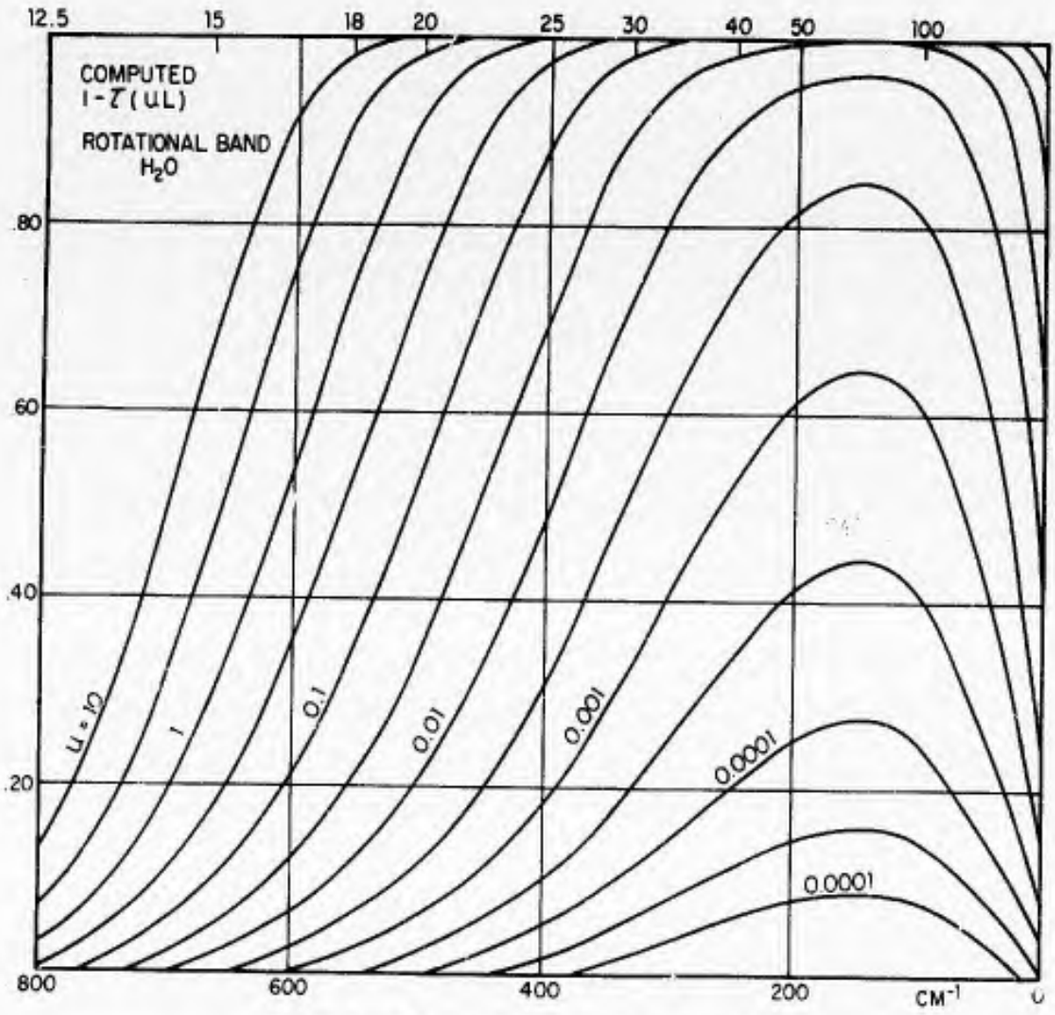

FIG. 26. Actual absorption of rotational water-vapor band.

by a transmission function, $\tau = e^{-kx}$, for a straight beam; the corresponding transmission function for a slab may be obtained from (45) in the form

$$\tau_s(ku) = 2\int_1^\infty \tau(\xi u)d\xi/\xi^3 = 2Ei_3(ku) \qquad (65)$$

where Ei_3 is the third exponential integral in the usual designation. We have plotted this function in fig. 27 together with the slab-transmissivity function corresponding to our adopted transmissivity for the water-vapor bands, as shown in fig. 19. The function Ei_3 has, however, been shifted to the left by one decadic cycle of the logarithmic u scale—that is, by a factor of ten. This was done for the following practical reason: mostly, the absorption in the window region is rather small, and, by shifting the continuum transmissivity in this way, the two curves of fig. 27 are made to run close to each other in the critical region of small absorption, and the difference in their behavior is made apparent. Now, however, it becomes necessary

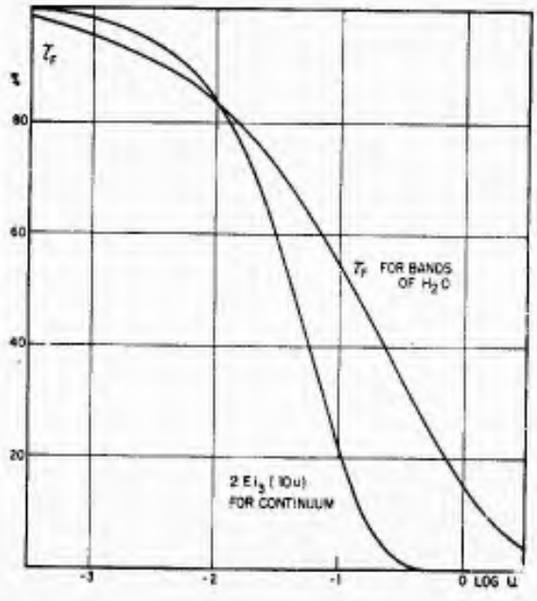

FIG. 27. Comparison of slab transmissivities of water-vapor bands (corresponds to beam transmissivity of fig. 19) and continuum.

to shift the curve of the generalized absorption coefficient for the continuum correspondingly—namely, downward by one cycle in the logarithmic scale of fig. 24. It is seen that in the absence of this shift the absorption coefficient would indeed run very closely to Yamamoto's values, only slightly above the latter.

The total transmission in the window was computed from the formula

$$\tau_{\text{total}} = \tau_{\text{cont.}} \cdot \tau_{\text{band}}. \tag{66}$$

A formula such as (66) is rigorously correct if two continuous transmissions are superposed. It should therefore represent a fair degree of approximation for the case where at least one of the components is a continuum. A radiation chart for the window region was next computed by using τ_{total}, and the final radiation chart for water vapor was obtained by adding up the charts for the two bands and the window. The window region as defined here (660–1220 cm^{-1}, with the terms of the numerical integration centered at multiples of 40 cm^{-1}—*i.e.*, from 680 cm^{-1} to 1200 cm^{-1}) extends into the two adjacent bands. Hence, on adding up the three contributions, a correction term has to be subtracted, representing the fact that the band edges, above 660 cm^{-1} and below 1220 cm^{-1} respectively, have been counted twice. This should be noted by those who wish to use our figures for further studies of the spectroscopic details of water-vapor absorption.

All other bands of the water-vapor spectrum besides those treated are in the near infrared, in a region where the black-body intensity at atmospheric temperatures is vanishingly small.

V. THE TRANSFER EQUATIONS, TABLES AND CHARTS

1. Integration of the transfer equations

We now consider atmospheres with an arbitrary vertical distribution of radiating gases. These atmospheres will be assumed horizontally stratified—that is, u is independent of horizontal coordinates and a function of height only. In place of (38), we now write

$$du^* = du \frac{p}{p_0} \sqrt{\frac{T_0}{T}}. \tag{67}$$

Often, the square-root dependence on temperature is rather slight and might be omitted. In practice, the integration of (67) is carried out by a numerical approximation, dividing the atmospheres into layers of finite thickness whose contributions are added up. As before, we propose to omit the asterisk in this chapter *and designate by u the reduced vertical path* as defined by (67). If u is measured in the vertical, the path of an inclined beam through a layer of thickness u is $u \sec \vartheta$ (fig. 5). This becomes infinite for $\vartheta = \pi/2$, and, in order to avoid this singularity, it is convenient to split the transfer equation into two parts, one equation referring to beams having an upward component of travel and another equation referring to beams having a downward component. In accordance with this splitting, we may assume $0 \leq \vartheta < \pi/2$ so that $\sec \vartheta$ is always positive. We may further assume that u is always measured in the same direction—say, increasing upward. We let the intensity, I, of flux f, be positive in the direction of propagation of each beam. For an inclined beam, the equation of transfer (12) now becomes

$$\begin{aligned} dI/du &= -k \sec \vartheta [I - I_b] \quad \text{(up)} \\ dI/du &= k \sec \vartheta [I - I_b] \quad \text{(down)} \end{aligned} \tag{68}$$

where I_b is again the black-body intensity.

On integrating (68) for the actual atmosphere and a given radiating gas, we need to remember that, in any one atmosphere, $u(z)$ and $T(z)$ are given functions of height, z. The pressure effect on the radiation has been taken into account by (67), and the pressure need no longer be considered (except of course when we want to use it as independent variable in place of z). On eliminating z, we can, for any one radiating gas, characterize a specific atmosphere by the functional relationship

$$u = u(T) \text{ or } T = T(u). \tag{69}$$

We shall write down the integral of the second equation (68); this differs from that for the first only by the algebraic sign. Equations (68) refer to an infinitesimal spectral interval. For such an interval, now, let

$$\tau(u) = e^{-ku \sec \vartheta}. \tag{70}$$

The integral of the second equation (68) giving the downward flux at level u_0 is

$$I(u_0) = -\int_{u_0}^{u_1} I_b(u) \frac{\partial \tau(u - u_0)}{\partial u} du \tag{71}$$

as may readily be verified by direct substitution by using (70). I_b is a function of temperature only, and $I_b(u)$ is defined by (69). At the upper boundary, $u_1 = 0$, we have $I(0) = 0$. Sometimes we are concerned

with an atmospheric layer of finite thickness bounded from above by a cloud. The cloud surface may be considered a black body for all practical purposes. Let us assume for the sake of generality that the temperature of the cloud bottom is not identical with that of the air adjacent to it; we may write $I_b(bd)$ for the black-body radiation emerging from this boundary. If we let $u = u_0$ at the boundary, the solution fulfilling the correct boundary condition is

$$I(u_0) = I_b(bd)\tau(u_1 - u_0) - \int_{u_0}^{u_1} I_b(u)\frac{\partial\tau(u - u_0)}{\partial u}du. \quad (72)$$

Formula (72) becomes a solution of the first equation (68), applying to an upward beam, by changing the sign of the integral. It is to be remembered that I is always positive in our definition. The lower boundary may now be the ground, or else a cloud top, usually radiating as a black body.

For simplicity, let us next confine ourselves to (71) where there is no separate boundary term. We can perform two linear operations on this equation—namely, the integration over the spectrum and the integration over the angles.

The integration over the spectrum is carried out in two steps. First, we go from the monochromatic transmissivity (70) to the transmissivity averaged over a finite interval $\Delta\nu$—that is, to $\tau(uL)$ where L is the generalized absorption coefficient. This τ is defined by (16) and, on suitable normalization of I (or else f) per unit spectral interval, we may set $\Delta\nu = 1$. Under this operation, (71) remains formally unchanged. Thereafter, we can carry out the full integration over the spectrum.

By integrating next over the polar angles, ϑ, φ, we found in section II.6 that this does not change the basic transfer formalism; we merely have to replace the intensity I by the flux f and replace τ by the flux transmissivity τ_F. We write B_ν for the black-body flux, where by (42) we have $B_\nu = \pi I_b$.

Now (71) becomes, if F designates the integrated flux,

$$F(u_0) = -\int d\nu \int_{u_0}^{u_1} B_\nu \frac{\partial\tau_F(u - u_0)}{\partial u}du. \quad (73)$$

A similar transformation applies to (72) and the corresponding formula for the upward flux. Equation (73) and similar ones with boundary terms obtained by integrating (72) over the spectrum and angles solve the radiative-transfer problem.

2. Construction of tables and charts

Equation (73) may be used for the numerical computation of radiative fluxes. Instead, the process may be carried out graphically on a nomogram, a radiation chart. Thus, Möller's (1943) radiation chart has $\log u$ as abscissa and the quantity, say

$$P(u, T) = -\int B_\nu(T)\frac{d\tau_F(u)}{du}d\nu, \quad (74)$$

as ordinate. Isotherms, curves of constant T, are permanently drawn on the chart. By using these curves, one can plot the relationship $T(u)$ representing a given atmosphere. The flux at u_0 then becomes

$$F(u_0) = \int_{u_0}^{u_1} P(u - u_0, T)du, \quad (75)$$

and may be interpreted as the area under the $T(u)$ curve which area is most readily evaluated by means of a planimeter. Thus, radiative fluxes can be determined rapidly.

There is clearly a great variety of ways in which the basic integrals of the transfer equations can be obtained numerically or graphically. There seems to be little point here in reproducing some of the contents of a text on numerical analysis or of one on nomographic methods. The transformations between the various methods are as a rule straightforward, and various patterns will occur to anyone who is confronted with the task of evaluating a considerable number of radiative fluxes. We shall therefore omit altogether the description of numerical techniques of evaluating these fluxes and shall instead exemplify the whole method in terms of a graphical procedure only. This does not mean that this method is superior; quite often the numerical approach might be more convenient, but the graphical method is more easily demonstrated.

In the charts of the author and of Yamamoto, among others, a change of variables has been performed. Instead of u, the temperature, T, is used as the independent variable by Elsasser (1942) and the black-body flux B by Yamamoto (1952). Subject the second integral in (73) to an integration by parts,

$$\int_{u_0}^{u_1} B_\nu \frac{d\tau_F(u)}{du}du = \left| B_\nu\tau_F \right|_{u_0}^{u_1} - \int_{u_0}^{u_1}\frac{dB_\nu}{dT}\tau_F(u)du = \left| B_\nu\tau_F \right|_{T_0}^{T_1} - \int_{T_0}^{T_1}\frac{dB_\nu}{dT}\tau_F(u)dT, \quad (76)$$

where it is to be remembered that in a given atmosphere the functional relation (69) holds. In analogy to (74), we introduce a function of *two* variables,

$$Q(u, T) = \int \frac{dB_\nu(T)}{dT}\tau_F(u)d\nu, \quad (77)$$

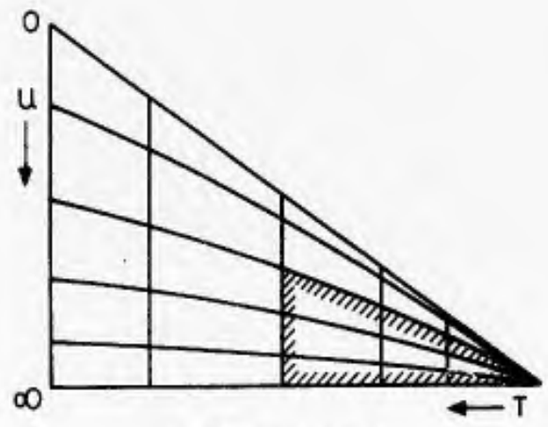

FIG. 28. Radiation chart.

integrated over the spectrum. By carrying (76) and (77) into (73), we get

$$F(u_0) = -\left|\int B_{\nu\tau_F}(u-u_0)d\nu\right|_{T_0}^{T_1} + \int_{T_0}^{T_1} Q(u-u_0,\ T)dT, \tag{78}$$

where the path of the integral is along the actual relationship, $u(T)$, valid for the atmosphere considered. A glance at (77) will show that the two boundary terms ahead of the integral in (78) are equivalent to integrals of the form

$$\int_0^T QdT \text{ taken along } u = const.$$

Furthermore, by replacing $u - u_0$ by u in the last integral in (78), which can be done without loss of generality as will presently appear, this formula becomes

$$F = \int_0^{T_0} Q(0,\ T)dT + \int_{T_0}^{T_1} Q(u(T),\ T)dT + \int_{T_1}^{0} Q(u_1,\ T)dT. \tag{79}$$

This form shows the integral extended along a *closed* path in the T-Q plane. The integration goes from the absolute zero of temperature along the path $u = u_0$ to the temperature T_0, thence along the actual $u(T)$ relationship in the atmospheric layer considered to T_1, and from there back to the absolute zero along $u = u_1$. The replacement of $u - u_0$ by u in the second integral means simply that the zero of optical thickness must, in this system of evaluation, be taken at the level for which the flux is computed.

Let us remark that the quantity tabulated in section VI is not Q itself but is

$$R(u,\ T) = \frac{dB}{dT} - Q(u,\ T) = \int \frac{dB_\nu}{dT}(1-\tau(u))d\nu. \tag{80}$$

The advantage is that R vanishes for all points of the spectrum where the substance considered is transparent, whereas $Q = dB/dT$ in this part of the spectrum.

3. Use of a radiation chart

We shall exemplify the determination of radiative fluxes by means of the type of chart used earlier by the author (1942). If we take the temperature as abscissa and Q as ordinate, we get a diagram in which $Q_{max} = 4\sigma T^3$ is the upper edge. This is inconvenient and we transform to new variables, say

$$x = aT^2 \qquad y = Q/2aT. \tag{81}$$

This transformation preserves areas, and the upper edge is now a straight line, giving the chart a triangular shape (fig. 28). On the chart are drawn curves of constant u, *isopleths* of u as we shall call them, implicitly defined by (77). The abscissas are labelled in terms of T, increasing from right to left, the ordinates are labelled in terms of the u isopleths, and a standard area is provided for calibration of the planimeter. We may remark here that Yamamoto's chart (1952) is very similar but rectangular, the abscissa being proportional to $B = \sigma T^4$ and the ordinate to Q/T^3.

A radiative flux is equivalent to an area on the radiation chart; we shall illustrate this by a series of examples of increasing complexity. We shall first assume a substance such as water vapor which is opaque over the whole of the far infrared spectrum for a layer of sufficient thickness. The isopleth $u = 0$ coincides with the upper edge of the chart, whereas the isopleth $u = \infty$ coincides with the horizontal axis. It is readily seen that a triangle bounded on the left by a vertical line $T = \text{const.}$ is equal to the black-body flux, $B = \sigma T^4$. This graphical representation embodies the rather obvious theorem that an isothermal layer of infinite thickness of a substance which is nowhere in the spectrum completely transparent radiates as a black body. Next, take the nearly triangular area shaded in fig. 28 which is bounded from above by an isopleth, $u = \text{const.}$ It represents the quantity

$$\int_{u=\text{const.}} QdT = \int B_{\nu\tau_F}(u)d\nu, \tag{82}$$

that is, the radiation transmitted by a slab of thickness u (itself not radiating) upon which the black body flux B impinges. The area above the shaded region and bounded on the left by the same vertical line is then,

$$\int_{u=\text{const.}} RdT = \int B_\nu(1 - \tau_F(u))d\nu, \tag{83}$$

that is, the emission of an isothermal layer of thickness u and temperature T. All these results can readily be derived from (77).

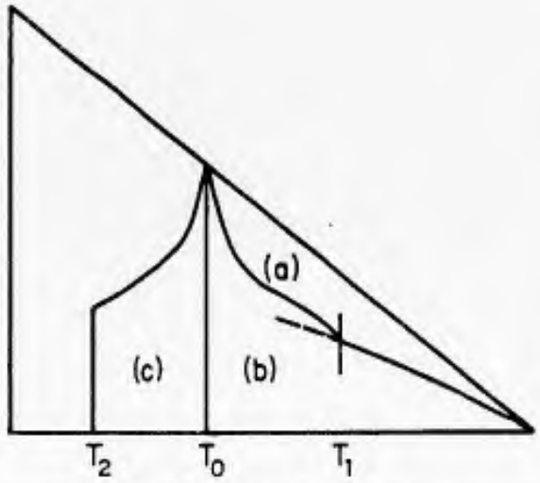

FIG. 29. Computation of flux on radiation chart.

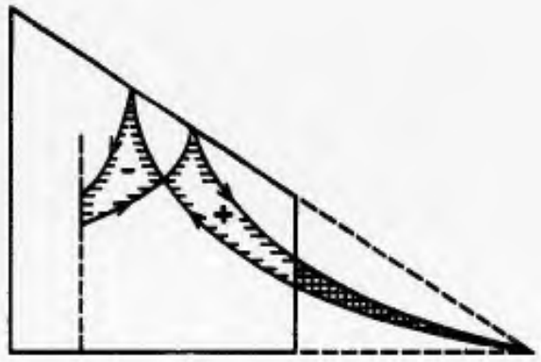

FIG. 30. Computation of cooling of a slab on radiation chart.

Next consider the emission of a layer with arbitrary stratification. This is given by (79), and one readily verifies that this flux is represented by the area (a) in fig. 29. We recall that the zero of optical thickness must here be taken at the level for which the flux is determined. At any level in the atmosphere, there will be a flux in either direction, and the net flux, counted positive if going upward, will be the difference,

$$F_{\text{net}} = F_{\text{up}} - F_{\text{down}}. \tag{84}$$

For instance, if the surface considered is at the ground, the up-going flux will be the black-body radiation of the ground whose temperature may now be T_0. It follows at once that area (b) in fig. 29 represents the net flux leaving the ground. Again, assume that we want to determine the net flux at a higher level in the atmosphere; now, let T_0 stand for the temperature at that level. The significance of area (a) with respect to the downward flux is the same as before. We now plot the actual relation $u(T)$ going downward from the reference level, with the reference level as zero. We can proceed in this way until we have reached the ground. We may next replace the ground by an isothermal layer of infinite optical thickness at temperature T_2. This is graphically represented by going downwards along the vertical T_2 to the axis of abscissae. This is shown in fig. 29, the net upward flux at the reference level of temperature T_0 being now given by the area (a) + (b) + (c). Since (a) is the downgoing flux, it follows that the net flux (84) at the reference level is represented by (b) + (c). In a slightly more complicated case, the temperature of the ground, say T_3, may be somewhat different from the temperature T_2 of the air immediately adjacent to the ground. This corresponds to the earlier equation (72) now integrated over the spectrum and the angles. One now goes along the actual atmospheric curve $u(T)$ to T_2, then along the u-isopleth to T_3 and from there on vertically downwards.

Almost all cloud surfaces may be considered black bodies and may be accounted for in the radiation chart on replacing them by an isothermal layer of infinite thickness. If, for instance, in the case shown in fig. 29, there is a cloud base at a level of temperature T_1 and if the reference level T_0 is between this and the ground, the net radiation at T_0 would be (b′) + (c) where (b′) is the truncated part of area (b) to the left of a vertical line at T_1.

The $u(T)$ curve as drawn in fig. 29 assumes that the temperature decreases with increasing height, which is the usual case in the atmosphere. If temperature inversions are present, the curves to be drawn on the radiation chart become a little more complicated, and closer attention may have to be paid to the algebraic sign of the different areas; however, there is no particular difficulty, and we may leave out details that can readily be supplied as needed.

An area such as that on the right of the vertical $T = T_1$ in fig. 29 must be evaluated in all radiative flux calculations. To facilitate this repetitive process, the areas, given by (83) have been evaluated once and for all for a sufficiently low temperature. Table 20 gives the areas for a temperature of − 80C for all the bands considered. Having these, it is possible to design a truncated radiation chart, leaving out the triangular area to the right of − 80C. This is shown schematically in fig. 30. The area cross-hatched there is the difference of two such areas.

Let us finally lift the restriction that for sufficient thickness the substance in question is completely opaque in all parts of the spectrum. This is true for water vapor, and the earlier radiation charts applied to water vapor. Carbon dioxide and ozone, on the other hand, cover only a small part of the far infrared spectrum. In this case, it is convenient to define a spectral interval within which absorption is everywhere appreciable at the largest thicknesses encountered in the atmosphere. One may then repeat all the

formal arguments of this section for the limited interval envisaged, and one may construct a radiation chart whose edge represents the fraction of the black-body flux which is contained in the interval selected. For the case of carbon-dioxide, we shall revert to this question when we deal with the spectral overlap of H_2O and CO_2. For ozone in the stratosphere, no problem arises once the limiting interval is chosen (*e.g.*, 970–1130 cm^{-1}), since water vapor may be considered transparent in the window region except for the emission of layers of large moisture near the ground which, on combining it with the radiation of the ground, may, relative to the ozone band, be considered as external black-body radiation of a suitable representative temperature.

4. Radiative cooling

Assume now two levels in the atmosphere, say (1) and (2), where we shall take (2) to be the higher level. With the convention (84) which makes the net flux positive upwards, the net loss of radiant energy per unit time suffered by the layer between (1) and (2) is

$$\Delta F = F_{\text{net}}^{(2)} - F_{\text{net}}^{(1)} \tag{85}$$

where ΔF is positive for cooling. The evaluation of such an expression on the radiation chart is shown in fig. 30, the peak corresponding to level (1) being on the left, that to level (2) on the right. The rate of cooling averaged over the layer is now

$$-\rho c_p \Delta z \frac{\partial T}{\partial t} = \Delta F \tag{86}$$

where ρ is the mean air density in the layer, c_p specific heat at constant pressure, and Δz the thickness of the layer. From the barometric equation, this can be written

$$\frac{\partial T}{\partial t} = \frac{g}{c_p}\frac{\Delta F}{\Delta p} \tag{87}$$

where Δp is the pressure difference between the boundaries of the layer. If ΔF is in gcal per square cm day, if Δp is in millibars, and if t is in days, the numerical value of the constant on the right of (87) is 4.09.

In order to compute radiative cooling in the free atmosphere, it is usually adequate to subdivide the atmosphere into layers of finite thickness and to use such formulas as (87). The more rigorous procedure would of course be to go to the limit of infinitesimal vertical differences, giving

$$\frac{\partial T}{\partial t} = \frac{g}{c_p}\frac{dF}{dp} = \frac{g}{c_p}\left(\frac{\partial F}{\partial T}\frac{\partial T}{\partial p} + \frac{\partial F}{\partial u}\frac{\partial u}{\partial p}\right). \tag{88}$$

However, $\partial F/\partial T$ vanishes, as may most readily be seen by noting that $F = \int R dT$ where the integration with respect to T is over a closed contour. Hence, (88) becomes

$$\frac{\partial T}{\partial t} = \frac{g}{c_p}\frac{du}{dp}\frac{\partial F}{\partial u} = \frac{g}{c_p}\frac{d\log u}{dp}\frac{\partial F}{\partial \log u}$$

$$= \frac{g}{c_p}\frac{d\log u}{dp}\int \frac{\partial R}{\partial \log u} dT \tag{89}$$

where the integration is again over a closed contour. Thus, the determination of radiative cooling can be carried out quite directly by means of a nomogram in which the quantity $\partial R/\partial \log u$ appears as ordinate. This quantity is tabulated in section VI for all three gases. These tables are less accurate than those for R because the numerical differentiation engenders a certain loss of accuracy. The procedure of using these "flux divergence charts" is analogous to that for the radiation chart outlined above. Such charts have been designed for water vapor by Bruinenberg (1946), Hales (1951), and Yamamoto and Onishi (1953) among others.

5. The carbon-dioxide—water overlap

In the region of the spectrum where carbon dioxide absorbs, there is also some water-vapor absorption. A detailed quantitative treatment of this effect upon atmospheric radiation would be extremely laborious, and we must confine ourselves to a rather crude method. This is not too serious, because the spectral region involved here contributes at most about 18 per cent of the total black-body flux, and often much less. Thus, a moderate percentage error in the overlap effect corresponds to a comparatively small error in the total fluxes. We shall follow the method used by Yamamoto (1952).

The approximation is essentially based upon the assumption, already used in (66), that the total transmissivity is the product of the transmissivities corresponding to the two gases. In other words, in the interval of overlap, we replace τ_P by $\tau_P(H_2O)\tau_P(CO_2)$. This product rule is of course rigorously correct only for the superposition of continuous spectra and is inadequate for band spectra. Nevertheless, one can expect to get a moderately good approximation owing to the fact that most of the absorption takes place in the wings of the lines which act somewhat like a continuum (the case of absorption proportional to the square root of the optical path). We may apply this correction either to a water-vapor calculation or else to a carbon-dioxide calculation. Consider first the former. Referring to the definition (77) of Q, we replace it by

$$Q_{\text{corr}} = Q - \Delta Q, \qquad R_{\text{corr}} = R - \Delta R \tag{90}$$

where now

$$\Delta Q = -\Delta R = \int \frac{dB_\nu}{dT} \tau_F(H_2O)[1 - \tau_F(CO_2)]d\nu \quad (91)$$

which, with the integration taken over the spectral interval of overlap, effects the replacement considered in this interval. Similarly, of course, if we want to correct CO_2 radiation for underlying water-vapor absorption, we write

$$\Delta Q = -\Delta R = \int \frac{dB_\nu}{dT} \tau_F(CO_2)[1 - \tau_F(H_2O)]d\nu. \quad (92)$$

In the tables of these quantities given in the appendix, we have taken the spectral interval as 540–820 cm^{-1}. This particular choice of interval resulted from our replacing the integrations in (91) and (92) by simple summations over intervals 40 cm^{-1} wide, with dB_ν/dT taken at the centers of the intervals. The first and the last centers were 560 cm^{-1} and 800 cm^{-1}, respectively. The numerical computation of (91) or (92) would still be prohibitively lengthy since there are three parameters, the temperature and the optical paths of both water vapor and carbon dioxide. By a fortunate circumstance, the proportion of the black-body radiation contained in this interval relative to the total black-body radiation changes rather little with temperature (except at the very lowest temperatures, since the fraction must clearly go to zero for $T = 0$). Since the overlap is in practice most important in the lowest layers of the atmosphere, the calculations have been carried through for a temperature of 20C throughout. The values of (91) and (92) are given in tables 21 and 22.

The computation, numerical or graphical, of the correction term $\int \Delta Q dt$ proceeds in exactly the same way as the computation of the flux $\int Q dT$. Yamamoto presents a graph on which ΔQ is read off, the abscissae and ordinates being the carbon dioxide and water vapor paths, respectively. He then has lines ΔQ = const. printed on his water vapor radiation chart; these lines are at the bottom of the chart, the horizontal axis being $\Delta Q = 0$, and the higher values of ΔQ cover a strip above the axis. One then draws a curve corresponding to the actual atmosphere, and the net flux of water vapor radiation corrected for CO_2 is the area between the upper and the lower curves (fig. 31).

In actual calculations of radiative transfer the application of the Yamamoto corrections (91) and (92) might offer some difficulties. Note that this correction amounts in (91) essentially to replacing $\int B'_F(H_2O)d\nu$ by the term $\int B'\tau_F(H_2O)\tau_F(CO_2)d\nu$ within the region of the overlap, and conversely in (92). Thus if we corrected both the water vapor chart and the carbon dioxide chart, we would introduce the cross term (the last integral) twice. Notice, however, that water vapor has a sufficient concentration to absorb or emit in the region of the overlap only in the lowest layers, say the lowest 1-3 km, of the atmosphere. Thus for the computation of outgoing radiation and atmospheric cooling it might commonly suffice to correct only the CO_2 chart, leaving the H_2O chart uncorrected. In any event, if the usual procedure is applied of obtaining the black-body radiation of the ground by introducing a layer of infinite optical thickness, one must be sure that the region covered by the CO_2 band is not counted twice in the black-body contribution. Another way of applying the overlap correction would consist in taking the arithmetical mean of (91) and (92) and applying this correction once to the combined result of the H_2O and CO_2 charts. The elaboration of a suitable procedure that takes account of the problems posed by the coexistence, in one region, of bands originating from two different gases, is best done by those who are actively engaged in practical calculations of this type. The present author has not done such calculations in recent years, and therefore has confined himself to presenting such numerical tables as can be obtained from an evaluation of laboratory measurements made separately on each gas.

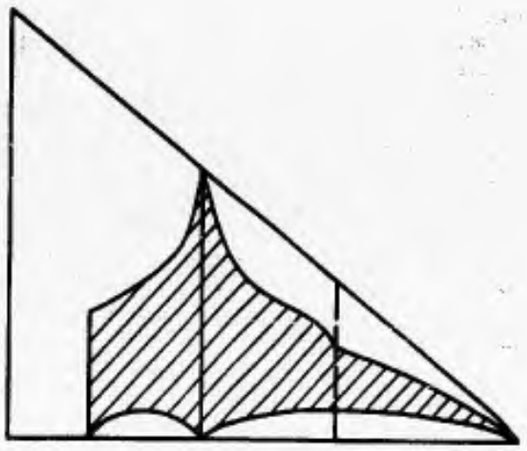

FIG. 31. Carbon-dioxide overlap correction arranged at bottom of water-vapor radiation chart.

REFERENCES

Anderson, P. W., 1949: Pressure broadening in the microwave and infrared regions. *Phys. Rev.*, **76**, 647–661.

Bell, E. E., 1956: *Interim engineering report for period July–September 1956.* Ohio State Univ., Contract AF 33(616)-3312 with Wright Air Development Center.

Born, M., 1933: *Optik.* Berlin, J. Springer, 615 pp.

Bruinenberg, A., 1946: *A numerical method for the calculation of temperature changes by radiation in the free atmosphere (in Dutch).* Kon. Nederl. Meteor. Inst., Meded. en Verhand. Serie B, Deel 1, No. 1, 57 pp.

Chandrasekhar, S., 1950: *Radiative transfer.* Oxford, Clarendon Press, 393 pp.

Cloud, W. H., 1952: *The 15 micron band of CO_2 broadened by nitrogen and helium.* Prog. Rept., Johns Hopkins Univ., Contract N-onr 248-01, 56 pp.

Cohen, E. R., J. W. M. DuMond, T. W. Layton, and J. S. Rollett, 1955: Analysis of variance of the 1952 data on the atomic constants and a new adjustment, 1955. *Revs. Mod. Phys.*, **27**, 363–380.

Daw, H. A., 1956: *Transmission of radiation through water vapor subject to pressure broadening in the region 4.2 microns to 23 microns.* Tech. Rep. No. 10, Univ. Utah, Contract AF 19(122)–392 with AFCRC, 70 pp.

Dorsey, N. E., 1940: *Properties of ordinary water substance.* New York, Reinhold Publ. Co., 673 pp (see p. 298).

Elsasser, W. M., 1938: Mean absorption and equivalent absorption coefficient of a band spectrum. *Phys. Rev.*, **54**, 126–129.

Elsasser, W. M., 1942: *Heat transfer by infrared radiation in the atmosphere.* Harvard Meteor. Studies, No. 6, Cambridge, Harvard Univ. Press, 107 pp.

Elsasser, W. M., and J. I. King, 1953: *Transmission data for the far infrared bands of carbon dioxide and ozone.* Tech. Rep. No. 9, Univ. Utah, Contract AF 19(122)–392 with AFCRC, 44 pp.

Goody, R. M., 1952: A statistical model for water vapor absorption. *Quart. J. r. Meteor. Soc.*, **78**, 165–169.

Goody, R. M., 1954: *The physics of the stratosphere.* Cambridge, England, Cambridge Univ. Press, 87 pp.

Hales, J. V., 1951: *An atmospheric radiation flux divergence chart and meridional cross sections of water vapor radiational heat losses computed through its use.* Thesis, unpubl., Univ. California at Los Angeles, 90 pp.

Herzberg, G., 1945: *Molecular spectra and molecular structure, Vol. II, infrared and raman spectra.* New York, Van Nostrand, 632 pp.

Howard, J. N., D. L. Burch, and D. Williams, 1956: Infrared transmission of synthetic atmospheres. *J. Opt. Soc. Amer.*, **46**, 186–189, 237–247, 334–338, 452–455. (Further data in: Geophys. Res. Pap. No. 40, AFCRC, November 1955, 245 pp.)

Hughes, R. H., 1953: The microwave spectrum and structure of ozone. *J. Chem. Phys.*, **21**, 959–960.

Kaplan, L. D., 1950: Line intensities and absorption for the 15 micron carbon dioxide band. *J. Chem. Phys.*, **18**, 186–189.

Kaplan, L. D., 1952: On the pressure dependence of radiative heat transfer in the atmosphere. *J. Meteor.*, **9**, 1–12.

Kaplan, L. D., 1953: *A quasi-static approach to the calculation of atmospheric transmission.* Proc. Toronto Meteor. Conf., 43–48.

Kaplan, L. D., and D. F. Eggers, 1956: Intensity and line width of the 15 micron CO_2 band determined by a curve-of-growth method. *J. Chem. Phys.*, **25**, 876–883.

Kaplan, L. D., M. V. Migeotte, and L. Neven, 1956: 9.6 micron band of teliuric ozone and its rotational analysis. *J. Chem. Phys.*, 24, 1183–1186.

Ladenburg, R., and F. Reiche, 1911: Ueber Selektive Absorption. *Ann. der Phys.*, **42**, 181–203.

Mitchell, A. C., and M. K. Zemansky, 1934: *Resonance radiation and excited atoms.* New York, MacMillan, 385 pp.

Möller, F., 1943: *Das strahlungsdiagramm.* Berlin, Springer, 9 pp.

Mügge, R., and F. Möller, 1932: Zur berechnung von Strahlungsströmen und Temperaturanderungen in Atmosphären von beliebigem Aufbau. *Z. f. Geophys.*, **8**, 53–64.

Plass, G. N., 1958: Models for spectral band absorption. *J. Opt. Soc. Amer.*, **48**, 690–703.

Plass, G. N., and D. Warner, 1952: Influence of line shift and asymmetry of spectral lines on atmospheric heat transfer. *J. Meteor.*, **9**, 333–339.

Plass, G. N., and D. I. Fivel, 1953: Influence of Doppler effect and damping on line-absorption coefficient and atmospheric radiation transfer. *Astrophys. J.*, **117**, 225–233.

Plass, G. N., and D. I. Fivel, 1955: A method for the integration of the radiative transfer equation. *J. Meteor.*, **12**, 191–200.

Randall, H. M., D. M. Dennison, N. Ginsburg, and L. R. Weber, 1937: The far infrared spectrum of water vapor. *Phys. Rev.*, **52**, 160–174.

Roach, W. T., and R. M. Goody, 1958: Absorption and emission in the atmospheric window from 770 to 1250 cm^{-1}. *Quart. J. r. Meteor. Soc.*, **84**, 319–333.

Robinson, G. D., 1950: Note on the measurement and estimation of atmospheric radiation-2. *Quart. J. r. Meteor. Soc.*, **76**, 37–51.

Strong, J., and G. N. Plass, 1950: The effect of pressure broadening of spectral lines on atmospheric temperature. *Astrophys. J.*, **112**, 365–379.

Summerfield, M., 1941: *Pressure dependence of the absorption in the 9.6 micron band of ozone.* Thesis, Calif. Inst. Tech., unpubl., 65 pp.

Van Vleck, J. H., and V. F. Weisskopf, 1945: On the shape of collision-broadened lines. *Revs. Mod. Phys.*, **17**, 227–236.

Walshaw, C. D., 1957: Integrated absorption by the 9.6 μ band of ozone. *Quart. J. r. Meteor. Soc.*, **83**, 315–321.

Whittacker, E. T., and G. N. Watson, 1940: *Modern analysis*, fourth ed. Cambridge, England, Cambridge Univ. Press, 595 pp.

Wilson, M. K., and R. M. Badger, 1948: A reinvestigation of the vibration spectrum of ozone. *J. Chem. Phys.*, **16**, 74.

Yamamoto, G., 1952: On a radiation chart. *Sci. Rep. Tôhoku Univ., Series 5, Geophys.*, **4**, 9–23.

Yamamoto, G., and G. Onishi, 1953: A chart for the calculation of radiative temperature changes. *Sci. Rep. Tôhoku Univ., Series 5, Geophys.* **4**, 108–115.

Yamamoto, G., and T. Sasamori, 1958: Calculation of the absorption of the 15 μ carbon-dioxide band. *Sci. Rep. Tôhoku Univ., Series 5, Geophys.*, **10**, 37–45.

VI. NUMERICAL TABLES

For definitions, refer to the following formulas:

dB_ν/dT ..... (6) computed from Planck formula,

τ ..... (16) determined empirically for each gas,

τ_F ..... (45) by numerical integration from τ,

L ..... (39) determined empirically for each band,

R ..... (80) $R(u,T) = \int \frac{dB_\nu}{dT}(1 - \tau_F)d\nu$,

$\int_{(u=\text{const.})} RdT$ ... (83) $\int_{(u=\text{const.})} RdT = \int B_\nu(1 - \tau_F)d\nu$, and

$-\Delta R$. (90) (91) overlap corrections $H_2O - CO_2$.

The unit of heat flow is gcal per sq cm day throughout. The optical path, u, stands for the "reduced"

path up/p_0 where p_0 is standard pressure; otherwise, use the more accurate reduction formula (67). For carbon dioxide and ozone, the vertical thickness u is measured by the height in cm of a column reduced to standard pressure and temperature. For water vapor, it is measured in g per sq cm, or the height of the equivalent column of precipitable water. All logarithms used in this work are to base ten.

TABLE 1. $(dB_\nu/dT)\cdot 10^6$.

ν (cm^{-1})	−80°	−70°	−60°	−50°	−40°	−30°	−20°	−10°	0°	+10°	+20°	+30°	+40°
40	85	85	85	85	85	85	85	85	85	85	85	85	85
80	333	334	335	335	336	337	337	338	338	338	339	339	339
120	723	727	731	735	738	741	743	745	747	749	750	752	753
160	1222	1235	1247	1258	1267	1275	1282	1289	1295	1300	1305	1309	1313
200	1790	1821	1848	1872	1893	1912	1929	1944	1958	1971	1982	1992	2001
240	2384	2443	2495	2541	2583	2620	2653	2683	2710	2734	2757	2777	2796
280	2964	3062	3150	3229	3300	3363	3421	3473	3520	3564	3603	3639	3672
320	3493	3642	3777	3899	4010	4110	4201	4284	4360	4429	4492	4550	4603
360	3945	4155	4347	4522	4682	4829	4962	5085	5198	5301	5396	5483	5564
400	4299	4577	4834	5071	5290	5492	5678	5849	6007	6153	6288	6413	6528
440	4546	4896	5223	5529	5813	6078	6324	6552	6764	6960	7143	7313	7471
480	4684	5106	5505	5883	6238	6571	6883	7174	7447	7702	7940	8162	8370
520	4719	5208	5678	6128	6555	6959	7342	7702	8042	8361	8660	8942	9207
560	4661	5211	5746	6265	6763	7240	7694	8126	8536	8924	9290	9637	9964
600	4523	5124	5717	6299	6865	7411	7937	8441	8923	9383	9820	10235	10629
640	4320	4961	5603	6240	6866	7478	8073	8648	9201	9733	10242	10729	11193
680	4069	4737	5416	6099	6778	7449	8107	8748	9372	9974	10555	11114	11651
720	3784	4467	5172	5889	6612	7333	8047	8750	9438	10109	10760	11391	11999
760	3479	4165	4883	5624	6379	7141	7904	8661	9408	10142	10860	11560	12239
800	3165	3843	4563	5317	6094	6887	7688	8491	9291	10082	10861	11626	12373
840	2852	3513	4225	4980	5769	6582	7412	8252	9095	9937	10771	11595	12406
880	2547	3183	3879	4626	5415	6239	7088	7955	8833	9717	10599	11476	12345
920	2257	2861	3533	4263	5044	5868	6727	7612	8516	9432	10355	11278	12198
960	1985	2554	3194	3900	4665	5481	6339	7233	8153	9094	10048	11010	11974
1000	1734	2264	2869	3545	4286	5085	5936	6829	7757	8713	9690	10682	11683
1040	1506	1994	2560	3202	3914	4690	5524	6409	7336	8299	9291	10304	11334
1080	1299	1746	2272	2875	3553	4301	5112	5981	6900	7862	8860	9887	10936
1120	1115	1521	2005	2568	3209	3923	4706	5552	6455	7409	8405	9438	10500
1160	953	1318	1761	2283	2883	3561	4311	5129	6011	6948	7936	8967	10034
1200	810	1137	1539	2019	2579	3217	3931	4717	5571	6487	7459	8481	9547
1240	685	976	1339	1779	2296	2894	3569	4319	5142	6031	6982	7989	9045
1280	577	835	1161	1560	2037	2592	3227	3939	4726	5584	6509	7495	8536
1320	485	711	1002	1363	1799	2313	2906	3578	4328	5151	6045	7005	8025
1360	405	603	862	1187	1584	2057	2608	3239	3949	4735	5594	6524	7519
1400	338	510	738	1029	1389	1823	2333	2922	3590	4337	5160	6056	7021
1440	281	430	631	890	1215	1610	2080	2628	3254	3960	4744	5604	6536
1480	232	362	537	767	1059	1417	1849	2356	2941	3605	4349	5170	6066
1520	192	303	456	660	920	1244	1638	2106	2650	3273	3975	4755	5613
1560	158	253	386	565	797	1090	1448	1877	2381	2963	3623	4363	5181
1600	130	211	326	483	689	951	1276	1669	2134	2675	3294	3992	4769
1640	106	175	275	412	594	829	1122	1480	1908	2409	2987	3644	4379
1680	87	145	231	351	511	720	984	1310	1702	2165	2703	3318	4012
1720	71	120	194	297	439	624	861	1156	1514	1941	2440	3015	3667
1760	57	99	162	252	376	540	752	1018	1344	1736	2198	2733	3345
1800	46	82	135	213	321	466	656	895	1191	1550	1976	2473	3045
1840	38	67	113	180	274	402	570	785	1054	1381	1773	2233	2766
1880	30	55	94	151	233	346	495	688	930	1228	1587	2013	2508
1920	24	45	78	127	198	297	429	601	819	1090	1419	1811	2271
1960	20	37	64	106	168	254	371	524	721	966	1266	1626	2052
2000	16	30	53	89	142	217	320	457	633	855	1128	1458	1851
2040	12	24	44	74	120	186	276	397	555	755	1003	1305	1667
2080	10	20	36	62	101	158	238	345	486	666	891	1167	1499
2120	8	16	30	52	85	135	204	299	424	586	790	1041	1346
2160	6	13	24	43	72	115	175	259	370	515	699	928	1207
2200	5	10	20	36	60	97	150	224	323	453	618	826	1081
2240	4	8	16	29	51	82	129	193	281	397	546	734	966
2280	3	7	13	24	42	70	110	167	244	348	482	652	863
2320	2	5	11	20	35	59	94	143	212	304	424	578	770
2360	2	4	9	17	29	50	80	123	184	266	373	512	686
2400	1	3	7	14	25	42	68	106	159	232	328	453	610

TABLE 2. τ for carbon dioxide.

Log u	−6	−5	−4	−3	−2	−1	0	1	2
0.0		99.91	97.66	92.18	81.70	60.	27.27	3.60	0.14
0.1		99.82	97.27	91.41	80.19	57.62	23.89	2.66	0
0.2		99.70	96.85	90.59	78.56	54.58	20.66	1.96	
0.3		99.55	96.39	89.72	76.80	51.42	17.63	1.47	
0.4		99.37	95.90	88.79	74.91	48.15	14.84	1.13	
0.5		99.16	95.38	87.80	72.88	44.78	12.30	0.89	
0.6		98.92	94.82	86.74	70.71	41.33	10.02	0.71	
0.7		98.65	94.22	85.61	68.39	37.82	8.01	0.56	
0.8	100.00	98.35	93.58	84.40	65.92	34.28	6.27	0.42	
0.9	99.97	98.02	92.90	83.10	63.30	30.75	4.80	0.28	
1.0	99.91	97.66	92.18	81.70	60.53	27.27	3.60	0.14	

TABLE 3. τ_F for carbon dioxide.

Log u	−6	−5	−4	−3	−2	−1	0	1	2
0.0		99.52	96.62	90.24	77.93	53.83	20.67	2.19	
0.1		99.37	96.15	89.35	76.14	50.69	17.73	1.63	
0.2		99.18	95.65	88.40	74.22	47.46	15.00	1.23	
0.3		98.97	95.12	87.39	72.17	44.13	12.51	0.94	
0.4		98.72	94.55	86.30	69.97	40.74	10.28	0.73	
0.5		98.45	93.94	85.14	67.64	37.31	8.30	0.57	
0.6		98.14	93.29	83.90	65.15	33.87	6.58	0.43	
0.7		97.81	92.60	82.57	62.53	30.44	5.12	0.31	
0.8	99.74	97.44	91.86	81.13	59.76	27.07	3.91	0.19	
0.9	99.65	97.04	91.08	79.59	56.86	23.80	2.94	0.10	
1.0	99.52	96.62	90.24	77.93	53.83	20.67	2.19	0.02	

TABLE 4. τ for ozone.

Log u	−5	−4	−3	−2	−1
0.0		97.6	88.1	63.8	15.1
0.1		96.8	86.6	60.0	10.8
0.2		96.0	84.9	55.9	7.4
0.3		95.2	83.0	51.5	4.8
0.4		94.4	80.9	46.8	2.9
0.5		93.6	78.6	41.8	1.5
0.6		92.7	76.1	36.6	0.5
0.7	100.0	91.7	73.4	31.2	0
0.8	99.2	90.6	70.5	25.7	
0.9	98.4	89.4	67.3	20.2	
1.0	97.6	88.1	63.8	15.1	

TABLE 5. τ_F for ozone.

Log u	−5	−4	−3	−2	−1
0.0		95.7	84.1	54.6	8.4
0.1		94.9	82.2	50.3	5.7
0.2		94.1	80.0	45.7	3.6
0.3		93.2	77.7	40.8	2.1
0.4		92.2	75.1	35.8	1.1
0.5		91.2	72.3	30.7	0.4
0.6		90.0	69.3	25.7	0.1
0.7	98.2	88.8	66.1	20.7	
0.8	97.4	87.4	62.5	16.0	
0.9	96.6	85.8	58.7	11.9	
1.0	95.7	84.1	54.6	8.4	

TABLE 6. τ for water vapor.

Log u	−4	−3	−2	−1	0	1
0.0		97.05	87.11	62.72	22.58	1.03
0.1		96.33	85.56	59.15	18.74	0.49
0.2		95.56	83.84	55.41	15.18	0
0.3	100.00	94.75	81.94	51.52	11.98	
0.4	99.90	93.89	79.84	47.50	9.20	
0.5	99.67	92.98	77.53	43.38	6.87	
0.6	99.32	92.00	75.00	39.19	5.00	
0.7	98.87	90.94	72.25	34.97	3.57	
0.8	98.33	89.78	69.28	30.76	2.50	
0.9	97.72	88.51	66.10	26.61	1.68	
1.0	97.05	87.11	62.72	22.58	1.03	

TABLE 7. τ_F for water vapor.

Log u	−4	−3	−2	−1	0	1
0.0		95.22	83.04	54.52	15.54	0.45
0.1		94.39	81.09	50.67	12.45	0.19
0.2		93.50	78.95	46.71	9.73	0
0.3	99.32	92.55	76.61	42.67	7.41	
0.4	98.98	91.53	74.06	38.59	5.50	
0.5	98.54	90.42	71.30	34.50	3.98	
0.6	98.01	89.21	68.33	30.44	2.81	
0.7	97.40	87.88	65.15	26.46	1.93	
0.8	96.73	86.42	61.78	22.61	1.28	
0.9	96.00	84.81	58.23	18.95	0.80	
1.0	95.22	83.04	54.52	15.54	0.45	

TABLE 8. Log L for carbon dioxide.

ν	Log L (+20°)	ν	Log L (+20°)
560	0.03–5	690	0
570	0.95–5	700	0.66–1
580	0.70–4	710	0.28–1
590	0.37–3	720	0.92–4
600	0.94–3	730	0.50–2
610	0.50–2	740	0.12–2
620	0.95–2	750	0.73–3
630	0.39–1	760	0.33–3
640	0.79–1	770	0.92–4
650	0.16	780	0.48–4
660	0.38	790	0.07–4
670	0.43	800	0.61–5
680	0.32	810	0.17–5

TABLE 9. Log L for ozone.

ν	Log L (+20°)	ν	Log L 14 μ band estim.
970	0.8–3		
980	0.6–2	610	0.4–5
990	0.2–1	630	0.7–4
1000	0.6–1	650	0.3–3
1010	0.95–1	670	0.7–3
1020	0.2	690	0.9–3
1030	0.3	710	0.7–3
1037	0.5	725	–2
1045	0.9–1	740	0.9–2
1052	0.5	760	0.6–3
1060	0.35	780	0.2–3
1070	0.3–1	800	0.6–4
1080	0.75–2	820	0.8–5
1090	0.7–2		
1100	0.8–2		
1110	–1		
1120	0.7–2		
1130	0.5–3		

TABLE 10. Absorption coefficients for water vapor.

6.2-μ band				Window			Rotational band			
ν	Log L (20°)	ν	Log L (20°)	ν	Log L (20°)	log k (cont.)	ν	Log L (20°)	ν	Log L (20°)
1000	0.77–5	1640	2.08	680	0.58–2	0.22–2	(0)	(1.10)	480	0.60
1040	0.31–4	1680	2.29	720	0.08–2	0.12–2	40	2.04	520	0.23
1080	0.85–4	1720	2.17	760	0.56–3	0.02–2	80	2.47	560	0.85–1
1120	0.38–3	1760	1.86	800	–3	0.94–3	120	2.67	600	0.45–1
1160	0.93–3	1800	1.38	840	0.41–4	0.89–3	160	2.69	640	0.03–1
1200	0.47–2	1840	0.91	880	0.80–5	0.86–3	200	2.61	680	0.58–2
1240	0.07–1	1880	0.50	920	0.20–5	0.83–3	240	2.45	720	0.08–2
1280	0.74–1	1920	0.14	960	0.25–5	0.82–3	280	2.23	760	0.56–3
1320	0.35	1960	0.79–1	1000	0.77–5	0.82–3	320	1.96	800	–3
1360	0.85	2000	0.41–1	1040	0.31–4	0.83–3	360	1.65	840	0.41–4
1400	1.27	2040	0.04–1	1080	0.85–4	0.85–3	400	1.30	880	0.80–5
1440	1.64	2080	0.60–2	1120	0.38–3	0.91–3	440	0.95		
1480	2.05	2120	0.12–2	1160	0.93–3	0.98–3				
1520	2.46	2160	0.58–3	1200	0.47–2	0.07–2				
1560	2.01	2200	0.97–4							
1590	1.49	2240	0.31–4							
1600	1.56	2280	0.59–5							

TABLE 11. R for carbon dioxide.

Log u	−80°	−70°	−60°	−50°	−40°	−30°	−20°	−10°	0°	+10°	+20°	+30°	+40°
−4	0.004	0.005	0.006	0.007	0.007	0.008	0.009	0.009	0.009	0.010	0.011	0.012	0.012
−4+0.3	0.006	0.007	0.008	0.009	0.010	0.011	0.012	0.013	0.013	0.014	0.015	0.016	0.016
−4+0.7	0.009	0.010	0.012	0.013	0.015	0.016	0.018	0.019	0.020	0.021	0.022	0.023	0.024
−3	0.012	0.014	0.016	0.018	0.020	0.022	0.024	0.026	0.028	0.030	0.031	0.032	0.034
−3+0.3	0.017	0.020	0.022	0.025	0.028	0.031	0.033	0.036	0.039	0.042	0.044	0.046	0.048
−3+0.7	0.027	0.031	0.035	0.039	0.044	0.048	0.052	0.056	0.060	0.065	0.069	0.073	0.076
−2	0.038	0.043	0.049	0.055	0.062	0.068	0.074	0.079	0.085	0.091	0.097	0.103	0.108
−2+0.3	0.053	0.060	0.069	0.078	0.087	0.096	0.105	0.112	0.121	0.129	0.137	0.145	0.153
−2+0.7	0.083	0.095	0.109	0.123	0.138	0.153	0.167	0.180	0.193	0.206	0.219	0.232	0.245
−1	0.117	0.135	0.155	0.175	0.196	0.217	0.237	0.257	0.276	0.295	0.314	0.333	0.351
−1+0.3	0.162	0.188	0.216	0.244	0.273	0.302	0.331	0.360	0.388	0.415	0.442	0.469	0.495
−1+0.7	0.233	0.272	0.313	0.355	0.398	0.441	0.485	0.529	0.572	0.614	0.655	0.695	0.734
0	0.288	0.337	0.389	0.443	0.498	0.553	0.609	0.665	0.721	0.776	0.829	0.881	0.932
0.3	0.342	0.402	0.465	0.531	0.598	0.666	0.734	0.803	0.872	0.940	1.006	1.071	1.135
0.7	0.412	0.487	0.565	0.646	0.729	0.814	0.899	0.985	1.071	1.157	1.241	1.324	1.406
+1	0.463	0.549	0.638	0.730	0.825	0.922	1.020	1.119	1.218	1.317	1.415	1.512	1.608
1.3	0.513	0.609	0.709	0.812	0.919	1.028	1.139	1.251	1.363	1.475	1.587	1.698	1.808
1.7	0.578	0.687	0.801	0.919	1.042	1.167	1.295	1.424	1.553	1.683	1.813	1.942	2.070
2	0.626	0.745	0.869	0.998	1.133	1.270	1.410	1.551	1.693	1.836	1.979	2.121	2.262
2.3	0.673	0.802	0.936	1.076	1.222	1.371	1.523	1.676	1.831	1.986	2.141	2.296	2.449
2.7	0.735	0.877	1.024	1.178	1.339	1.503	1.671	1.840	2.011	2.181	2.351	2.521	2.689
3	0.781	0.932	1.089	1.253	1.425	1.600	1.779	1.960	2.142	2.323	2.503	2.682	2.860
3.3	0.826	0.986	1.153	1.327	1.509	1.695	1.885	2.077	2.269	2.460	2.649	2.836	3.022

TABLE 12. $-\partial R/\partial \log u$ for carbon dioxide.

Log u	−80°	−70°	−60°	−50°	−40°	−30°	−20°	−10°	0°	+10°	+20°	+30°	+40°
−4	0.005	0.006	0.007	0.008	0.009	0.010	0.010	0.011	0.011	0.011	0.011	0.012	0.012
−4+0.3	0.006	0.007	0.008	0.009	0.010	0.011	0.012	0.013	0.014	0.014	0.015	0.016	0.016
−4+0.7	0.009	0.010	0.012	0.013	0.014	0.016	0.018	0.020	0.021	0.022	0.024	0.025	0.026
−3	0.013	0.015	0.017	0.019	0.021	0.023	0.026	0.028	0.030	0.032	0.034	0.036	0.038
−3+0.3	0.019	0.022	0.025	0.028	0.031	0.034	0.037	0.040	0.043	0.046	0.049	0.052	0.055
−3+0.7	0.030	0.035	0.040	0.045	0.050	0.055	0.060	0.064	0.069	0.074	0.079	0.084	0.089
−2	0.042	0.049	0.056	0.064	0.072	0.079	0.086	0.093	0.100	0.107	0.113	0.120	0.127
−2+0.3	0.059	0.069	0.080	0.091	0.102	0.113	0.124	0.134	0.144	0.153	0.162	0.171	0.180
−2+0.7	0.096	0.113	0.130	0.148	0.165	0.182	0.199	0.216	0.233	0.249	0.265	0.281	0.297
−1	0.132	0.155	0.178	0.202	0.226	0.250	0.275	0.300	0.325	0.349	0.373	0.396	0.419
−1+0.3	0.164	0.193	0.223	0.253	0.284	0.316	0.349	0.382	0.414	0.445	0.476	0.506	0.536
−1+0.7	0.182	0.217	0.253	0.290	0.328	0.367	0.407	0.447	0.487	0.527	0.566	0.605	0.643
0	0.182	0.218	0.256	0.295	0.335	0.376	0.418	0.460	0.502	0.545	0.587	0.629	0.671
0.3	0.178	0.215	0.253	0.292	0.332	0.374	0.416	0.459	0.502	0.546	0.590	0.634	0.678
0.7	0.172	0.209	0.247	0.285	0.324	0.365	0.407	0.450	0.494	0.539	0.584	0.630	0.676
+1	0.168	0.204	0.241	0.279	0.318	0.358	0.400	0.443	0.487	0.532	0.577	0.623	0.670
1.3	0.165	0.199	0.235	0.273	0.312	0.352	0.394	0.437	0.480	0.524	0.569	0.615	0.661
1.7	0.161	0.194	0.229	0.266	0.305	0.345	0.386	0.428	0.470	0.513	0.557	0.602	0.646
2	0.158	0.191	0.225	0.261	0.300	0.340	0.380	0.421	0.462	0.504	0.547	0.590	0.632
2.3	0.156	0.188	0.222	0.257	0.295	0.334	0.374	0.414	0.454	0.494	0.535	0.575	0.614
2.7	0.154	0.185	0.218	0.252	0.288	0.326	0.365	0.404	0.442	0.479	0.515	0.550	0.583
3	0.152	0.183	0.215	0.248	0.283	0.320	0.358	0.395	0.431	0.465	0.497	0.527	0.555
3.3	0.150	0.181	0.212	0.244	0.278	0.313	0.349	0.384	0.417	0.448	0.476	0.501	0.523

TABLE 13. R for ozone.

Log u	−80°	−70°	−60°	−50°	−40°	−30°	−20°	−10°	0°	+10°	+20°	+30°	+40°
−4	0.006	0.008	0.010	0.013	0.015	0.017	0.020	0.023	0.026	0.029	0.033	0.036	0.039
−4+0.3	0.009	0.012	0.015	0.019	0.023	0.027	0.031	0.036	0.041	0.046	0.052	0.057	0.062
−4+0.7	0.015	0.020	0.026	0.032	0.039	0.046	0.054	0.063	0.072	0.081	0.091	0.100	0.109
−3	0.022	0.029	0.038	0.047	0.057	0.068	0.080	0.093	0.107	0.121	0.135	0.149	0.163
−3+0.3	0.032	0.042	0.054	0.067	0.082	0.099	0.117	0.136	0.156	0.176	0.197	0.218	0.239
−3+0.7	0.050	0.065	0.083	0.103	0.127	0.154	0.183	0.213	0.244	0.276	0.309	0.343	0.377
−2	0.066	0.086	0.110	0.137	0.169	0.205	0.244	0.284	0.326	0.369	0.414	0.460	0.506
−2+0.3	0.084	0.110	0.141	0.176	0.217	0.263	0.313	0.365	0.419	0.475	0.534	0.594	0.655
−2+0.7	0.109	0.144	0.185	0.232	0.286	0.347	0.412	0.480	0.552	0.627	0.706	0.787	0.869
−1	0.127	0.169	0.217	0.273	0.337	0.409	0.485	0.565	0.651	0.740	0.834	0.931	1.029
−1+0.3	0.144	0.192	0.248	0.312	0.386	0.468	0.554	0.646	0.745	0.848	0.956	1.068	1.182
−1+0.7	0.164	0.220	0.285	0.359	0.445	0.538	0.637	0.745	0.859	0.979	1.105	1.234	1.366
0	0.177	0.238	0.309	0.389	0.482	0.582	0.690	0.808	0.932	1.063	1.200	1.340	1.483
0.3	0.188	0.253	0.329	0.414	0.512	0.618	0.733	0.858	0.990	1.130	1.275	1.424	1.576
0.7	0.200	0.269	0.349	0.439	0.542	0.653	0.774	0.905	1.044	1.191	1.343	1.499	1.658
+1	0.207	0.278	0.360	0.452	0.557	0.670	0.793	0.926	1.067	1.216	1.370	1.528	1.689

TABLE 14. $-\partial R/\partial \log u$ for ozone.

Log u	−80°	−70°	−60°	−50°	−40°	−30°	−20°	−10°	0°	+10°	+20°	+30°	+40°
−4	0.01	0.01	0.02	0.02	0.02	0.03	0.03	0.04	0.04	0.05	0.05	0.06	0.06
−4+0.3	0.01	0.02	0.02	0.03	0.03	0.04	0.04	0.05	0.06	0.07	0.08	0.08	0.09
−4+0.7	0.02	0.03	0.03	0.04	0.05	0.06	0.07	0.08	0.10	0.11	0.12	0.14	0.15
−3	0.03	0.04	0.05	0.06	0.07	0.09	0.10	0.12	0.14	0.16	0.18	0.20	0.22
−3+0.3	0.04	0.05	0.06	0.08	0.10	0.12	0.14	0.16	0.19	0.21	0.24	0.27	0.29
−3+0.7	0.05	0.07	0.08	0.10	0.13	0.16	0.19	0.22	0.25	0.28	0.32	0.36	0.39
−2	0.06	0.08	0.10	0.12	0.15	0.18	0.22	0.26	0.29	0.34	0.38	0.42	0.47
−2+0.3	0.06	0.08	0.11	0.14	0.17	0.20	0.24	0.28	0.32	0.37	0.42	0.47	0.52
−2+0.7	0.06	0.09	0.11	0.14	0.17	0.21	0.25	0.29	0.34	0.38	0.43	0.49	0.54
−1	0.06	0.08	0.11	0.14	0.17	0.20	0.24	0.28	0.32	0.37	0.42	0.47	0.52
−1+0.3	0.05	0.08	0.10	0.13	0.16	0.19	0.22	0.26	0.30	0.35	0.40	0.44	0.49
−1+0.7	0.05	0.06	0.09	0.11	0.13	0.16	0.19	0.23	0.26	0.30	0.34	0.38	0.42
0	0.04	0.06	0.07	0.09	0.11	0.14	0.16	0.19	0.22	0.25	0.28	0.32	0.35
0.3	0.03	0.05	0.06	0.07	0.09	0.11	0.13	0.15	0.17	0.19	0.22	0.24	0.27
0.7	0.03	0.03	0.04	0.05	0.06	0.07	0.08	0.09	0.10	0.11	0.12	0.14	0.15

TABLE 15. R for 6.3-μ water-vapor band.

Log u	−80°	−70°	−60°	−50°	−40°	−30°	−20°	−10°	0°	+10°	+20°	+30°	+40°
−5	0.01	0.01	0.02	0.03	0.04	0.06	0.08	0.10	0.12	0.15	0.19	0.23	0.27
−5+0.3	0.01	0.02	0.03	0.04	0.05	0.07	0.09	0.12	0.15	0.19	0.23	0.28	0.34
−5+0.7	0.01	0.02	0.03	0.05	0.07	0.09	0.12	0.16	0.20	0.26	0.31	0.38	0.45
−4	0.02	0.03	0.04	0.06	0.09	0.12	0.15	0.20	0.25	0.32	0.39	0.47	0.56
−4+0.3	0.02	0.03	0.05	0.08	0.11	0.14	0.19	0.25	0.32	0.39	0.48	0.58	0.70
−4+0.7	0.03	0.04	0.07	0.10	0.14	0.19	0.25	0.33	0.42	0.52	0.64	0.77	0.92
−3	0.03	0.05	0.08	0.12	0.17	0.23	0.31	0.40	0.51	0.63	0.78	0.94	1.13
−3+0.3	0.04	0.06	0.10	0.14	0.20	0.28	0.37	0.48	0.61	0.77	0.94	1.14	1.37
−3+0.7	0.05	0.08	0.12	0.18	0.25	0.35	0.46	0.61	0.77	0.97	1.19	1.45	1.73
−2	0.06	0.09	0.14	0.21	0.29	0.40	0.54	0.70	0.90	1.13	1.39	1.69	2.02
−2+0.3	0.06	0.10	0.16	0.23	0.33	0.46	0.61	0.80	1.02	1.28	1.59	1.93	2.32
−2+0.7	0.07	0.12	0.18	0.27	0.38	0.53	0.71	0.93	1.19	1.49	1.85	2.25	2.70
−1	0.08	0.13	0.20	0.30	0.42	0.58	0.78	1.02	1.31	1.65	2.03	2.48	2.99
−1+0.3	0.09	0.14	0.22	0.32	0.46	0.64	0.85	1.11	1.43	1.79	2.22	2.71	3.27
−1+0.7	0.10	0.16	0.25	0.36	0.51	0.71	0.95	1.24	1.58	1.99	2.46	3.01	3.63
0	0.11	0.17	0.26	0.39	0.55	0.76	1.02	1.33	1.70	2.14	2.65	3.23	3.90
0.3	0.12	0.19	0.28	0.42	0.59	0.82	1.09	1.42	1.82	2.29	2.83	3.46	4.18
0.7	0.13	0.21	0.31	0.46	0.65	0.89	1.19	1.56	1.99	2.50	3.09	3.78	4.56
+1	0.14	0.22	0.33	0.49	0.69	0.95	1.27	1.66	2.12	2.66	3.29	4.02	4.84
1.3	0.15	0.23	0.36	0.52	0.74	1.01	1.35	1.76	2.25	2.83	3.49	4.26	5.13
1.7	0.16	0.25	0.39	0.57	0.80	1.10	1.46	1.91	2.43	3.05	3.76	4.57	5.50

TABLE 16. R for rotational water-vapor band.

Log u	−80°	−70°	−60°	−50°	−40°	−30°	−20°	−10°	0°	+10°	+20°	+30°	+40°
−5	0.04	0.04	0.04	0.04	0.04	0.05	0.05	0.05	0.05	0.05	0.06	0.06	0.06
−5+0.3	0.06	0.06	0.06	0.07	0.07	0.07	0.08	0.08	0.08	0.08	0.09	0.09	0.09
−5+0.7	0.09	0.10	0.10	0.11	0.11	0.12	0.13	0.13	0.14	0.14	0.15	0.15	0.16
−4	0.13	0.14	0.15	0.16	0.16	0.17	0.18	0.19	0.20	0.21	0.21	0.22	0.23
−4+0.3	0.18	0.19	0.20	0.22	0.23	0.24	0.25	0.26	0.28	0.29	0.30	0.31	0.33
−4+0.7	0.26	0.28	0.30	0.32	0.34	0.36	0.38	0.40	0.42	0.44	0.46	0.48	0.50
−3	0.34	0.37	0.40	0.42	0.45	0.47	0.50	0.53	0.55	0.58	0.61	0.63	0.66
−3+0.3	0.43	0.47	0.50	0.53	0.57	0.60	0.64	0.67	0.71	0.75	0.78	0.82	0.86
−3+0.7	0.56	0.61	0.65	0.70	0.75	0.80	0.85	0.90	0.95	1.00	1.05	1.11	1.16
−2	0.66	0.72	0.77	0.83	0.89	0.95	1.01	1.08	1.14	1.21	1.28	1.35	1.42
−2+0.3	0.76	0.83	0.90	0.97	1.04	1.11	1.19	1.27	1.35	1.43	1.51	1.60	1.69
−2+0.7	0.89	0.98	1.06	1.15	1.24	1.34	1.43	1.53	1.64	1.74	1.85	1.96	2.07
+1	0.99	1.09	1.19	1.29	1.40	1.51	1.62	1.74	1.86	1.98	2.11	2.24	2.37
−1+0.3	1.09	1.20	1.31	1.43	1.55	1.68	1.81	1.95	2.09	2.23	2.37	2.52	2.68
−1+0.7	1.22	1.35	1.48	1.62	1.76	1.91	2.07	2.23	2.39	2.56	2.73	2.91	3.10
0	1.31	1.46	1.61	1.76	1.92	2.09	2.26	2.44	2.62	2.81	3.01	3.21	3.41
0.3	1.41	1.56	1.73	1.90	2.07	2.26	2.45	2.64	2.85	3.06	3.27	3.50	3.72
0.7	1.53	1.70	1.89	2.07	2.27	2.48	2.69	2.92	3.15	3.38	3.63	3.87	4.13
+1	1.61	1.80	2.00	2.20	2.42	2.64	2.87	3.11	3.36	3.62	3.88	4.15	4.42
1.3	1.70	1.90	2.11	2.33	2.56	2.80	3.04	3.30	3.57	3.84	4.12	4.41	4.70
1.7	1.80	2.02	2.25	2.48	2.73	2.99	3.27	3.55	3.84	4.13	4.43	4.74	5.05

TABLE 17. R for water-vapor window (660–1220 cm^{-1}).

Log u	−80°	−70°	−60°	−50°	−40°	−30°	−20°	−10°	0°	+10°	+20°	+30°	+40°
−2	0	0	0.01	0.01	0.01	0.01	0.01	0.01	0.01	0.01	0.01	0.01	0.01
−2+0.3	0.01	0.01	0.01	0.02	0.02	0.02	0.02	0.03	0.03	0.03	0.03	0.04	0.04
−2+0.7	0.03	0.03	0.04	0.05	0.05	0.06	0.07	0.08	0.09	0.09	0.10	0.11	0.12
−1	0.05	0.07	0.08	0.09	0.11	0.12	0.14	0.15	0.17	0.18	0.20	0.22	0.24
−1+0.3	0.09	0.11	0.14	0.16	0.19	0.21	0.24	0.27	0.30	0.33	0.36	0.39	0.42
−1+0.7	0.19	0.23	0.27	0.32	0.37	0.42	0.48	0.54	0.60	0.66	0.72	0.78	0.85
0	0.30	0.37	0.44	0.52	0.61	0.70	0.79	0.89	0.99	1.09	1.19	1.29	1.40
0.3	0.47	0.57	0.69	0.82	0.95	1.10	1.25	1.40	1.56	1.72	1.89	2.05	2.22
0.7	0.77	0.95	1.15	1.37	1.60	1.84	2.10	2.36	2.64	2.91	3.19	3.48	3.76
+1	1.00	1.24	1.51	1.80	2.11	2.43	2.77	3.13	3.49	3.86	4.24	4.62	5.00
1.3	1.18	1.46	1.78	2.12	2.49	2.88	3.29	3.71	4.14	4.59	5.04	5.49	5.95
1.7	1.26	1.57	1.91	2.28	2.68	3.10	3.54	3.99	4.46	4.94	5.43	5.92	6.42

TABLE 18. R for water vapor, total.

Log u	−80°	−70°	−60°	−50°	−40°	−30°	−20°	−10°	0°	+10°	+20°	+30°	+40°
−5	0.045	0.053	0.062	0.073	0.086	0.103	0.123	0.148	0.176	0.208	0.243	0.282	0.325
−5+0.3	0.066	0.076	0.088	0.103	0.120	0.142	0.168	0.199	0.234	0.275	0.320	0.371	0.426
−5+0.7	0.105	0.119	0.137	0.158	0.183	0.214	0.250	0.292	0.341	0.397	0.460	0.530	0.607
−4	0.146	0.164	0.188	0.216	0.248	0.288	0.334	0.388	0.451	0.522	0.602	0.691	0.790
−4+0.3	0.199	0.223	0.254	0.291	0.333	0.384	0.443	0.512	0.592	0.682	0.783	0.896	1.022
−4+0.7	0.291	0.326	0.370	0.421	0.480	0.550	0.632	0.726	0.834	0.957	1.094	1.248	1.419
−3	0.375	0.421	0.477	0.541	0.616	0.704	0.807	0.925	1.060	1.213	1.385	1.577	1.789
−3+0.3	0.470	0.528	0.597	0.677	0.771	0.881	1.009	1.156	1.323	1.512	1.725	1.962	2.223
−3+0.7	0.608	0.684	0.773	0.877	1.000	1.144	1.311	1.502	1.720	1.967	2.244	2.552	2.892
−2	0.715	0.806	0.912	1.036	1.183	1.355	1.553	1.780	2.040	2.335	2.665	3.032	3.438
−2+0.3	0.824	0.931	1.056	1.202	1.374	1.575	1.806	2.072	2.376	2.721	3.106	3.535	4.010
−2+0.7	0.975	1.106	1.259	1.437	1.645	1.887	2.166	2.487	2.853	3.267	3.729	4.244	4.815
−1	1.095	1.246	1.422	1.627	1.865	2.141	2.459	2.824	3.239	3.707	4.229	4.812	5.460
−1+0.3	1.224	1.398	1.600	1.834	2.105	2.419	2.780	3.193	3.661	4.186	4.772	5.427	6.155
−1+0.7	1.421	1.633	1.877	2.159	2.484	2.857	3.284	3.769	4.315	4.926	5.609	6.369	7.211
0	1.603	1.852	2.138	2.468	2.845	3.275	3.764	4.316	4.935	5.626	6.395	7.248	8.190
0.3	1.823	2.120	2.460	2.850	3.293	3.794	4.360	4.995	5.704	6.491	7.362	8.324	9.382
0.7	2.177	2.554	2.985	3.474	4.027	4.649	5.345	6.120	6.977	7.921	8.957	10.091	11.329
+1	2.431	2.869	3.368	3.933	4.569	5.282	6.077	6.959	7.930	8.993	10.153	11.416	12.787
1.3	2.610	3.092	3.640	4.261	4.960	5.743	6.613	7.576	8.634	9.790	11.047	12.410	13.884
1.7	2.686	3.182	3.751	4.397	5.127	5.946	6.858	7.866	8.973	10.182	11.497	12.922	14.461

TABLE 19. $-\partial R/\partial \log u$ for water vapor, total.

Log u	−80°	−70°	−60°	−50°	−40°	−30°	−20°	−10°	0°	+10°	+20°	+30°	+40°
−5+0.3	0.08	0.09	0.10	0.11	0.13	0.15	0.17	0.19	0.22	0.26	0.29	0.33	0.38
−5+0.7	0.12	0.13	0.15	0.17	0.19	0.22	0.25	0.28	0.32	0.37	0.42	0.47	0.54
−4	0.16	0.17	0.19	0.22	0.25	0.28	0.32	0.37	0.42	0.48	0.54	0.61	0.69
−4+0.3	0.20	0.22	0.25	0.28	0.32	0.36	0.41	0.47	0.53	0.60	0.68	0.77	0.86
−4+0.7	0.26	0.29	0.33	0.37	0.42	0.47	0.54	0.61	0.69	0.78	0.89	1.00	1.12
−3	0.30	0.34	0.38	0.43	0.49	0.55	0.63	0.72	0.82	0.93	1.06	1.19	1.34
−3+0.3	0.33	0.37	0.42	0.48	0.55	0.62	0.71	0.81	0.93	1.06	1.21	1.37	1.55
−3+0.7	0.35	0.40	0.45	0.52	0.60	0.69	0.79	0.90	1.04	1.19	1.36	1.55	1.76
−2	0.36	0.41	0.47	0.54	0.62	0.72	0.83	0.95	1.10	1.26	1.44	1.64	1.86
−2+0.3	0.37	0.43	0.49	0.57	0.65	0.75	0.87	1.00	1.15	1.32	1.51	1.72	1.95
−2+0.7	0.39	0.46	0.53	0.61	0.70	0.81	0.94	1.08	1.24	1.42	1.61	1.83	2.08
−1	0.41	0.49	0.57	0.66	0.76	0.88	1.02	1.17	1.34	1.53	1.73	1.96	2.22
−1+0.3	0.45	0.54	0.63	0.73	0.85	0.99	1.14	1.31	1.49	1.69	1.91	2.16	2.44
−1+0.7	0.55	0.66	0.78	0.92	1.08	1.25	1.43	1.63	1.85	2.10	2.37	2.65	2.95
0	0.67	0.81	0.97	1.15	1.35	1.56	1.79	2.04	2.30	2.59	2.91	3.25	3.62
0.3	0.81	0.99	1.19	1.41	1.65	1.91	2.19	2.50	2.83	3.19	3.58	3.99	4.43
0.7	0.90	1.10	1.33	1.59	1.87	2.18	2.52	2.88	3.26	3.66	4.08	4.52	4.98
+1	0.74	0.92	1.13	1.36	1.61	1.89	2.19	2.51	2.85	3.21	3.59	4.00	4.43
1.3	0.40	0.51	0.63	0.76	0.90	1.06	1.24	1.44	1.66	1.90	2.16	2.44	2.74
1.7	0.06	0.06	0.06	0.07	0.09	0.12	0.16	0.21	0.27	0.34	0.42	0.51	0.61

TABLE 20. Chart areas, $\int RdT$ at −80° (u = const.).

Log u		Log u	O_3	H_2O total	6.3 μ band	Rotat. band	Window
−4	.18	−5		3.72	0.13	3.59	
−4+0.3	0.24	−5+0.3		5.49	0.16	5.33	
−4+0.7	0.35	−5+0.7	0.09	8.93	0.22	8.72	
−5	0.47	−4	0.14	12.43	0.26	12.17	
−3+0.3	0.65	−4+0.3	0.22	16.96	0.32	16.64	
−3+0.7	1.02	−4+0.7	0.38	24.44	0.42	24.02	
−2	1.42	−3	0.56	31.14	0.51	30.63	
−2+0.3	1.93	−3+0.3	0.79	38.44	0.61	37.83	
−2+0.7	3.15	−3+0.7	1.20	48.38	0.77	47.61	
−1	4.45	−2	1.60	55.54	0.89	54.65	
−1+0.3	6.17	−2+0.3	2.06	62.63	1.02	61.30	0.31
−1+0.7	8.91	−2+0.7	2.66	71.67	1.19	69.54	0.93
0	11.04	−1	3.08	78.40	1.33	75.27	1.79
0.3	13.15	−1+0.3	3.47	85.36	1.48	80.80	3.08
0.7	15.86	−1+0.7	3.99	95.35	1.67	87.67	6.01
+1	17.82	0	4.34	104.04	1.83	92.55	9.65
1.3	19.73	0.3	4.64	113.98	2.00	97.07	14.91
1.7	22.24	0.7	4.94	129.17	2.23	102.70	24.23
2	24.10	1	5.12	140.28	2.41	106.63	31.23
2.3	25.91	1.3		149.16	2.60	110.29	36.27
2.7	28.30	1.7		156.21	2.87	114.74	38.60
3	30.0						
3.3	31.83						

TABLE 21. $-\Delta R$, to correct water-vapor chart for CO_2 overlap.

u_{H_2O} \ u_{CO_2}	−4+0.7	−3	−3+0.3	−3+0.7	−2	−2+0.3	−2+0.7	−1	−1+0.3	−1+0.7	0	0.3	0.7	1	1.3	1.7	2	2.3	2.7	3
−4+0.7																1.820	1.992	2.160	2.374	2.528
−3											0.828	1.005	1.239	1.414	1.587	1.816	1.988	2.155	2.368	2.522
−3+0.3						0.137	0.220	0.315	0.443	0.654	0.825	1.001	1.234	1.408	1.580	1.808	1.979	2.145	2.357	2.510
−3+0.7				0.067	0.096	0.136	0.218	0.312	0.438	0.647	0.816	0.990	1.221	1.393	1.563	1.788	1.957	2.121	2.331	2.482
−2	0.022	0.030	0.042	0.066	0.094	0.134	0.215	0.307	0.431	0.637	0.804	0.975	1.203	1.373	1.541	1.763	1.929	2.091	2.298	2.447
−2+0.3	0.021	0.029	0.041	0.065	0.092	0.131	0.210	0.300	0.421	0.623	0.787	0.954	1.177	1.343	1.508	1.726	1.888	2.047	2.250	2.396
−2+0.7	0.021	0.028	0.039	0.062	0.088	0.125	0.200	0.286	0.402	0.595	0.752	0.912	1.125	1.284	1.442	1.651	1.807	1.959	2.154	2.294
−1	0.020	0.027	0.037	0.059	0.084	0.119	0.190	0.271	0.381	0.564	0.713	0.865	1.067	1.218	1.368	1.567	1.716	1.861	2.047	2.180
−1+0.3	0.019	0.025	0.034	0.054	0.078	0.111	0.176	0.251	0.353	0.522	0.660	0.801	0.988	1.128	1.267	1.452	1.590	1.725	1.899	2.024
−1+0.7	0.016	0.021	0.029	0.045	0.065	0.093	0.148	0.212	0.299	0.442	0.559	0.679	0.839	0.959	1.078	1.236	1.354	1.470	1.621	1.731
0	0.013	0.017	0.023	0.036	0.052	0.074	0.119	0.171	0.241	0.358	0.454	0.553	0.685	0.784	0.883	1.014	1.112	1.209	1.336	1.430
0.3	0.009	0.012	0.016	0.025	0.037	0.053	0.085	0.122	0.172	0.258	0.328	0.401	0.498	0.571	0.645	0.744	0.819	0.893	0.991	1.065
0.7	0.004	0.006	0.007	0.011	0.017	0.025	0.040	0.058	0.082	0.124	0.159	0.195	0.244	0.282	0.320	0.371	0.410	0.449	0.504	0.545
+1	0.002	0.003	0.003	0.004	0.007	0.010	0.017	0.024	0.034	0.052	0.067	0.083	0.104	0.120	0.136	0.158	0.175	0.192	0.216	0.236
1.3	0.001	0.001	0.001	0.001	0.002	0.003	0.006	0.008	0.011	0.017	0.022	0.027	0.033	0.038	0.043	0.049	0.053	0.057	0.063	0.069
1.7	0	0	0	0	0	0	0.001	0.001	0.002	0.003	0.004	0.005	0.006	0.007	0.008	0.008	0.008	0.008	0.009	0.010
2	0	0	0	0	0	0	0	0	0	0.001	0.001	0.001	0.001	0.001	0.002	0.002	0.002	0.002	0.002	0.003

TABLE 22. $-\Delta R$, to correct carbon-dioxide chart for H_2O overlap.

u_{CO_2} \ u_{H_2O}	−4+0.7	−3	−3+0.3	−3+0.7	−2	−2+0.3	−2+0.7	−1	−1+0.3	−1+0.7	0	0.3	0.7	1	1.3	1.7	2
−4+0.7					0.116	0.176	0.298	0.433	0.615	0.946	1.278	1.676	2.244	2.593	2.792	2.864	2.871
−3					0.116	0.176	0.297	0.432	0.613	0.943	1.274	1.671	2.238	2.586	2.784	2.856	2.863
−3+0.3					0.116	0.176	0.296	0.430	0.610	0.939	1.268	1.663	2.227	2.574	2.772	2.844	2.851
−3+0.7				0.073	0.115	0.175	0.294	0.427	0.605	0.930	1.256	1.647	2.206	2.550	2.747	2.819	2.826
−2				0.073	0.114	0.173	0.291	0.423	0.600	0.921	1.243	1.630	2.183	2.524	2.719	2.790	2.797
−2+0.3			0.035	0.072	0.113	0.171	0.287	0.417	0.592	0.908	1.224	1.605	2.150	2.486	2.679	2.749	2.756
−2+0.7			0.035	0.071	0.111	0.167	0.279	0.405	0.574	0.880	1.186	1.554	2.082	2.410	2.599	2.667	2.673
−1			0.035	0.070	0.108	0.162	0.270	0.391	0.554	0.849	1.143	1.496	2.005	2.322	2.506	2.572	2.578
−1+0.3			0.035	0.068	0.104	0.155	0.258	0.373	0.528	0.808	1.085	1.418	1.901	2.204	2.381	2.445	2.450
−1+0.7			0.034	0.065	0.098	0.145	0.239	0.344	0.485	0.739	0.990	1.292	1.731	2.010	2.175	2.234	2.239
0		0.017	0.032	0.061	0.092	0.136	0.223	0.320	0.450	0.683	0.913	1.189	1.593	1.852	2.007	2.062	2.066
0.3		0.017	0.031	0.058	0.086	0.126	0.206	0.295	0.414	0.626	0.835	1.085	1.452	1.691	1.835	1.886	1.889
0.7		0.016	0.029	0.054	0.079	0.114	0.184	0.262	0.366	0.551	0.732	0.947	1.266	1.477	1.606	1.652	1.654
+1		0.016	0.028	0.051	0.074	0.105	0.168	0.238	0.331	0.496	0.656	0.845	1.129	1.318	1.436	1.478	1.479
1.3		0.015	0.026	0.047	0.068	0.096	0.152	0.214	0.296	0.441	0.581	0.745	0.993	1.160	1.267	1.305	1.306
1.7	0.006	0.013	0.023	0.041	0.059	0.083	0.130	0.182	0.250	0.368	0.481	0.613	0.813	0.951	1.042	1.074	1.075
2	0.006	0.013	0.022	0.038	0.053	0.073	0.114	0.159	0.216	0.314	0.407	0.516	0.680	0.796	0.874	0.902	0.903
2.3	0.006	0.012	0.020	0.034	0.047	0.064	0.098	0.136	0.183	0.262	0.336	0.422	0.551	0.645	0.710	0.734	0.735
2.7	0.005	0.010	0.017	0.029	0.039	0.052	0.078	0.107	0.142	0.198	0.248	0.305	0.391	0.454	0.501	0.520	0.520
3	0.005	0.010	0.016	0.026	0.034	0.044	0.064	0.086	0.113	0.154	0.188	0.225	0.278	0.320	0.353	0.367	0.367

UNCLASSIFIED